AD-A083 097 CALIFORNIA UNIV SAN DEIGO LA JOLLA DEPT OF ELECTRICA--ETC F/G 20/14
A SIMPLIFIED THEORY OF ELF PROPAGATION IN THE EARTH-IONOSPHERE --ETC(U)
MAR 80 H G BOOKER N00014-78-C-0682

UNCLASSIFIED NL

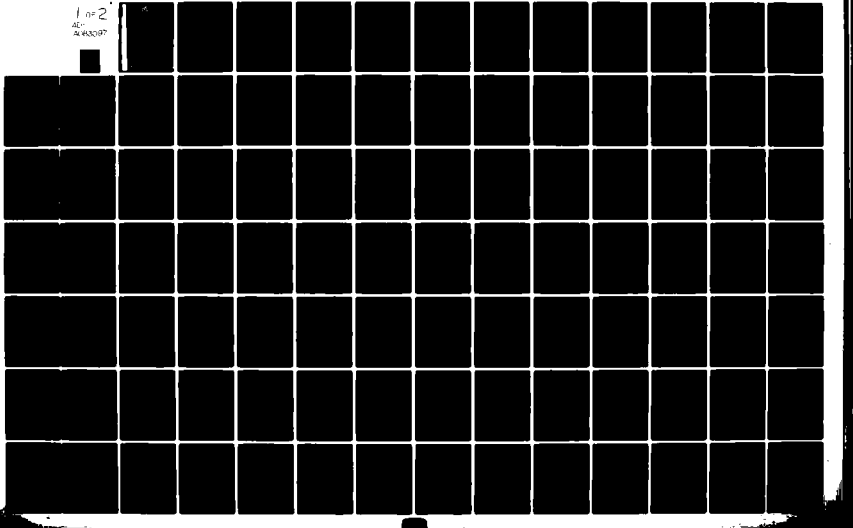

LEVEL II

(4)

Report N00014-78-C-0682-[redacted]1

A Simplified Theory of ELF Propagation In The Earth-Ionosphere Transmission Line And Its Worldwide Application

Henry G. Booker
Department of Electrical Engineering and Computer Sciences
University of California, San Diego
La Jolla, California 92093

31 March 1980

Final report for period 1 August 1978-31 March 1980
For public release; distribution unlimited

Prepared for
Office of Naval Research
800 North Quincy Street
Arlington, Virginia 22217

Report N00014-78-C-0682

A Simplified Theory of ELF Propagation In The Earth-Ionosphere Transmission Line And Its Worldwide Application

Henry G. Booker
Department of Electrical Engineering and Computer Sciences
University of California, San Diego
La Jolla, California 92093

31 March 1980

Final report for period 1 August 1978-31 March 1980
For public release; distribution unlimited

Prepared for
Office of Naval Research
800 North Quincy Street
Arlington, Virginia 22217

SECURITY CLASSIFICATION OF THIS PAGE (When Data Entered)

REPORT DOCUMENTATION PAGE		READ INSTRUCTIONS BEFORE COMPLETING FORM
1. REPORT NUMBER N00014-78-C-0682-[redacted]	2. GOVT ACCESSION NO.	3. RECIPIENT'S CATALOG NUMBER
4. TITLE (and Subtitle) A simplified theory of ELF Propagation in the Earth-Ionosphere Transmission Line and its Worldwide Application		5. TYPE OF REPORT & PERIOD COVERED Final Report, 1 August 1978 to 31 March 1980 6. PERFORMING ORG. REPORT NUMBER
7. AUTHOR(s) Henry G. Booker		8. CONTRACT OR GRANT NUMBER(s) N00014-78-C-0682 Mod
9. PERFORMING ORGANIZATION NAME AND ADDRESS University of California, San Diego La Jolla, California 92093		10. PROGRAM ELEMENT, PROJECT, TASK AREA & WORK UNIT NUMBERS
11. CONTROLLING OFFICE NAME AND ADDRESS Director, Arctic and Field Projects, Arctic and Earth Sciences Division, ONR, 800 N. Quincy St., Arlington, VA 22217		12. REPORT DATE 31 March 1980 13. NUMBER OF PAGES
14. MONITORING AGENCY NAME & ADDRESS (if different from Controlling Office)		15. SECURITY CLASS. (of this report) Unclassified 15a. DECLASSIFICATION/DOWNGRADING SCHEDULE
16. DISTRIBUTION STATEMENT (of this Report) For public release, distribution unlimited		
17. DISTRIBUTION STATEMENT (of the abstract entered in Block 20, if different from Report)		
18. SUPPLEMENTARY NOTES		
19. KEY WORDS (Continue on reverse side if necessary and identify by block number) ELF propagation Earth-ionosphere waveguide Earth-ionosphere cavity Schumann resonances Ionospheric D region Ionospheric E region		

20. ABSTRACT (Continue on reverse side if necessary and identify by block number)

An approximate theory of ELF propagation in the Earth-ionosphere transmission line is developed by combining the reflection theory of Booker and Lefeuvre (1977) with Greifinger and Greifinger's treatment (1978, 1979) of the effect of ionization below the level of reflection. The theory allows for the influence of the Earth's magnetic field, for reflection from the gradient on the under side of the D region (or, at night, of a ledge below the E region), for reflection from the gradient on the under side of the E region, and for reflection from the gradient on the top side of the E region. The procedure

DD FORM 1 JAN 73 1473 EDITION OF 1 NOV 65 IS OBSOLETE
S/N 0102-LF-014-6601

Unclassified
SECURITY CLASSIFICATION OF THIS PAGE (When Data Entered)

is to compare local vertical gradient with local wavelength, thereby classifying altitude into intervals where the gradient is high and ones where it is low. Where the gradient is low, the phase-integral treatment is adequate. An interval where the gradient is high may, to a first approximation, be replaced by a discontinuity. The amount of the discontinuity is the difference between the refractive indices at the top and bottom of the interval of high gradient, judged in relation to local wavelength. It is then a matter of combining reflections from the several discontinuities. This requires calculation of the complex phase-changes between the discontinuities. But these are the intervals where the phase-integral treatment is available. To a better approximation, there is a non-zero phase-change associated with an interval of high gradient. The method for incorporating this is described.

The theory is applied to a simplified worldwide model of the D and E regions, and of the Earth's magnetic field. At 1000 Hz by day, reflection is primarily from the gradient on the under side of the D region. At 300 Hz by day, reflection is primarily from the D region at low latitudes, but it is from the E region at high latitudes. Below 100 Hz by day, reflection is primarily from the gradient on the under side of the E region at all latitudes. By night, reflection from the gradient on the top side of the E region is important. There is then a resonant frequency (~ 300 Hz) at which the optical thickness of the E region for the whistler mode is half a wavelength. At the Schumann resonant frequency in the Earth-ionosphere cavity (~ 8 Hz) the nocturnal E region is almost completely transparent for the whistler mode and is semi-transparent for the Alfvén mode. Reflection then takes place from the F region. ELF propagation in the Earth-ionosphere transmission line by night is quite dependent on the magnitude of the drop in ionization density between the E and F regions. Nocturnal propagation at ELF therefore depends significantly on an ionospheric feature whose magnitude and variability are not well understood.

Table of Contents

List of Figures

List of Tables

Chapter 1. Introduction

This report is concerned with propagation, between the Earth's surface and the ionosphere, of electromagnetic waves having frequencies much lower than those customarily used for radio communications. The calculations refer to the frequency range 7.5-300 Hz. At these frequencies the height of the ionosphere is much less than the wavelength in free space. Consequently the Earth and the ionosphere constitute the two conductors of a transmission line. The problem is to calculate the effect of ionospheric phenomena on the propagation properties of such a transmission line, and to understand the physical reasons for the results obtained.

Use of extremely low frequencies for practical radio communications is discussed in a special issue of the IEEE Transactions on Communications edited by Wait (1974). Such a communications system would be able to penetrate considerably further into the ocean than is possible at conventional radio frequencies.

Another reason for interest in extremely low radio frequencies is that the space between the conducting Earth and the conducting ionosphere is a cavity resonator of enormous dimensions. The fundamental wavelength is controlled by the perimeter of the Earth, and corresponds to a frequency of about 8 Hz. The existence of this resonance was first pointed out by Schumann (1952a,b,c). It is excited by electromagnetic radiation from lightning flashes, distributed over the world. Such radiation constitutes atmospheric noise, and there are peaks of noise at the Schumann resonance frequency and at its low harmonics (Schumann and König 1954,

Schumann 1957, Balser and Wagner 1962a,b, Chapman and Jones 1964, Madden and Thompson 1965, Jones 1967, Larsen and Egeland 1968). The strength of these noise peaks, the precise frequencies at which they occur, and their bandwidths are related to the properties of the ionosphere. It is desirable to understand these features, and it may even be possible to use the structure of the Schumann resonances to derive some information about the physics of the ionosphere.

For many years the theory of ELF propagation in the Earth-ionosphere transmission line was based on the assumption that the ionosphere may be regarded as one or more homogeneous conducting slabs with discontinuous boundaries at heights chosen in a manner that was somewhat arbitrary but nevertheless reasonable (Watson 1919, Budden 1961a,b, Wait 1962, Galejs 1972). The scale-height of the ionosphere is small compared with the free-space wavelength, and in this sense the under boundary of the ionosphere is sharp. Nevertheless, a need existed to employ a continuous vertical profile of conductivity that had some relation to the known facts of ionospheric physics. A need also existed to take full account of the effect of the Earth's magnetic field.

Because of the long free-space wavelength, the phase-integral treatment (WKB approximation) cannot be used near the bottom of the ionosphere. On the other hand, full-wave treatments (Pappert and Moler 1974) lead to elaborate computer programs. These give numerical values for the propagation parameters in the Earth-ionosphere transmission line, but only limited insight into the physics of the propagation phenomena in the ionosphere (see Pappert and Moler 1978).

A need exists for an approximate treatment of ELF propagation that reveals the physics of what is happening in the ionosphere. Such a theory needs to take into account the ionospheric profiles of the electron density, of the ion densities, and of the collisional frequencies, as well as the effect of the Earth's magnetic field. It needs to be such that a particular propagation phenomenon can be traced to the feature of the ionospheric profiles that is principally responsible. Such a theory was attempted several years ago by Booker and Lefeuvre (1977), and their method is described in Chapter 2 of this report. The theory shows that ELF waves are reflected in a stratum where $1/(4\pi)$ times the local wavelength is of the same order of magnitude as the local scale-height of the ionospheric profile. However, the theory of Booker and Lefeuvre had two drawbacks.

Firstly, it did not take satisfactory account of the effect of ionization below the reflecting stratum. A method for doing this has since been developed by Greifinger and Greifinger (1978, 1979). Secondly, the theory of Booker and Lefeuvre assumed that only one reflecting stratum exists in the ionosphere whereas several are frequently encountered. By day, reflection occurs both from the gradient on the under side of the D region and from the gradient on the under side of the E region. By night, reflection occurs from the gradient on the top side of the E region as well as from the gradient on the under side of the E region. Below the ionic gyrofrequency by night, there is even reflection from the F region.

The theory of Booker and Lefeuvre (1977) has been extended in order (i) to cover the occurence of several reflecting strata, and (ii) to incorporate the Greifinger and Greifinger (1978, 1979)

treatment of ionization near the bottom of the ionosphere. The extended theory is described in Chapter 3 of this report.

On the basis of this theory, calculations have been carried out by Amir B. Behroozi-Toosi, a graduate student studying for a Master's degree. A simplified worldwide model of the ionosphere is employed to describe approximately the behavior of the D and E regions as functions of latitude, time of day, season of the year, and year in the sunspot cycle. A central dipole model is used for the Earth's magnetic field. The F region was omitted on the assumption that it is not important for ELF propagation in the Earth-ionosphere transmission line--an assumption that proved to be less true than anticipated. On the basis of the theory presented in Chapter 3, calculations were made for the frequency range 7.5-300 Hz, and results are presented in the diagrams of Chapter 4. These are designed so as not only to describe the propagation characteristics of the Earth-ionosphere transmission line but also to bring out the physical reasons for the results obtained.

A comparison is made between the results obtained by the method of Chapter 3 and those obtained by the method of Pappert and Moler (1974). The comparison is presented in Tables 4 and 5 on page 153, the latter table being provided through the courtesy of the Naval Ocean Systems Center. At present, and probably for a long time to come, overall error in such calculations will be controlled by ignorance concerning worldwide behavior of the ionosphere. For this reason, little is gained by going from moderate accuracy to high accuracy in the propagation calculations. On the other hand, much is

gained by understanding what features of the ionospheric model control what propagation phenomena. It is believed that the method described in Chapter 3 and applied in Chapter 4 provides just what is required. It gives more physical insight than any other method currently available. It uses less effort than any other profile-based method currently available. In spite of approximations, it provides reasonable accuracy.

Bibliography

Balser, M., and Wagner, C. 1962a Diurnal power variations of the Earth-ionosphere cavity modes and their relationship to world-wide thunderstorm activity, Journal of Geophysical Research 67, 619-625.

Balser, M., and Wagner, C. 1962b On frequency variations of the Earth-ionosphere cavity modes, Journal of Geophysical Research 67, 4081-4083.

Booker, H.G., and Lefeuvre, F. 1977 The relation between ionospheric profiles and ELF propagation in the Earth-ionosphere transmission line, Journal of Atmospheric and Terrestrial Research 39, 1277-1292.

Budden, K.G. 1961a Radio waves in the ionosphere, Cambridge University Press, Cambridge.

Budden, K.G. 1961b The wave-guide mode theory of wave-propagation, Logos Press, London.

Chapman, F.W., and Jones, D.L. 1964 Observations of Earth-ionosphere cavity resonances and their interpretation in terms of a two-layer ionospheric model, Radio Science Journal of Research of the National Bureau of Standards 68D, 1177-1185.

Galejs, J. 1972 Terrestrial propagation of long electromagnetic waves, Pergamon Press, New York.

Greifinger, C. and Greifinger, P. 1978 Approximate method for determining ELF eigenvalues in the Earth-ionosphere wave-guide, Radio Science 13, 831-837.

Greifinger, C. and Greifinger, P. 1979 On the ionospheric parameters which govern high latitude ELF propagation in the Earth-ionosphere wave-guide, Radio Science 14, 889-895.

Jones, D.L.	1967	Schumann resonances and ELF propagation for inhomogeneous isotropic ionospheric profiles, Journal of Atmospheric and Terrestrial Physics 29, 1037-1044.
Larsen, T.R. and Egeland, A.	1968	Fine structure in the Earth-ionosphere cavity resonances, Journal of Geophysical Research 73, 4986-4989.
Madden, T., and Thompson, W.	1965	Low frequency electromagnetic oscillations of the earth-ionosphere cavity, Reviews of Geophysics 3, 211-253.
Pappert, R.A. and Moler, W.F.	1974	Propagation theory and calculations at lower ELF, IEEE Transactions on Communications 22, 438-451.
Pappert, R.A. and Moler, W.F.	1978	A theoretical study of ELF normal mode reflection and absorption produced by night-time ionospheres, Journal of Atmospheric and Terrestrial Physics 40, 1031-1045.
Schumann, W.O.	1952a	Über die strahlunglosen Eigenschwingungen einer leitenden Kügel, die von einer Luftschicht und einer Ionosphärenhulle ungenden ist, Z. Naturforsch. 7A, 149-154.
Schumann, W.O.	1952b	Über die Dampfung der elektromagnetischen Eigenschwingungen des Systems Erde-Luft-Ionosphäre, Z. Naturforsch. 7A, 250-252.
Schumann, W.O.	1952c	Über die Ausbreitung sehr langer elektrischer Wellen um die Erde and die Signale des Blitzes, Nuovo Cimento 9, 1116-1138.
Schumann, W.O. and König, H.	1954	Über die Beobactung von Atmospherics bie geringsten Frequenzen, Naturwiss. 41, 183-184.
Schumann, W.O.	1957	Über elektrische Eigenschwingungen des Hohlraumes Erde-Luft-Atmosphäre, erregt durch Blitzenladungen, Z. Angew. Phys. 9 373-378.

Wait, J.R. 1962 Electromagnetic waves in stratified media, Macmillan, New York.

Wait, J.R. 1974 Special issue on extremely low frequency (ELF) Communications, IEEE Transactions on Communications, 22 353-387.

Watson, G.N. 1919 The transmission of electric waves round the Earth, Proceedings of the Royal Society, A95, 546-563.

Chapter 2. The reflection theory of Booker and Lefeuvre (1977)

1. Introduction

Propagation of the transmission-line mode in the wave-guide between the conducting Earth and the conducting ionosphere was first studied by Watson (1919), and the theory has since been developed, particularly for application in the ELF band. It is summarized in books by Budden (1961b), Wait (1962) and Galejs (1972), and also in a special issue of the IEEE Transactions on Communications edited by Wait (1974). The earth, the atmosphere and the ionosphere are often regarded as three media that are homogeneous and isotropic. More elaborate versions of the theory take the ionosphere to involve two or more homogeneous isotropic layers (Wait, 1958; Chapman and Jones, 1964a; Jones, 1967). Theories involving a more-or-less continuously stratified ionosphere, isotropic or non-isotropic, have been developed mainly for VLF and higher frequencies, but they have also been used at ELF (Cole, 1965; Madden and Thompson, 1965; Hughes and Theisen, 1970; Barr, 1972; Pappert and Moler, 1974).

Even if it is agreed that a homogeneous ionosphere with a discontinuous under boundary is an adequate model at ELF, we need to know at what height to place the discontinuity and what parameters to assign to the ionosphere above this height. Furthermore, from experience at higher frequencies, one would expect the height of reflection and the other relevant parameters to depend on angle of incidence and frequency. Konrad and Poverlein (1958) and Chapman and Jones (1964b) have conjectured that the level of reflection should be higher at ELF than at

VLF. Nevertheless, it is frequently assumed that the same ionospheric discontinuity is satisfactory for all angles of incidence and all frequencies in the ELF band. If so, then it should be possible to give theoretical reasons for this result. At the Schumann resonant frequencies, this matter has been considered by Large and Wait (1968).

It is the objective of this chapter to start with a simple but reasonably realistic profile of ionization density, and to derive a method, suitable for use at ELF, for ascertaining at what level the ionosphere may best be cut off at the bottom and be replaced by a discontinuity. We shall also ascertain the dependence of this discontinuity-level on angle of incidence and frequency, and go on to assess the rate of attenuation in the Earth-ionosphere transmission line due to leakage of energy into the ionosphere above the level of reflexion.

We shall do this taking into account the effect of the Earth's magnetic field, but neglecting coupling between the ordinary and extraordinary waves (the O and X waves). It will be necessary to solve the mode transmission-problem in the Earth-ionosphere transmission line taking the ionospheric conductor as a non-isotropic medium. It should be noted that, in such circumstances, a mode involves, not two crossing plane waves, but four. There are a pair of upgoing waves and a pair of downgoing waves, the members of each pair having the elliptic polarization corresponding to the O and X waves in the ionosphere.

2. The level of reflection in the ionosphere at ELF

We shall base our discussion of the level of reflection in the ionosphere at ELF on an ionospheric model for which the index of refraction n varies with height z according to the formula

$$n^2 = 1 - (b\exp j\psi) \exp\{(z-a)/h\} \qquad (1)$$

where b and ψ are real constants, h is a scale-height, and a is a reference height. Such a profile of refractive index is not ideal, but gives a reasonable representation of the underside of the ionosphere in circumstances when the increase of ionization density with height is roughly exponential. The profile does not represent properly the variation of collisional frequency with height, as a result of which there is a tendency to underestimate absorption on one side of the level of reflection and to overestimate it on the other side.

For a plane wave incident upon a plane stratified ionosphere whose profile is described by Equation (1) there is an exact wave solution for horizontal polarization. We shall assume that this solution gives a reasonable clue to determination of the level of reflection in a practical ionosphere for the O and X waves. The solution is given by Budden (1961a, pp. 354-357) and by Wait (1962, pp. 72-74). It involves a Bessel function of an argument that is small at the bottom of the ionosphere and large well inside the ionosphere, with reflection occurring in the transition region between the two. For an angle of incidence θ ($S = \sin\theta$, $C = \cos\theta$), possibly complex, the change in complex phase between the incident wave (measured at the reference height a and the reflected wave (also measured at z = a) is

$$\Phi \approx \pi - \frac{4\pi hC}{\lambda_o} \ln \left\{ (b \exp j\psi) \left(\frac{2\pi h}{\lambda_o} \right)^2 \right\} - 2 \arg \Gamma \left(1 - j \frac{4\pi hC}{\lambda_o} \right) \quad (2)$$

where λ_o is the wavelength in free space. When $2\pi h/\lambda_o$ is large, Equation (2) corresponds to the phase-integral (or WKB) approximation (Budden, 1961a). On the other hand, at ELF $2\pi h/\lambda_o$ is small, and we may then write approximately

$$\Gamma \left(1 - j \frac{4\pi hC}{\lambda_o} \right) \approx \Gamma(1) - j\Gamma'(1) \frac{4\pi hC}{\lambda_o} \quad (3)$$

so that

$$2 \arg \Gamma \left(1 - j \frac{4\pi hC}{\lambda_o} \right) = -2 \frac{\Gamma'(1)}{\Gamma(1)} \frac{4\pi hC}{\lambda_o} \quad (4)$$

Let us define

$$\delta = -2 \frac{\Gamma'(1)}{\Gamma(1)} = 1.1544 \quad . \quad (5)$$

Then Equation (2) may be written at ELF

$$\Phi = \pi + \frac{4\pi hC}{\lambda_o}\left[\ln\left\{\frac{1}{b\exp j\delta}\left(\frac{\lambda_o}{2\pi h}\right)^2\right\} - 5\right]$$

or

$$\Phi = \pi + \frac{4\pi hC}{\lambda_o}\left[\ln\left\{\frac{1}{b}\left(\frac{\lambda_o}{2\pi h}\right)^2\right\} - (5 + j\psi)\right] \qquad (6)$$

For the ionospheric profile in Equation (1) the phase-integral approximation always applies at sufficiently large heights. A sufficiently large height is one for which the argument of the Bessel wave-function is appreciably greater than unity. Any height above the zone of transition from small argument to large argument satisfies this condition, and this zone is the reflecting stratum. Consequently we may simply say that the phase-integral approximation applies above the reflecting stratum.

Let us compare the result in Equation (6) with that for an ionosphere in which (i) the same refractive index profile is maintained above a certain level z_1, (ii) the phase-integral approximation is applied for $z > z_1$ and (iii) the refractive index is taken as unity for $z < z_1$. Let us see whether it is possible to adjust the level z_1 of the resulting discontinuity in refractive index so that, well below the level z_1, the phase-change ψ between an incident wave (measured at the reference height a) and the reflected wave (measured

also at $z = a$) is nearly the same as the right hand side of Equation (6).

Just above the level z_1 the square of the refractive index is

$$n_1^2 = 1 - (b\exp j\psi) \exp\{(z_1 - a)/h\} \tag{7}$$

and if we assume that this level is sufficiently far into the ionosphere to make $|n| \gg 1$, we may write approximately

$$n_1^2 = -(b\exp j\psi) \exp\{(z_1 - a)/h\} \tag{8}$$

For an angle of incidence whose cosine in C, the Fresnel reflection coefficient at the discontinuity at level z_1 is

$$\rho = \frac{C - (n_1^2 - 1 + C^2)^{1/2}}{C + (n_1^2 - 1 + C^2)^{1/2}} \tag{9}$$

Assuming that $|n_1| \gg 1 \gg C$, this becomes

$$\rho = -\left(1 - \frac{2C}{n_1}\right) \tag{10}$$

which is equivalent to a complex phase-change on reflection of

$$j \ln \rho = \tau - j\frac{2C}{n_1} \tag{11}$$

and does not differ much from π. This is the phase-change referred to z_1 as reference height. If a is used as the reference height, the complex phase-change between the incident and reflected waves is

$$\Phi' = \pi + \frac{4\pi C}{\lambda_o} (z_1 - a) - j \frac{2C}{n_1} \tag{12}$$

To put this result in approximately the same form as Equation (6), we note that Equation (8) may be rewritten

$$z_1 - a = h \ln \left(- \frac{n_1^2}{b \exp j\Psi} \right) \tag{13}$$

so that Equation (12) becomes

$$\Phi' = \pi + \frac{4\pi hC}{\lambda_o} \ln \left(- \frac{n_1^2}{b \exp j\Psi} \right) - j \frac{2C}{n_1}$$

or, again using Equation (8),

$$\Phi' = \pi + \frac{4\pi hC}{\lambda_o} \ln \frac{|n_1|^2}{b} + \frac{2C}{|n_1|} \left(\cos \frac{\Psi}{2} - j \sin \frac{\Psi}{2} \right) \tag{14}$$

We are now in a position to deduce from Equations (6) and (14) whether it is possible to choose z_1 (i.e. n_1) so as to make the complex phase-change Φ' for the discontinuity profile approximately the same as that for the original profile. We see that it is not possible to do so

precisely because of the terms following the logarithms in Equations (6) and (14). On the other hand, we also see that these terms are small compared with the logarithmic terms when $\lambda_o/(2\pi h)$ and $|n_1|$ are large, that is, at ELF. To make the dominant logarithmic terms equal we require that

$$|n_1| = \frac{\lambda_o}{2\pi h} \tag{15}$$

This means that the reflecting stratum in the ELF band occurs close to where the local reduced wavelength $\lambda_o/(2\pi|n_1|)$ is equal to the scale height h of the profile. Appreciably below the level corresponding to Equation (15) the local wavelength is large compared with the structure-scale of the ionization profile, which is therefore largely ignored by the waves. Appreciably above the level corresponding to Equation (15) the local wavelength is small compared with the structure-scale of the ionization profile and the phase-integral approximation is applicable. It is in the neighborhood of the level given by Equation (15) that the bulk of the reflection takes place.

Let us now examine the small terms following the logarithms in Equations (6) and (14). While it is not in general possible to adjust the level z_1 so as to make these terms exactly equal, it is possible to adjust the level in such as way as to minimize the difference between Φ and Φ'. From Equations (6) and (14) we deduce that

00 00 A083097 (U) FIELD/GROUP 000000

UNCLASSIFIED TITLE

A SIMPLIFIED THEORY OF ELF PROPAGATION IN THE EARTH-IONOSPHER TRANSMISSION

ABSTRACT

(U) AN APPROXIMATE THEORY OF ELF PROPAGATION IN THE EARTH-IONOSPHERE TRANS
EFLECTION THEORY OF BOOKER AND LEFEUVRE (1977) WITH GREIFINGER AND GREIFING
IONIZATION BELOW THE LEVEL OF REFLECTION. THE THEORY ALLOWS FOR THE INFLUE
CTION FROM THE GRADIENT ON THE UNDER SIDE OFTHE D REGION (OR, AT NIGHT, OF
FROM THE GRADIENT ON THE UNDER SIDE OF THE E REGION, AND FOR REFLECTION FRO
ON. THE PROCEDURE IS TO COMPARE LOCAL VERTICAL GRADIENT WITH LOCAL WAVELENG
ALS WHERE THE GRADIENT IS HIGH AND ONES WHERE IT IS LOW. WHERE THE GRADIENT
QUATE. AN INTERVAL WHERE THE GRADIENT IS HIGH MAY, TO A FIRST APPROXIMATION
OF THE DISCONTINUITY IS THE DIFFERENCE BETWEEN THE REFRACTIVE INDICES AT T
ADIENT, JUDGED IN RELATION TO LOCAL WAVELENGTH. IT IS THEN A MATTER OF COMB
UITIES. THIS REQUIRES CALCULATION OF THE COMPLEX PHASE-CHANGES BETWEEN THE
WHERE THE PHASE-INTEGRAL TREATMENT IS AVAILABLE. TO A BETTER APPROXIMATION
D WITH AN INTERVAL OF HIGH GRADIENT. THE METHOD FOR INCORPORATING THIS IS D

INDEX TERMS ASSIGNED

APPROXIMATION(MATHEMATICS)
EXTREMELY LOW FREQUENCY
GRADIENTS
NIGHT
THEORY
THEORY
PROPAGATION
IONIZATION
REFLECTION
REFRACTIVE INDE

TERMS NOT FOUND ON NLDB

CLASSIFYING ALTITUDE
EARTH-IONOSPHERE TRANSMISSION LINE
NON-ZERO PHASE-CHANGE
SIMPLIFIED THEORY
WORLDWIDE APPLICATION
EARTH-IONOSPHER
LOCAL VERTICAL
PHASE-INTEGRAL
TREATMENT 81978

HE EARTH-IONOSPHER TRANSMISSION LINE AND ITS WORLDWIDE APPLICATION.

ON IN THE EARTH-IONOSPHERE TRANSMISSION LINE IS DEVELOPED BY COMBINING THE R
77) WITH GREIFINGER AND GREIFINGER'S TREATMENT 81978, 1979) OF THE EFFECT OF
THE THEORY ALLOWS FOR THE INFLUENCE OF THE EARTH'S MAGNETIC FIELD, FOR REFLE
FTHE D REGION (OR, AT NIGHT, OF A LEDGE BELOW THE E REGION), FOR REFLECTION
E REGION, AND FOR REFLECTION FROM THE GRADIENT ON THE TOP SIDE OF THE F REGI
CAL GRADIENT WITH LOCAL WAVELENGTH, THEREBY CLASSIFYING ALTITUDE INTO INTERV
RE IT IS LOW. WHERE THE GRADIENT IS LOW, THE PHASE-INTEGRAL TREATMENT IS ADE
GH MAY, TO A FIRST APPROXIMATION, BE REPLACED BY A DISCONTINUITY. THE AMOUNT
WEEN THE REFRACTIVE INDICES AT THE TOP AND BOTTOM OF THE INTERVAL OF HIGH GR
GTH. IT IS THEN A MATTER OF COMBINING REFLECTIONS FROM THE SEVERAL DISCONTIN
MPLEX PHASE-CHANGES BETWEEN THE DISCONTINUITIES. BUT THESE ARE THE INTERVALS
LABLE. TO A BETTER APPROXIMATION, THERE IN A NON-ZERO PHASE-CHANGE ASSOCIATE
THOD FOR INCORPORATING THIS IS DESCRIBED.

INDEX TERMS ASSIGNED
THEORY
PROPAGATION
IONIZATION
REFLECTION
REFRACTIVE INDEX

TERMS NOT FOUND ON NLDB
EARTH-IONOSPHER TRANSMISSION LINE
LOCAL VERTICAL GRADIENT
PHASE-INTEGRAL TREATMENT
TREATMENT 81978

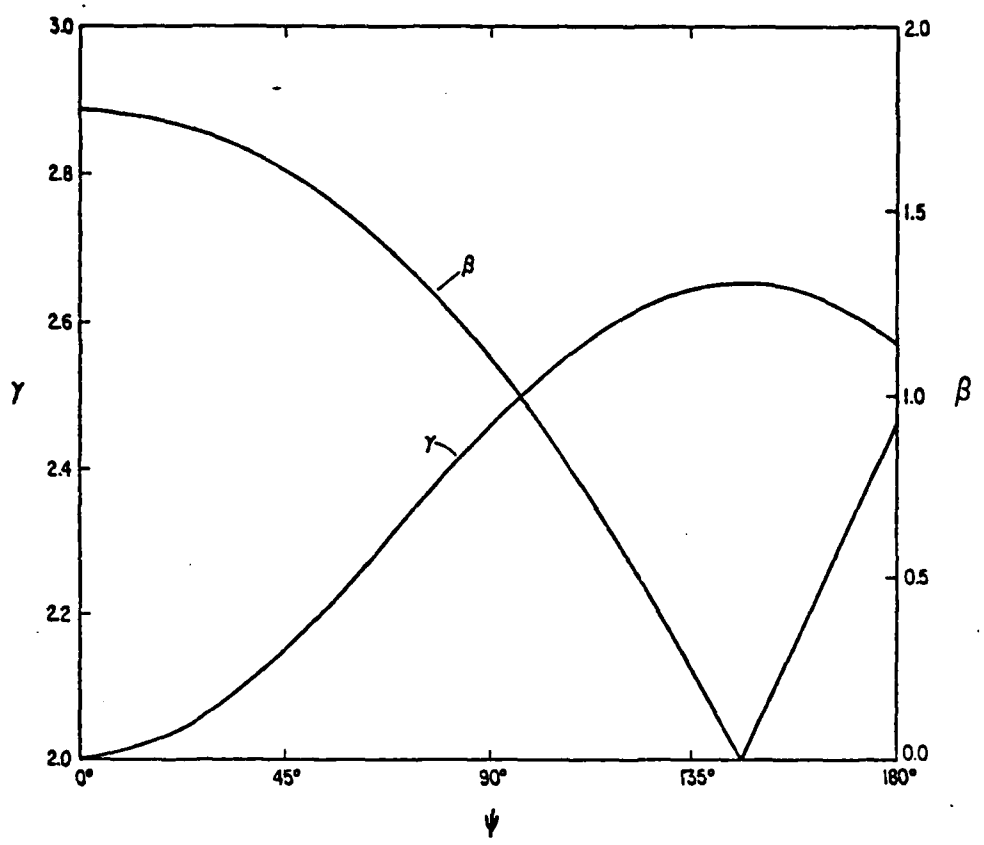

Figure 1. Illustrating (i) the value of γ required to minimize error in the complex phase-change on reflection, and (ii) the value of β to be used in expression (19) for estimating the resulting error.

$$\Phi - \Phi' = \left(\frac{4\pi hC}{\lambda_o}\right)\left[\left\{2 \ln\left(\frac{1}{|n_1|}\ \frac{\lambda_o}{2\pi h}\right) - \delta - \frac{1}{|n_1|}\ \frac{\lambda_o}{2\pi h}\ \cos\frac{\psi}{2}\right\}\right. \quad (16)$$

$$\left. -j\left\{\psi - \frac{1}{|n_1|}\ \frac{\lambda_o}{2\pi h}\ \sin\frac{\psi}{2}\right\}\right]$$

Hence

$$|\Phi - \Phi'|^2 = \left(\frac{4\pi hC}{\lambda_o}\right)^2 \left\{\left(2 \ln\gamma - \delta - \gamma \cos\frac{\psi}{2}\right)^2 + \left(\psi - \gamma \sin\frac{\psi}{2}\right)^2\right\} \quad (17)$$

where

$$|n_1| = \frac{1}{\gamma}\ \frac{\lambda_o}{2\pi h} \quad (18)$$

For a value of γ differing somewhat from unity, Equation (18) determines a height a little different from that given by Equation (15). We select γ so as to minimize the expression for $|\Phi - \Phi'|^2$ given in Equation (17). This value of γ turns out to be independent of frequency, of scale-height and of angle incidence, but to be dependent on the phase-angle ψ of the refractive index profile in Equation (1). The value of γ varies between the extreme values 2.00 and 2.65 as shown in Figure 1, and even less in practice. With the value of γ chosen in this way, the error in $|\Phi - \Phi'|$ has magnitude

$$\frac{4\pi hC}{\lambda_o}\,\beta \tag{19}$$

where β is as shown in Figure 1. This expression has to be compared with the logarithmic term in Equations (6) or (14), and therefore with the term

$$\frac{4\pi C}{\lambda_o}\,(z_1 - a) \tag{20}$$

in Equation (12). The condition that Φ may be replaced by Φ' in a mode calculation involving ionospheric reflexion at a height z_R above the surface of the earth is therefore

$$\frac{4\pi hC}{\lambda_o}\,\beta << \frac{4\pi C}{\lambda_o}\,z_R$$

or

$$\beta << z_R/h \tag{21}$$

Since z_R/h is of the order of 20 or more, and the maximum value of β in Figure 1 is 1.77, it is clear that the condition (21) is reasonably well satisfied.

This implies that, to a first approximation, one may abolish the ionosphere below the level where

$$|n| = \frac{1}{\gamma}\,\frac{\lambda_o}{2\pi h} \tag{22}$$

and apply the phase-integral approximation above this level. The

quantity γ is given by Figure 1 and is independent of the angle of incidence. It follows that the level at which a discontinuous ionospheric lower-boundary should be placed for ELF studies is in fact independent of the angle of incidence (including complex angles of incidence). On the other hand, the discontinuity-level does depend on frequency: not only does λ_o appear explicitly in Equation (22), but the refractive index n is also frequency dependent. Hence it is not advisable to use the same discontinuity-level throughout the ELF band, although at each frequency it is satisfactory to use the same discontinuity-level for all angles of incidence.

While the above deductions apply strictly to the refractive index profile in Equation (1), it is not difficult to devise a way to apply the results to more practical ionospheric profiles. For such a profile a scale-height can be defined at each height for each frequency by means of the equation

$$h = \left| \frac{1}{n^2 - 1} \frac{d}{dz} (n^2 - 1) \right|^{-1} \tag{23}$$

and it is then simple to ascertain the height where this is equal to the local reduced wavelength $\lambda_o / |2\pi n|$. This height is roughly the ELF height of reflection in accordance with Equation (15). At this height one can ascertain the value of the complex refractive index n_1 for the given profile and hence the quantity

$$\psi = \pi + 2 \arg n_1 \tag{24}$$

In accordance with Equation (8), this is approximately the value of ψ

to be used in Figure 1 in order to deduce a value for γ. We can now ascertain the level where the scale-height given by Equation (23) is equal to the corrected local reduced wavelength $\lambda_o/|2\pi\ \gamma\ n|$. In accordance with Equation (22) this height is a reasonable approximation to the ELF height of reflection for the selected frequency and for any angle of incidence. Substitution from Equation (23) into Equation (22) shows that the ELF height of reflection, defined in this way, is given approximately by

$$\left|\frac{1}{n^3}\ \frac{dn^2}{dz}\right| = \frac{2\pi\gamma}{\lambda_o} \tag{25}$$

In the presence of the Earth's magnetic field, the above technique may be applied to the refractive index profiles for O and X waves, provided that one neglects coupling between these waves. The refractive indices at the levels given by Equation (25) always turn out to be large compared with unity. Hence the ELF waves transmitted into the ionosphere may be assumed to travel almost vertically upwards regardless of the direction of the incident and reflected waves below the ionosphere. This greatly simplifies the handling of the Earth's magnetic field. The refractive indices to be used in Equation (25) for the O and X waves are simply those for vertical propagation in the ionosphere.

3. The mode theory at ELF

We derive the mode theory in the Earth-ionosphere wave-guide at ELF on the assumption that curvature of the Earth may be neglected, that the height of reflection is given by Equation (22), that the phase-integral approximation may be applied above this level, and that the ionosphere may be abolished below this level. Reflection at the resulting discontinuity is then determined by the refractive index immediately above the discontinuity.

We derive separate heights of reflection z_0 and z_X for the O and X waves from Equation (22) using the refractive indices for the O and X waves for vertical propagation. Just above the associated discontinuities, let n_0 and n_X be the refractive indices for the O and X waves, so that the impedances looking vertically upwards at the location of the discontinuities are ζ_o/n_0 and ζ_o/n_X, where ζ_o is the impedance of free space (377 ohms). If we take axes as shown in Figure 2, with z vertically upwards and the yz plane as the vertical plane of propagation of the mode, then we have, in terms of the components of the complex electromagnetic fields $\underset{\sim}{E}^O$, $\underset{\sim}{H}^O$ for the O wave and $\underset{\sim}{E}^X$, $\underset{\sim}{H}^X$ for the X wave at their respective levels of reflection,

$$-\frac{E_y^O}{H_x^O} = \frac{E_x^O}{H_y^O} = \frac{1}{n_O}\zeta_o , \quad z = z_O \tag{26}$$

$$-\frac{E_y^X}{H_x^X} = \frac{E_x^X}{H_y^X} = \frac{1}{n_X}\zeta_o , \quad z = z_X \tag{27}$$

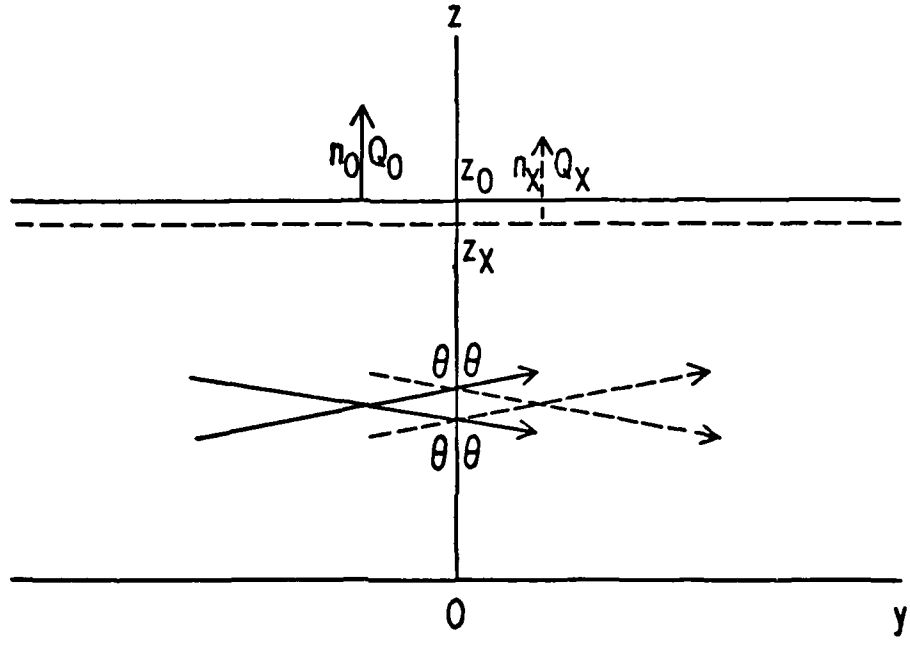

Chapter 2

Figure 2. Illustrating the four crossing plane waves involved in a mode in the Earth-ionsophere wave-guide.

Also, if Q_O and Q_X are the polarization ratios for the O and X waves at their respective levels of reflection, we have

$$-\frac{E_x^O}{E_y^O} = \frac{H_y^O}{H_x^O} = Q_O, \qquad z = z_O \tag{28}$$

$$-\frac{E_x^X}{E_y^X} = \frac{H_y^X}{H_x^X} = Q_X, \qquad z = z_X \tag{29}$$

A mode in the Earth-ionosphere wave-guide consists of a pair of crossing plane waves at an angle θ to the vertical ($S = \sin\theta$, $C = \cos\theta$) having an elliptic polarization whose horizontal projection corresponds to Equation (28) combined with a pair of crossing plane waves at the same angle θ having an elliptic polarization whose horizontal projection corresponds to Equation (29). From the vertical standing-wave pattern formed by these waves we may write down, by standard matrix methods for one-dimensional transmission systems (see, for example, Booker, 1948), the complex electromagnetic field ($\underset{\sim}{E}, \underset{\sim}{H}$) at the ground in terms of the electromagnetic fields at the levels of reflection. We obtain:

$$E_y = \cos\frac{2\pi z_O C}{\lambda_o} E_y^O - j\zeta_o C \sin\frac{2\pi z_O C}{\lambda_o} H_x^O$$
$$+ \cos\frac{2\pi z_X C}{\lambda_o} E_y^X - j\zeta_o C \sin\frac{2\pi z_X C}{\lambda_o} H_x^X \tag{30}$$

$$H_x = -j \frac{1}{\zeta_o C} \sin \frac{2\pi z_o C}{\lambda_o} E_y^O + \cos \frac{2\pi z_o C}{\lambda_o} H_x^O$$

$$-j \frac{1}{\zeta_o C} \sin \frac{2\pi z_X C}{\lambda_o} E_y^X + \cos \frac{2\pi z_X C}{\lambda_o} H_x^X \qquad (31)$$

$$E_x = \cos \frac{2\pi z_o C}{\lambda_o} E_x^O + j \frac{\zeta_o}{C} \sin \frac{2\pi z_o C}{\lambda_o} H_y^O$$

$$+ \cos \frac{2\pi z_X C}{\lambda_o} E_x^X + j \frac{\zeta_o}{C} \sin \frac{2\pi z_X C}{\lambda_o} H_y^X \qquad (32)$$

$$H_y = j \frac{C}{\zeta_o} \sin \frac{2\pi z_o C}{\lambda_o} E_x^O + \cos \frac{2\pi z_o C}{\lambda_o} H_y^O$$

$$+ j \frac{C}{\zeta_o} \sin \frac{2\pi z_X C}{\lambda_o} E_x^X + \cos \frac{2\pi z_X C}{\lambda_o} H_y^X \qquad (33)$$

To satisfy the mode condition these values of E_x, E_y, H_x and H_y must obey the boundary conditions at the surface of the earth.

By employing the ratios (26), (27), (28) and (29) one can express all the electromagnetic field components on the right hand sides of Equations (30), (31), (32) and (33) in terms of H_x^O and H_x^X, which are the components of the magnetic field for the O and X waves at their levels of reflection, taken in the direction transverse to that of propagation in the Earth-ionosphere wave-guide. We obtain:

$$E_y = -\left\{ \frac{1}{n_O} \cos \frac{2\pi z_O C}{\lambda_o} + jC \sin \frac{2\pi z_O C}{\lambda_o} \right\} \zeta_o H_x^O$$

$$- \left\{ \frac{1}{n_X} \cos \frac{2\pi z_X C}{\lambda_o} + jC \sin \frac{2\pi z_X C}{\lambda_o} \right\} \zeta_o H_x^X \tag{34}$$

$$H_x = \left\{ j \frac{1}{n_O C} \sin \frac{2\pi z_O C}{\lambda_o} + \cos \frac{2\pi z_X C}{\lambda_o} \right\} H_x^O$$

$$+ \left\{ j \frac{1}{n_X C} \sin \frac{2\pi z_X C}{\lambda_o} + \cos \frac{2\pi z_X C}{\lambda_o} \right\} H_x^X \tag{35}$$

$$E_x = \left\{ \frac{1}{n_O} \cos \frac{2\pi z_O C}{\lambda_o} + j \frac{1}{C} \sin \frac{2\pi z_O C}{\lambda_o} \right\} Q_O \zeta_o H_x^O$$

$$+ \left\{ \frac{1}{n_X} \cos \frac{2\pi z_X C}{\lambda_o} + j \frac{1}{C} \sin \frac{2\pi z_X C}{\lambda_o} \right\} Q_X \zeta_o H_x^X \tag{36}$$

$$H_y = \left\{ j \frac{C}{n_O} \sin \frac{2\pi z_O C}{\lambda_o} + \cos \frac{2\pi z_O C}{\lambda_o} \right\} Q_O H_x^O$$

$$+ \left\{ j \frac{C}{n_X} \sin \frac{2\pi z_X C}{\lambda_o} + \cos \frac{2\pi z_X C}{\lambda_o} \right\} Q_X H_x^X \tag{37}$$

We will now restrict ourselves to the transmission-line mode, for which the angles

$$\frac{2\pi z_O C}{\lambda_o} \quad \text{and} \quad \frac{2\pi z_X C}{\lambda_o}$$

are sufficiently small that their sines may be replaced by the angles and their cosines by unity. Equations (34) - (37) may then be written

$$E_y = -\left(\frac{1}{n_O} + j\,\frac{2\pi z_O}{\lambda_o} C^2\right) \zeta_o H_x^O - \left(\frac{1}{n_X} + j\,\frac{2\pi z_X}{\lambda_o} C^2\right) \zeta_o H_x^X \tag{38}$$

$$H_x = \left(j\,\frac{1}{n_O}\,\frac{2\pi z_O}{\lambda_o} + 1\right) H_x^O + \left(j\,\frac{1}{n_X}\,\frac{2\pi z_X}{\lambda_o} + 1\right) H_x^X \tag{39}$$

$$E_x = \left(\frac{1}{n_O} + j\,\frac{2\pi z_O}{\lambda_o}\right) Q_O \zeta_o H_x^O + \left(\frac{1}{n_X} + j\,\frac{2\pi z_X}{\lambda_o}\right) Q_X \zeta_o H_x^X \tag{40}$$

$$H_y = \left(j\,\frac{1}{n_O}\,\frac{2\pi z_O}{\lambda_o} C^2 + 1\right) Q_O H_x^O + \left(j\,\frac{1}{n_X}\,\frac{2\pi z_O}{\lambda_o} C^2 + 1\right) Q_X H_x^X \tag{41}$$

In these equations the quantities

$$\frac{1}{n_O},\ \frac{1}{n_X},\ \frac{2\pi z_O}{\lambda_o},\ \frac{2\pi z_X}{\lambda_o} \text{ and } C^2 \tag{42}$$

are all small in practice. Care is therefore necessary in making further approximations in Equations (38) and (40). However, Equations (39) and (41) can safely be simplified to

$$H_x = H_x^O + H_x^X \tag{43}$$

$$H_y = Q_O H_x^O + Q_X H_x^X \tag{44}$$

These equations relate the two Cartesian components (H_x, H_y) of the horizontal magnetic field of the wave at the Earth's surface to the quantities H_x^O and H_x^X that measure the strengths of the O and X waves at their respective levels of reflection.

We now have to satisfy the boundary conditions at the Earth's surface. There is, of course, some leakage of energy into the Earth from the Earth-ionosphere transmission line. We know how to calculate the corresponding contribution to attenuation in the transmission line (Wait 1962) and we know that it is additive to the ionospheric contribution. Since we are at present interested in calculating the ionospheric contribution, we can take the Earth as a perfect conductor and write the boundary condition at the Earth's surface as

$$E_x = E_y = 0, \quad z = 0 \tag{45}$$

It follows from Equations (38) and (40) that

$$\left(\frac{1}{n_O} + j \frac{2\pi z_O}{\lambda_o} C^2\right) H_x^O + \left(\frac{1}{n_X} + j \frac{2\pi z_X}{\lambda_o} C^2\right) H_x^X = 0 \tag{46}$$

$$\left(\frac{1}{n_O} + j \frac{2\pi z_O}{\lambda_o}\right) Q_O H_x^O + \left(\frac{1}{n_X} + j \frac{2\pi z_X}{\lambda_o}\right) Q_X H_x^X = 0 \tag{47}$$

Elimination of the ratio H_x^O/H_x^X between this pair of equations gives the equation for the value of C appropriate to the transmission-line mode:

$$\left(\frac{1}{n_O} + j\,\frac{2\pi z_O}{\lambda_o}\,C^2\right)\left(\frac{1}{n_X} + j\,\frac{2\pi z_X}{\lambda_o}\right)Q_X = \left(\frac{1}{n_O} + j\,\frac{2\pi z_O}{\lambda_o}\right)\left(\frac{1}{n_X} + j\,\frac{2\pi z_X}{\lambda_o}\,C^2\right)Q_O \tag{48}$$

The solution of this equation is

$$C^2 = j\,\frac{Q_O\left(\frac{2\pi z_O}{\lambda_o} - j\,\frac{1}{n_O}\right)\frac{1}{n_X} - Q_X\left(\frac{2\pi z_X}{\lambda_o} - j\,\frac{1}{n_X}\right)\frac{1}{n_O}}{Q_O\left(\frac{2\pi z_O}{\lambda_o} - j\,\frac{1}{n_O}\right)\frac{2\pi z_X}{\lambda_o} - Q_X\left(\frac{2\pi z_X}{\lambda_o} - j\,\frac{1}{n_X}\right)\frac{2\pi z_O}{\lambda_o}} \tag{49}$$

The complex propagation constant along the Earth-ionosphere transmission line is then

$$\frac{2\pi S}{\lambda_o} \tag{50}$$

where

$$S = (1 - C^2)^{1/2} \tag{51}$$

and C^2 is given by Equation (49). The real part of S is the ratio of velocity of light to the velocity of phase propagation in the Earth-ionosphere transmission line, while the imaginary part of expression (50) with the sign reversed is the rate of attenuation in nepers per unit distance.

If one is interested in the relative degree of excitation of the O and X waves, this is given by Equation (47) in the form

$$\frac{H_x^O}{H_x^X} = -\frac{Q_X}{Q_O}\,\frac{\frac{2\pi z_X}{\lambda_o} - j\,\frac{1}{n_X}}{\frac{2\pi z_O}{\lambda_o} - j\,\frac{1}{n_O}} \tag{52}$$

If one is interested in the slight degree of horizontal elliptic polarization existing at ground level, one divides Equation (44) by Equation (43) and uses Equation (52) to obtain

$$\frac{H_y}{H_x} = \frac{\left(\frac{2\pi z_O}{\lambda_o} - j\frac{1}{n_O}\right) - \left(\frac{2\pi z_X}{\lambda_o} - j\frac{1}{n_X}\right)}{\frac{1}{Q_X}\left(\frac{2\pi z_O}{\lambda_o} - j\frac{1}{n_O}\right) - \frac{1}{Q_O}\left(\frac{2\pi z_X}{\lambda_o} - j\frac{1}{n_X}\right)} \tag{53}$$

4. Useful analytical approximations

While for numerical purposes there is no problem about making mode calculations using Equations (49) - (53), it should be noted that, for analytical purposes, some further approximations can usefully be made. Although all the quantities (42) are small, they are not of the same order of smallness. In practice we have

$$\frac{1}{n_O} << \frac{2\pi z_O}{\lambda_o} , \quad \frac{1}{n_X} << \frac{2\pi z_X}{\lambda_o} \tag{54}$$

but we also have

$$\frac{1}{n_O} \not< \frac{2\pi z_O}{\lambda_o} C^2 , \quad \frac{1}{n_X} \not< \frac{2\pi z_X}{\lambda_o} C^2 \tag{55}$$

In consequence the brackets in Equation (40) simplify, whereas those in Equation (38) do not, and a corresponding statement applies for Equations (46) and (47). Hence Equation (49) simplifies to

$$C^2 = j \frac{\lambda_o}{2\pi} \frac{\frac{1}{z_O n_O Q_O} - \frac{1}{z_X n_X Q_X}}{\frac{1}{Q_O} - \frac{1}{Q_X}} \tag{56}$$

Moreover Equation (51) may usually be written approximately as

$$S = 1 - \frac{1}{2} C^2 \tag{57}$$

with the result that the value of S to be used in the propagation constant (50) is

$$S = 1 - j \frac{\lambda_o}{4\pi} \frac{\frac{1}{z_O n_O Q_O} - \frac{1}{z_X n_X Q_X}}{\frac{1}{Q_O} - \frac{1}{Q_X}} \tag{58}$$

Likewise Equation (52) for the relative excitation of the O and X waves becomes

$$\frac{H_x^O}{H_x^X} = - \frac{Q_X}{Q_O} \frac{z_X}{z_O} \tag{59}$$

while Equation (53) for the horizontal elliptic polarization at ground level becomes

$$\frac{H_y}{H_x} = \frac{z_O - z_X}{\frac{z_O}{Q_X} - \frac{z_X}{Q_O}} \tag{60}$$

The slight ellipticity in the horizontal field at ground level depends primarily on the small difference in the heights of reflection for the O and X waves.

5. Cold magneto-plasma relations

To apply the methods developed above, it is necessary to use expressions for the complex refractive indices and polarization ratios of the O and X waves. At ELF, it is desirable to take into account ions, positive and negative, atomic and molecular. Five species of charge carriers are therefore involved: electrons (e), positive atomic ions (a +), negative atomic ions (a -), positive molecular ions (m +), and negative molecular ions (m -). For each of these species we can define angular magnetic gyro frequencies $-\omega_{Me}$, $+\omega_{Ma+}$, $-\omega_{Ma-}$, $+\omega_{Mm+}$ and $-\omega_{Mm-}$; notice that the definitions of ω_{Me}, ω_{Ma-} and ω_{Mm-} are such that they are numerically negative. For each of the species we can define angular plasma frequencies ω_{Ne}, ω_{Na+}, ω_{Na-}, ω_{Nm+} and ω_{Nm-}. Moreover we may employ a collisional frequency ν_e for the electrons and a collision frequency ν_i for the ions. In terms of these quantities we may define, for an angular wave frequency ω, complex angular gyro and plasma frequencies as follows (Booker, 1975):

$$\Omega_{Me} = \frac{\omega_{Me}}{1 - j\frac{\nu_e}{\omega}} \qquad \Omega_{Ne}^2 = \frac{\omega_{Ne}^2}{1 - j\frac{\nu_e}{\omega}}$$

$$\Omega_{Ma+} = \frac{\omega_{Ma+}}{1 - j\frac{\nu_i}{\omega}} \qquad \Omega_{Na+}^2 = \frac{\omega_{Na+}^2}{1 - j\frac{\nu_i}{\omega}}$$

$$\Omega_{Ma-} = \frac{\omega_{Ma-}}{1 - j\frac{\nu_i}{\omega}} \qquad \Omega^2_{Na-} = \frac{\omega^2_{Na-}}{1 - j\frac{\nu_i}{\omega}}$$

$$\Omega_{Mm+} = \frac{\omega_{Mm+}}{1 - j\frac{\nu_i}{\omega}} \qquad \Omega^2_{Nm+} = \frac{\omega^2_{Nm+}}{1 - j\frac{\nu_i}{\omega}}$$

$$\Omega_{Mm-} = \frac{\omega_{Mm-}}{1 - j\frac{\nu_i}{\omega}} \qquad \Omega^2_{Nm-} = \frac{\omega^2_{Nm-}}{1 - j\frac{\nu_i}{\omega}}$$

Using these quantities, the longitudinal, transverse and Hall susceptibilities of a plasma at angular frequency ω are respectively

$$\varkappa_L = -\frac{1}{\omega^2}\sum\Omega^2_N, \quad \varkappa_T = \sum\frac{\Omega^2_N}{\Omega^2_M - \omega^2}, \quad \varkappa_H = \frac{1}{j\omega}\sum\frac{\Omega^2_N\,\Omega_M}{\Omega^2_M - \omega^2} \tag{61}$$

For vertical propagation in the ionosphere at a latitude where the inclination of the Earth's magnetic field to the horizontal is I, the complex refractive indices of the O and X waves are given by

$$\left.\begin{matrix} n^2_O \\ n^2_X \end{matrix}\right\} = (1 + \varkappa_L)\,\frac{1 + \varkappa_T - \varkappa_H\left\{\frac{1}{2}\tau\cos^2 I \mp \left(\frac{1}{4}\tau^2\cos^4 I - \sin^2 I\right)^{1/2}\right\}}{(1 + \varkappa_L) - (\varkappa_L - \varkappa_T)\cos^2 I} \tag{62}$$

where

$$\tau = \frac{(1 + \varkappa_T)(\varkappa_L - \varkappa_T) - \varkappa_H^2}{\varkappa_H(1 + \varkappa_L)} \tag{63}$$

The transition between quasi-longitudinal and quasi-transverse propagation occurs where

$$|\tau| = \frac{2 \sin |I|}{\cos^2 I} \tag{64}$$

At a magnetic pole of the Earth the O and X waves are the waves for which the electromagnetic vectors rotate respectively in the left and right handed senses round the positive direction of the Earth's magnetic field. Except at the magnetic equator the O and X waves may also be referred to as the L and R waves respectively.

Care is necessary in evaluating the polarization ratios Q used in earlier sections because the axes of coordinates that it has been convenient to use in this chapter differ from those often used in the cold plasma wave theory. The relation between the sets of axes involved is shown in Figure 3. The axes (x,y,z) are those used in this paper, with z vertically upwards and y in the horizontal direction of transmission in the Earth-ionosphere transmission line. Let us assume that this direction points at an angle Δ east of magnetic north. The axes (N, W, V) in Figure 3 have the respective directions of magnetic north, magnetic west and upward vertical. These are the axes often used by ionospherists in the cold plasma wave theory for vertical propagation. The V axis coincides with the z axis but the (N,W) axes are rotated through an angle

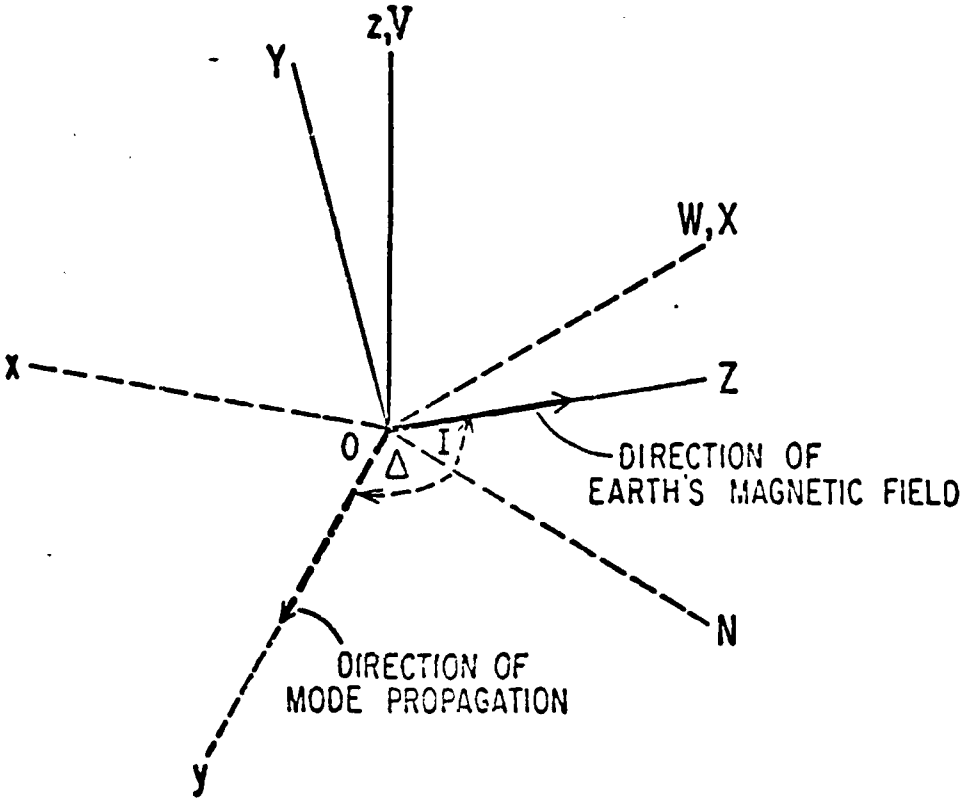

Chapter 2

Figure 3. Illustrating the relation between the axes (x,y,z), (X,Y,Z) and (N,W,V).

$\frac{1}{2}\pi + \Delta$ relative to the (x,y) axes. The polarization ratio commonly used in association with the (N,W,V) axes is

$$P = \frac{E_W}{E_N} \tag{65}$$

where E_W and E_N are the westerly and northerly components of the complex electric field of the wave. The polarization ratio that it has been convenient to use in this paper is (Equations 28 and 29)

$$Q = -\frac{E_x}{E_y} \ . \tag{66}$$

It is easily shown that the relation between the two is

$$Q = \frac{\sin\Delta + P\cos\Delta}{\cos\Delta - P\sin\Delta} \tag{67}$$

However, it must further be noticed that, if one is to make use of the coefficients of susceptibility listed in Equations (61) in a susceptibility tensor of the form

$$\begin{pmatrix} \varkappa_T & \varkappa_H & 0 \\ -\varkappa_H & \varkappa_T & 0 \\ 0 & 0 & \varkappa_L \end{pmatrix} \tag{68}$$

the axes involved are those marked (X,Y,Z) in Figure 3, in which the X axis is westerly and the Z axis is in the direction of the Earth's mag-

netic field. If one performs the cold plasma wave calculations with these axes, one uses the polarization ratios (Booker, 1975)

$$\frac{E_X}{E_Y} = Q_1 = \frac{\varkappa_H}{n^2 - 1 - \varkappa_T} \tag{69}$$

$$\frac{E_Z}{E_Y} = Q_2 = \frac{n^2 \cos I \sin I}{n^2 \cos^2 I - 1 - \varkappa_L} \tag{70}$$

and in terms of these expressions the polarization ratio (65) is, from Figure 3,

$$P = \frac{Q_1}{Q_2 \cos I - \sin I} \tag{71}$$

Sustitution from this equation into Equation (67) then gives

$$Q = \frac{\sin I \sin \Delta - Q_1 \cos \Delta - Q_2 \cos I \sin \Delta}{\sin I \cos \Delta + Q_1 \sin \Delta - Q_2 \cos I \cos \Delta} \tag{72}$$

To obtain Q_O and Q_X for use in previous sections of this paper, we use for n^2 in Equations (69) and (70) the values n_O^2 and n_X^2 from Equations (62) and then substitute into Equation (72).

It should be noted that the limiting values of Q_2 in Equation (70) at the equator (I = 0) are

$$Q_2 = \begin{cases} \infty & \text{O wave} \\ 0 & \text{X wave} \end{cases}$$

This is because, for the O wave, the denominator of Q_2 also tends to zero.

6. Quasi-transverse and quasi-longitudinal approximations

(a) Equatorial behavior

At the magnetic equator vertical propagation of the O wave involves no westerly component of the electric vector, and that of the X wave involves no northerly component. Hence

$$P_O = 0 , \quad P_X = \infty \tag{73}$$

and it follows from Equation (67) that

$$Q_O = \tan \Delta , \quad Q_X = - \cot \Delta \tag{74}$$

Substitution into Equations (58), (59) and (60) then gives

$$S = 1 - j \frac{\lambda_o}{4\pi} \left(\frac{1}{z_O n_O} \cos^2 \Delta + \frac{1}{z_X n_X} \sin^2 \Delta \right) \tag{75}$$

$$\frac{H_x^O}{H_y^X} = \frac{z_X}{z_O} \cot^2 \Delta \tag{76}$$

$$\frac{H_y}{H_x} = - \frac{(z_O - z_X) \sin \Delta \cos \Delta}{z_O \sin^2 \Delta + z_X \cos^2 \Delta} \tag{77}$$

For equatorical propagation in the south-north direction ($\Delta = 0$) we deduce from Equation (76) that only the O wave is excited, and we verify from Equation (75) that the propagation properties of the Earth-ionosphere transmission-line depend only on the ionospheric behavior of the O wave; we also deduce from Equation (77) that the

horizontal elliptic polarization at ground-level is linear (perpendicular to the direction of propagation). Similar statements are true for the X wave for equatorial propagation in the east-west direction ($\Delta = \frac{1}{2}\pi, -\frac{1}{2}\pi$).

We may note that, if the Earth's magnetic field were completely neglected, we would have

$$\left.\begin{aligned} n_O &= n_X = n_R \\ z_O &= z_X = z_R \end{aligned}\right\} \tag{78}$$

and Equation (75) would become

$$S = 1 - j \frac{\lambda_o}{4\pi} \frac{1}{z_R n_R} \tag{79}$$

in accordance with Wait (1962, p. 290).

(b) Quasi-longitudinal behavior

Vertical propagation of the O and X waves is quasi-longitudinal at the level of reflexion in the ELF band over a large part of the world. Under these circumstances

$$P_O = -j, \quad P_X = j \tag{80}$$

from which it follows that

$$Q_O = -j, \quad Q_X = j \tag{81}$$

and consequently that

$$S = 1 - j \frac{\lambda_o}{8\pi} \left(\frac{1}{z_O n_O} + \frac{1}{n_X n_X} \right) \tag{82}$$

$$\frac{H_x^O}{H_x^X} = -\frac{z_X}{z_O} \tag{83}$$

and

$$\frac{H_y}{H_x} = j \frac{z_O - z_X}{z_O + z_X} \tag{84}$$

These equations are independent of Δ.

Since z_0 and z_X are normally not very different numerically, we deduce from Equation (84) that the transmission-line mode, under quasi-longitudinal conditions in the ionosphere, is nearly but not quite linearly polarized perpendicular to the direction of propagation, and from Equation (83) that the degree of excitation of the 0 and X waves at their respective levels of reflection is nearly but not quite the same.

We can also see from Equation (82) that, so far as S is concerned, the effects of the 0 and X waves are mathematically additive. However, the corresponding physical significance requires a rather different statement. At the level of ELF reflection under quasi-longitudinal conditions the 0 wave behaves largely evanescently and n_0 in Equation (82) is close to a pure imaginary, whereas the X wave is the whistler mode and n_X in Equation (82) is close to a real quantity.

This meant that the O wave term in Equation (82) contributes mainly to the real part of S and therefore to the departure of the velocity of propagation in the Earth-ionosphere transmission-line from c. On the other hand, the X wave term in Equation (82) contributes mainly to the imaginary part of S and therefore to the rate of attenuation. In other words, the modification in the velocity of transmission of ELF waves is associated mainly with storage of energy by the O wave immediately above the level of reflection, whereas attenuation of ELF waves in the Earth-ionosphere transmission line due to leakage of energy into the region above the level of reflection is associated mainly with the X wave (the whistler wave).

(c) Relative importance of the quasi-longitudinal and quasi-transverse approximations

In the ELF band there is a drastic difference between the practical importance of the quasi-longitudinal approximation and that of the quasi-transverse approximation. Application of Equation (64) shows that, for vertical transmission in the D and E regions in this band, propagation is quasi-longitudinal at practically all latitudes. The change from quasi-longitudinal to quasi-transverse propagation occurs extremely close to the magnetic equator. Even at a magnetic latitude of 1^{o}, vertical propagation is quasi-longitudinal at all heights less than 100 km and all frequencies less than 300 Hz. At these frequencies, therefore, the equatorial zone, where there can be significant departure from quasi-longitudinal propagation, is less than $\lambda_{o}/(2\pi)$ in width, and consequently has little influence on world-wide propagation of ELF waves in the Earth-ionosphere transmission line, at least by day.

The almost complete dominance of the quasi-longitudinal approximation for calculation of ELF propagation in the Earth-ionosphere transmission line has a practical consequence of the greatest importance. Under quasi-longitudinal or quasi-transverse conditions coupling between the O and X waves is unimportant. It is only in the transition between quasi-longitudinal and quasi-trasnverse propagation that coupling is liable to be important, and even then not at all heights. The almost complete dominance of the quasi-longitudinal approximation implies, therefore, that coupling between the O and X waves is unlikely to be of much importance for ELF communications. This constitutes a major simplification in the theory of ELF propagation in the Earth-ionosphere transmission line.

7. The frequency dependence of the height of reflection

The general character of the frequency dependence of the height of reflexion given by Equation (22) may be illustrated in the following way. Except very close to the equator, vertical propagation in the ionosphere at ELF is quasi-longitudinal. Moreover, as we move above the level where

$$\nu_e = |\omega_{Me} \sin I| \tag{85}$$

electronic collisions contribute a relative minor correction to the magnitude of the complex refractive index. Since the level (85) occurs at about 70 km except near the equator and since the level (22) is frequently above the level (85), electronic collisions usually have only a limited influence in determining the level of reflexion.

On the other hand, for ions of angular gyro frequency ω_{Mi}, the level

$$\nu_i = |\omega_{Mi} \sin I| \tag{86}$$

occurs at about 120 km or higher and is appreciably above the level of ELF reflexion. Below the level (86) the ions are prevented by collisions from developing much motion and consequently from contributing in a major way to the magnitude of the complex refractive index. Between the levels (85) and (86), whistler-band behavior extends downwards in frequency below the ionic gyro-frequency because the ions are

largely held at rest by collisions. Consequently, over most of the ELF band and over most of the world, useful approximations to the refractive indices of the O and X waves are often provided by the whistler-band formulae

$$\left.\begin{matrix} n_O^2 \\ n_X^2 \end{matrix}\right\} = 1 \mp \frac{\omega_{Ne}^2}{\omega\,|\omega_{Me} \sin I|} \tag{87}$$

For an exponential increase of electron density with height (scale-height h), Equation (87) has the form of Equation (1) with

$$\psi = \begin{cases} 0 & O \text{ wave} \\ \pi & X \text{ wave} \end{cases} \tag{88}$$

$$\tag{89}$$

The corresponding values of γ in Figure 1 are

$$\begin{cases} \gamma(0) = 2.00 & O \text{ wave} \\ \gamma(\pi) = 2.57 & X \text{ wave} \end{cases} \tag{90}$$

$$\tag{91}$$

If the quantity

$$\frac{\omega_{Ne}^2}{|\omega_{Me} \sin I|} \tag{92}$$

evaluated at the reference height $z = a$ is written ω_o, and if the unity in Equation (87) is dropped, the height variations of the refractive indices of the O and X waves become

$$\left.\begin{matrix} n_O^2 \\ n_X^2 \end{matrix}\right\} = \mp \frac{\omega_o}{\omega} \exp \frac{z - a}{h} \tag{93}$$

so that

$$|n_O| = |n_X| = \left(\frac{\omega_o}{\omega}\right)^{1/2} \exp \frac{z-a}{2h} \tag{94}$$

Equation (22) for the heights of reflection z_0 and z_X of the O and X waves therefore gives

$$\left(\frac{\omega_o}{\omega}\right)^{1/2} \exp \frac{z_O - a}{2h} = \frac{1}{\gamma(0)} \frac{\lambda_o}{2\pi h} \tag{95}$$

$$\left(\frac{\omega_o}{\omega}\right)^{1/2} \exp \frac{z_X - a}{2h} = \frac{1}{\gamma(\pi)} \frac{\lambda_o}{2\pi h} \tag{96}$$

From these equations we deduce the following approximate expressions for the ELF reflexion heights:

$$z_O = a + 2h \ln \left[c / \{ \gamma(0) (\omega\omega_o)^{1/2} h \} \right] \quad (97)$$

$$z_X = a + 2h \ln \left[c / \{ \gamma(\pi) (\omega\omega_o)^{1/2} h \} \right] \quad (98)$$

Equations (97) and (98) illustrate the fact that heights of reflection in the ELF band increase as the frequency decreases. This behavior continues below the ionic gyro-frequency until tunnel-effect through to the Alfvén region above the level(86) results in penetration of the ionosphere at micropulsation frequencies. The rise in the level of reflection as the frequency is decreased through the ELF band, culminating in penetration of the ionosphere in the micro-pulsation band, is to be compared and contrasted with the rise in the level of reflection as the frequency is increased through the LF, MF and HF bands, culminating in penetration of the ionosphere in the VHF band.

Because $\gamma(0) < \gamma(\pi)$ in accordance with Equations (90) and (91), it follows from Equations (97) and (98) that $z_0 > z_X$. This illustrates the fact that the level of reflection for the O wave in the ELF band is normally a little greater than that for the X wave.

Finaily, let us deduce, for refractive index profiles based on Equations (87), the propagation properties of the transmission-line mode in the Earth-ionosphere wave-guide. From Equations (93)-(96), the complex refractive indices for the O and X waves at their respective levels of reflection may be written

$$n_O = -j \frac{1}{\gamma(0)} \frac{\lambda_o}{2\pi h} \tag{99}$$

$$n_X = \frac{1}{\gamma(\pi)} \frac{\lambda_o}{2\pi h} \tag{100}$$

Substitution into Equation (82) then gives

$$S = 1 + \frac{\gamma(0)}{4} \frac{h}{z_O} - j \frac{\gamma(\pi)}{4} \frac{h}{z_X} \tag{101}$$

For a profile that is not precisely exponential we would deduce the scale-height from Equation (23) and obtain slightly different values h_0 and h_X at the levels z_0 and z_X respectively. Equation (101) would then become

$$S = 1 + \frac{\gamma(0)}{4} \frac{h_O}{z_O} - j \frac{\gamma(\pi)}{4} \frac{h_X}{z_X} \tag{102}$$

or, using Equations (90) and (91),

$$S = 1 + 0.50 \frac{h_O}{z_O} - j\, 0.64 \frac{h_X}{z_X} \tag{103}$$

It follows that, over a large part of the world under commonly encountered ionospheric conditions, the phase velocity in the Earth-ionsophere transmission line is decreased below the velocity of light

while the attenuation rate due to leakage into the upper ionosphere in nepers per $\lambda_o/(2\pi)$ is approximately

$$0.64 \frac{h_X}{z_X} \tag{104}$$

In decibels per megameter at a frequency f measured in hertz, the attenuation rate is approximately

$$0.117 \, f \frac{h_X}{z_X} \tag{105}$$

Bibliography

Barr, R.	1972	Some new features of ELF attenuation, Journal of Atmospheric and Terrestrial Physics 34, 411-420.
Booker, H. G.	1948	The elements of wave propagation using the impedance concept, Journal of the IEE 94, 171-204.
Booker, H. G.	1975	Electromagnetic and hydromagnetic waves in a cold magnetoplasma, Philosophical Transactions of the Royal Society of London A280, 57-93.
Booker, H. G. and Lefeuvre, F.	1977	The relations between ionospheric profiles and ELF propagation in the Earth-ionosphere transmission line, Journal of Atmospheric and Terrestrial Physics, 39, 1277-1292.
Budden, K. G.	1961a	Radio waves in the ionosphere, Cambridge University Press, Cambridge.
Budden, K. G.	1961b	The wave-guide mode theory of wave propagation, Logos Press, London.
Chapman, F. W. and Jones, D. L.	1964a	Observations of Earth-ionospheric cavity resonances and their interpretation in terms of a two-layer ionospheric model, Radio Science Journal of Research of the National Bureau of Standards 68D, 1177-1185.
Chapman, F. W. and Jones, D. L.	1964b	Earth-ionosphere cavity resonances and effective ionosphere parameters, Proceedings of the Seventh Meeting of the AGARD Ionospheric Research Committee, Pergamon Press, London.
Cole, R. K.	1965	The Schumann resonances, Radio Science Journal of Research of the National Bureau of Standards 69D, 1345-1349.

Galejs, J.	1972	Terrestrial propagation of long electro-magnetic waves, Pergamon Press, New York.
Hughes, H. G. and Theisen, J. F.	1970	Diurnal variations in the apparent attenuations of ELF atmospherics over two different propagation paths, Journal of Geophysical Research 75, 2795-2801.
Jones, D. L.	1967	Shumann resonances and ELF propagation for inhomogeneous isotropic ionospheric profiles, Journal of Atmospheric and Terrestrial Physics 29, 1037-1044.
Konrad, A. and Poverlein, H.	1972	Schnelle und langsame Wellenmodes bei extrem niedrigen Frequenzen, Kleinheubacher Berichte 15, 197-207.
Large, D. B. and Wait, J. R.	1968	Theory of electromagnetic coupling phenomena in the Earth-ionosphere cavity, Journal of Geophysical Research 73, 4335-4362.
Madden, T. and Thompson, W.	1965	Low frequency electromagnetic oscillations of the Earth-ionosphere cavity, Reviews of Geophysics 3, 211-253.
Pappert, R. A. and Moler, W. F.	1974	Propagation theory and calculations at lower ELF, IEEE Transactions on Communications 22, 438-451.
Wait, J. R.	1958	An extension of the mode theory of VLF ionospheric propagation, Journal of Geophysical Research 63, 125-135.
Wait, J. R.	1962	Electromagnetic waves in stratified media, Macmillan, New York.
Wait, J. R.	1974	Special issue on extremely low frequency communications, IEEE Transactions on Communications 22, 353-587.
Watson, G. N.	1919	The transmission of electric waves round the earth, Proceedings of the Royal Society A95, 546-563.

Chapter 3. Theory of ELF Propagation in the Earth-ionosphere Transmission Line

1. Introduction

Numerous attempts have been made to devise simple methods for handling ELF propagation of the transmission-line mode of propagation between the conducting Earth and the ionosphere. Many of these are summarized in books by Budden (1961a,b), Wait (1962) and Galejs (1972), and also in a special issue of the IEEE Transactions on Communications edited by Wait (1974). Further efforts in this direction have been made by Booker and Lefeuvre (1977) as described in Chapter 2, and by Greifinger and Greifinger (1978,1979). These pairs of authors will be referred to as BL and GG.

Both BL and GG find that there is an identifiable reflecting stratum for the return of ELF waves from the ionosphere. Moreover, in spite of different approaches, they come to the same conclusion concerning the location of the stratum. The thickness is about one scale-height h, defined in terms of the profile of n^2-1, where n is the ionospheric refractive index. The center of the reflecting stratum occurs where $1/(2\pi)$ times the local wavelength λ is equal to γ times the local scale-height h, where γ is a number between 2 and 3. The BL treatment of the value of γ is slightly different from that of GG. Preference will be given to the BL treatment.

Above the reflecting stratum, the ionosphere is a good approximation to a slowly varying medium. It is a slowly varying medium in which the ordinary (O) and extraordinary (X) waves can nearly

always be assumed to propagate independently. Moreover, because of the high numerical value of the refractive index, phase propagation above the reflecting stratum (but not, in general, group propagation) is almost exactly vertical regardless of the directions of propagation of the incident and reflected waves below the ionosphere. Major simplifications arise from these considerations.

Neither BL nor GG draw explicit attention to another important feature of the reflecting stratum. When a downcoming magneto-ionic component (O wave or X wave) leaves the ionosphere, a location is reached below which no further important change in elliptical polarization takes place. This occurs because a magnetoplasma does not react in a doubly refracting manner unless the refractive indices of O and X waves differ by more than about $\lambda/(2\pi h)$ where λ is the local wavelength and h is the local scale-height (Booker 1936, Budden 1952, Hayes 1971). In the HF band the level thus determined can usually be regarded as the "bottom" of the ionosphere. In the ELF band, however, because of the much bigger free-space wavelength λ_0, the level below which the ionosphere fails to respond as a doubly refracting medium is approximately the same as the level of reflection. Consequently the reflecting stratum as identified by BL and GG has the property that, above it, the ionosphere is a slowly-varying non-isotropic medium whereas, below it, the ionosphere responds primarily as an isotropic medium.

However, BL overlooked an important feature taken into account by GG. BL took the isotropic medium below the reflecting stratum as free space, allowing for collisional absorption in this region by a

method similar to that employed for dielectric loss in an engineering transmission line. GG emphasized that the isotropic medium below the level of reflection is strictly equivalent to free space only below the level where the refractive index begins to approach unity. Between this level and the level of reflection, propagation is essentially vertical almost regardless of the directions of incidence and reflection below the bottom of the ionosphere. At ELF the transition from nearly horizontal propagation to nearly vertical propagation takes place, not in the reflecting stratum, but in a refracting stratum at the bottom of the ionosphere. What GG show is that the vertical standing-wave pattern for the horizontal electric field below the level of reflection is substantially what it is in free space subject to the following remarkable proviso. Propagation of phase is in the nearly horizontal directions of incidence and reflection below the bottom of the ionosphere but, between the bottom of the ionosphere and the level of reflection, change of phase is to be calculated to a first approximation on the basis of vertical propagation in free space.

This unusual result is an indispensable key to understanding ELF propagation. The way in which the various components of the electromagnetic field behave is described by GG using wave theory.
The result seems unusual because, between the refracting stratum at the bottom of the ionosphere and the reflecting stratum higher up, we are dealing with a rapidly varying stratifed medium and there is a lack of familiarity with solutions of the wave equation in these circumstances. In particular, it is essential to realize that there is remarkably little change of phase in passing through such a rapidly varying

medium in comparison with what would be mistakenly calculated using the theory for a slowly varying medium.

In this chapter the ideas of BL and GG are combined into a single approach. In taking the Earth's magnetic field into account there is no restriction to quasi-longitudinal propagation. In Chapter 4 the theory is applied to a simple worldwide model of the ionosphere.

2. The equivalent complex height of reflection

We neglect the curvature of the Earth and suppose that the horizontal direction of propagation in the Earth-ionosphere transmission line is at an angle Δ east of north. We take the magnitude and direction of the Earth's magnetic field to be specified functions of the height z above the Earth's surface. Likewise we take the electron density, the ion densities and the collisional frequencies to be specified functions of z.

Although propagation of phase is nearly horizontal below the ionosphere, we take it to be nearly vertical above the bottom of the ionosphere. For vertical propagation, calculations can be made of the complex refractive indices n_0 and n_X for the 0 and X waves, as well as their complex elliptical polarizations Q_0 and Q_X. The necessary formulae are summarized in Section 5 of Chapter 2, and a more complete account is given by Booker (1975). It should be noted that the definitions of the 0 and X waves used by BL may not be the most convenient. There exist a height z_C and a magnetic latitude Λ_C where there is a branch point at which $n_0 = n_X$. The branch point is located in the E region close to the magnetic equator. BL maintained continuity of wave nomenclature at latitude Λ_C for $z > z_C$, whereas it might be more convenient to do so for $z < z_C$. Nevertheless we shall preserve the BL nomenclature.

At each height z in the ionosphere we define the scale heights h_0 and h_X for vertically propagating 0 and X waves by means of the equations (Equation 23 of Chapter 2)

$$h_0 = \left| \frac{1}{n_0^2 - 1} \frac{d}{dz} (n_0^2 - 1) \right|^{-1}, \quad h_X = \left| \frac{1}{n_X^2 - 1} \frac{d}{dz} (n_X^2 - 1) \right|^{-1} \tag{1}$$

The levels of reflection z_0 and z_X for the 0 and X waves are then such that (Equation 22 of Chapter 2)

$$|n_0| = \frac{1}{\gamma_0} \frac{\lambda_o}{2\pi h_0}, \quad |n_X| = \frac{1}{\gamma_X} \frac{\lambda_o}{2\pi h_X} \tag{2}$$

where the numbers γ_0 and γ_X are read from Figure 1 of Chapter 2. The procedure for determining γ_0 and γ_X is one of successive approximation. First assume that $\gamma_0 = 2.00$, $\gamma_X = 2.57$ and use Equations (2) to determine a first approximation to z_0 and z_X. For these heights evaluate (Equation 24 of Chapter 2)

$$\psi_0 = \pi + 2 \arg n_0, \quad \psi_X = \pi + 2 \arg n_X \tag{3}$$

Use these values of ψ_0 and ψ_X in Figure 1 of Chapter 2 to determine improved values of γ_0 and γ_X. Use these values in Equations (2) to obtain improved values for z_0 and z_X.

Knowing the levels of reflection z_0 and z_X, and the corresponding values n_0 and n_X of the refractive indices, we are now in a position to calculate equivalent complex heights of reflection for the 0 and X waves. These are defined by the equations

$$\tilde{z}_{R0} = z_0 - j \frac{\lambda_o}{2\pi n_0}, \quad \tilde{z}_{RX} = z_X - j \frac{\lambda_o}{2\pi n_X} \tag{4}$$

In Section 4 these equivalent complex heights of reflection will turn out to play a key role in calculating the phase velocity and attenuation rate in Earth-ionosphere transmission line.

It should be noted that, because n_0 and n_X are complex, the real parts of $\tilde{z}_{R0}$ and $\tilde{z}_{RX}$ differ from the actual heights of reflection z_0 and z_X. Except near the equator, it is quite common for n_X to be almost real and for n_0 to be almost purely imaginary. The real part of $\tilde{z}_{RX}$ in the second of Equations (4) is then almost equal to z_X, and there is an imaginary part linked primarily to leakage of energy into the upper ionosphere via the whistler mode. But the transmitted 0 wave behaves evanescently. Consequently $\tilde{z}_{R0}$ in the first of Equations (4) is nearly real but larger than z_0; this is linked to a phase change on reflection that affects the velocity of propagation in the Earth-ionosphere transmission line. In general, there are negative imaginary parts to $\tilde{z}_{R0}$ and $\tilde{z}_{RX}$, and also real parts that differ from z_0 and z_X respectively. It is frequently true that the difference between z_0 and z_X is small, but it is seldom feasible to neglect the difference between $\tilde{z}_{R0}$ and $\tilde{z}_{RX}$.

3. The equivalent complex height of the bottom of the ionosphere

The GG method for taking into account the effect of ionization below the level z_R of reflection depends on the assumption that the horizontal complex magnetic field H(z) of the wave in the Earth-ionosphere transmission line is almost independent of height between $z = 0$ and $z = z_R$. For an angle of incidence whose sine is S(complex for a wave-guide mode), the wave equation for H(z) is

$$\frac{d}{dz}\left\{\frac{1}{n^2(z)}\ \frac{dH}{dz}\right\} + \left(\frac{2\pi}{\lambda_o}\right)^2 \left\{1 - \frac{S^2}{n^2(z)}\right\} H(z) = 0 \qquad (5)$$

Let E(z) be the corresponding horizontal component of the complex electric field. E(z) is derived from H(z) by means of the equation

$$E(z) = -j\,\zeta_o\ \frac{\lambda_o}{2\pi}\ \frac{1}{n^2(z)}\ \frac{dH}{dz} \qquad (6)$$

where ζ_o is the impedance of free space. By integrating Equation (5) with respect to z and substituting into Equation (6) it follows that, if the horizontal electric field vanishes at ground-level, then at the level of reflection we have

$$E(z_R) = j\,\zeta_o\ \frac{2\pi}{\lambda_o} \int_0^{z_R} \left\{1 - \frac{S^2}{n^2(z)}\right\} H(z)dz \qquad (7)$$

The assumption is now made that, in this integral, H(z) may be taken as constant across the Earth-ionosphere transmission line. It follows that

$$E(z_R) = j\,\zeta_o H\,\frac{2\pi}{\lambda_o}\int_0^{z_R}\left\{1 - \frac{S^2}{n^2(z)}\right\}dz \tag{8}$$

and therefore that

$$E(z_R) = j\,\zeta_o\,(2\pi/\lambda_o)(z_R - S^2\tilde{z}_B)H \tag{9}$$

where

$$\tilde{z}_B = \int_0^{z_R}\frac{dz}{n^2(z)} \tag{10}$$

The integrand in Equation (10) is unity below the ionosphere but, in the ELF band, it decreases rapidly as the ionosphere is entered. Consequently $\tilde{z}_B$ is a measure of the height of the bottom of the ionosphere. However, because n(z) is complex, it follows that $\tilde{z}_B$ is complex. As shown by GG, the positive imaginary part of $\tilde{z}_B$ plays an important role in connection with attenuation in the Earth-ionosphere transmission line caused by ionization below the level of reflection. The quantity $\tilde{z}_B$ is the equivalent complex height of the bottom of the ionosphere.

Equation (9) arises from the vertical standing-wave pattern existing between the Earth's surface and the level of reflection in the ionosphere. The quantity S is the sine of the complex angle of incidence below the ionosphere. When the boundary conditions at the level of reflection are satisfied, S is the eigenvalue of the mode problem. Its real and imaginary parts give the propagation properties of the Earth-ionosphere transmission line.

In Equation (9) let us replace S^2 by $1-C^2$, so that C is the cosine of the complex angle of incidence upon the ionosphere. We then obtain

$$E(z_R) = j\zeta_o \left\{ \frac{2\pi \tilde{z}_B}{\lambda_o} C^2 + \frac{2\pi(z_R - \tilde{z}_B)}{\lambda_o} \right\} \tag{11}$$

The corresponding result in the BL treatment of the region below the level of reflection is (Section 3, Chapter 2)

$$E(z_R) = j\zeta_o \frac{2\pi z_R}{\lambda_o} C^2 \tag{12}$$

Equation (12) arises from the vertical standing-wave pattern of horizontal electric field existing between the Earth's surface and the level of reflection on the assumption that we have waves propagating in free space at an angle of incidence and an angle of reflection whose cosine is C. Equation (11) shows that this is only appropriate below the bottom of the ionosphere; between the bottom of the ionosphere and the level of reflection, the vertical standing-wave pattern for horizontal electric field should be taken to be that for vertical propagation in free space. What the work of GG shows is that the BL treatment of the standing wave behavior across the Earth-ionosphere transmission line must be modified by replacing the right hand side of Equation (12) by the right hand side of Equation (11). This is easy to do and the results are given in the following section.

It may be noted that two definitions are possible for the equivalent complex height of the bottom of the ionosphere depending on whether the complex refractive index in Equation (10) is taken to

be that for the 0 wave or that for the X wave. The two definitions are:

$$\tilde{z}_{BO} = \int_0^{z_0} \frac{dz}{n_0^2(z)}, \qquad \tilde{z}_{BX} = \int_0^{z_X} \frac{dz}{n_X^2(z)} \tag{13}$$

There is not much difference between the two because n_0 and n_X only differ where they are numerically large. However, for north-south transmission at the equator, only the 0 wave is excited and $\tilde{z}_{BO}$ is to be preferred while, for east-west transmission at the equator, only the X wave is excited and $\tilde{z}_{BX}$ is to be preferred. On the other hand, at a magnetic pole, transmission in any horizontal direction excites the 0 and X waves above the level of reflection almost equally and an average of $\tilde{z}_{BO}$ and $\tilde{z}_{BX}$ is to be preferred. It is appropriate to weight $\tilde{z}_{BO}$ and $\tilde{z}_{BX}$ according to the relative degree of excitation of the 0 and X waves. This may be conveniently done in the following way.

As described in Chapter 2, the mode in the Earth-ionosphere transmission line consists of a quadruplet of crossing waves, one pair having the elliptical polarization of the 0 wave just above its level of reflection, and the other pair having the elliptical polarization of the X wave just above its level of reflection. For the pair of crossing waves with 0 polarization we shall write the factor in curly brackets on the right hand side of Equation (11) as

$$\frac{2\pi\tilde{z}_{BO}}{\lambda_o} C^2 + \frac{2\pi(\dot{z}_0 - \tilde{z}_{BO})}{\lambda_o} \tag{14}$$

where $\tilde{z}_{BO}$ is given by the first of Equations (13). On the other hand, for the pair of crossing waves with X polarization we shall write

$$\frac{2\pi\tilde{z}_{BX}}{\lambda_o} C^2 + \frac{2\pi(z_X - \tilde{z}_{BX})}{\lambda_o} \tag{15}$$

where $\tilde{z}_{BX}$ is given by the second of Equations (13).

4. Propagation velocity and attenuation rate

We are now in a position to adapt the BL theory of propagation in the Earth-ionosphere transmission line to incorporate the GG theory of the effect of ionization below the level of reflection. It is a matter of replacing the respective quantities $(2\pi z_0/\lambda_o)C^2$ and $(2\pi z_X/\lambda_o)C^2$ in Equations (38) - (41) of BL by expressions (14) and (15) in this Chapter, and then ascertaining the consequent changes in Equations (46) - (48) of Chapter 2. The upshot is that Equation (51) of Chapter 2 may be written

$$S = \left[\frac{Q_0^{-1} - Q_Y^{-1}}{Q_0^{-1}(\tilde{z}_{BO}/\tilde{z}_{RO}) - Q_X^{-1}(\tilde{z}_{BX}/\tilde{z}_{RX})}\right]^{\frac{1}{2}} \tag{16}$$

where $\tilde{z}_{RO}$ and $\tilde{z}_{RX}$ are given by Equations (4), $\tilde{z}_{BO}$ and $\tilde{z}_{BX}$ are given by Equations (13), and Q_0 and Q_X are the complex elliptical polarizations of the O and X waves at their respective levels of reflection. When the complex eigenvalue S has been calculated from Equation (16), the ratio of the velocity c of light to the phase velocity v in the Earth-ionosphere transmission line is given by

$$c/v = R(S) \tag{17}$$

and the rate of attenuation in nepers per unit distance by

$$\alpha = -(2\pi/\lambda_o)\, I(S). \tag{18}$$

where R and I denote real and imaginary parts.

Over a substantial part of the Earth, vertical propagation in the ionosphere is quasi-longitudinal at ELF and we have (Equations 81 of Chapter 2)

$$Q_0 = -j \qquad Q_X = +j \tag{19}$$

Equation (16) then becomes

$$S = [\tfrac{1}{2}\{(\tilde{z}_{BO}/\tilde{z}_{RO}) + (\tilde{z}_{BX}/\tilde{z}_{RX})\}]^{-\frac{1}{2}} \tag{20}$$

If we further assume that

$$\tilde{z}_{BO} \doteq \tilde{z}_{BX} \doteq \tilde{z}_B \tag{21}$$

Equation (20) becomes

$$S = \left(\frac{2\tilde{z}_B^{-1}}{\tilde{z}_{RO}^{-1} + \tilde{z}_{RX}^{-1}}\right)^{\frac{1}{2}} \tag{22}$$

If in addition we assume that

$$\tilde{z}_{RO} \doteq \tilde{z}_{RX} \doteq \tilde{z}_R \tag{23}$$

Equation (22) simplifies to

$$S = (\tilde{z}_R/\tilde{z}_B)^{\frac{1}{2}} \tag{24}$$

This corresponds to a result derived by GG. However, while the approximations in Equations (19) and (21) are often quite good, the approximation in Equation (23) is inadvisable. It is true that the actual heights of reflection of the O and X waves are often nearly the same, so that

$$z_0 \doteq z_X \tag{25}$$

But the corrections required in calculating $\tilde{z}_{RO}$ and $\tilde{z}_{RX}$ in accordance with Equations (4) are significantly different, because the X wave is the whistler mode (n_X almost real) whereas the O wave is quite evanescent (n_O almost purely imaginary).

Simplification of Equation (16) also occurs at the magnetic equator. For propagation in the Earth-ionosphere transmission line at an angle Δ east of north we have at the magnetic equator (Equations 74 of Chapter 2)

$$Q_O = \tan \Delta, \quad Q_X = -\cot \Delta \tag{26}$$

so that Equation (16) becomes

$$S = [(\tilde{z}_{BO}/\tilde{z}_{RO})\cos^2 \Delta + (\tilde{z}_{BX}/\tilde{z}_{RX})\sin^2 \Delta]^{-\frac{1}{2}} \tag{27}$$

For north-south transmission ($\Delta = 0, \pi$) we have

$$S = (\tilde{z}_{RO}/\tilde{z}_{BO})^{\frac{1}{2}} \tag{28}$$

and for east-west transmission ($\Delta = \pm \frac{1}{2} \pi$) we have

$$S = (\tilde{z}_{RX}/\tilde{z}_{BX})^{\frac{1}{2}} \tag{29}$$

In principle, propagation in the Earth-ionosphere transmission line at the magnetic equator is a function of the direction Δ of horizontal transmission, with only the O wave excited above the level of reflection for north-south transmission and only the X wave for east-west transmission. In practice, the numerical values of the expressions on the right hand sides of Equations (28) and (29) are

nearly equal at the equator, and no significant dependence on the angle of transmission Δ materializes. This is because vertical propagation of both the O and X waves immediately above the level of reflection at the magnetic equator is largely metallic, so that n_0 and n_X in Equations (4) are nearly equal both in absolute value and argument, the latter being close to $-\pi/4$.

It may be noticed that, in Equations (16), (20) and (27), the imaginary parts of the complex heights are usually small compared with the real parts, and that useful binomial expansions may be performed on this basis.

The approximations discussed in this section are often convenient for visualizing the physics of the propagation phenomenon. These approximations are, however, unnecessary in numerical calculations.

5. Simultaneous reflection from the D and E regions

So far, we have assumed that only a single reflecting stratum exists for each magneto-ionic component (O wave or X wave). This situation is illustrated in Figure 1. For the selected magneto-ionic component, the relevant Equation (2) has the solution $z = z_R$. At this level the complex refractive index for the magneto-ionic component is n_R. Reflection is calculated as though from a discontinuity of refractive index $n_R - 1$ at this height. Below this level the variation of complex phase with height is calculated by the theory of GG, and this involves a refracting stratum near the bottom of the ionosphere where nearly vertical propagation is converted to nearly horizontal propagation. The calculation based on an individual magneto-ionic component does not satisfy the boundary conditions at the surface of the Earth because the wave is elliptically polarized, but the combination of the O and X wave calculations does satisfy the boundary conditions. Below the reflecting stratum the medium behaves substantially isotropically; it is the combined field derived from the O and X wave calculations that is then significant.

However, it is quite easy for more than one reflecting stratum to exist below the level of maximum ionization density in the E region. This occurs when the profile of ionization density has a high gradient on the under side of the D region and a high gradient on the under side of the E region, with relatively low gradients between and above. As we shall see in detail in the next chapter, the behavior in the ELF band is then as follows.

The primary reflecting stratum at the Schumann resonant

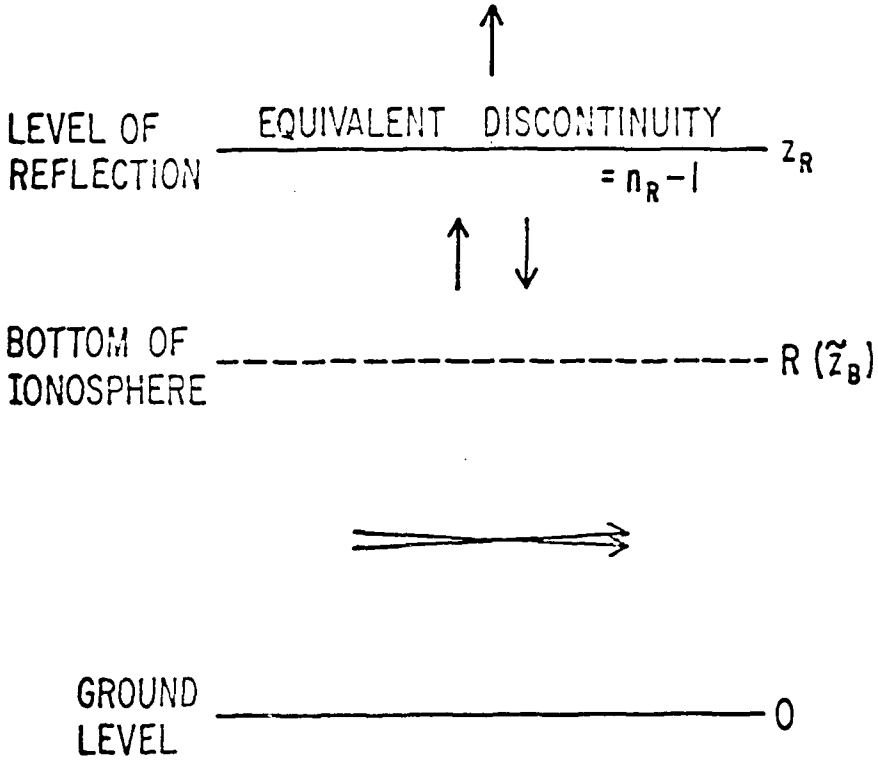

Chapter 3

Figure 1. Illustrating reflection of the O or X wave from the ionosphere at ELF when the relevant Equation (2) has only one solution.

frequency (~ 7.5 Hz) is located in the high gradient on the under side of the E region. But, as the frequency increases through about 30 Hz, partial reflection from the D region comes into play. Below about 100 Hz, the D region is an optically thin stratum that is quite transparent, so that reflection is still largely from the E region. But with sufficient increase of frequency, the high gradient on the under side of the D region takes over as the primary seat of reflection.

This behavior manifests itself in the process of solving Equations (2) to obtain the heights of reflection z_0 and z_X. For the two waves, let us introduce local wavelengths λ_0 and λ_X defined in terms of the wavelength λ_o in free space by

$$\lambda_0 = \lambda_o/|n_0|, \qquad \lambda_X = \lambda_o/|n_X| \tag{30}$$

Equations (2) may then be written

$$\frac{\lambda_0}{2\pi h_0} = \gamma_0, \qquad \frac{\lambda_X}{2\pi h_X} = \gamma_X \tag{31}$$

By plotting the quantities on the left-hand sides of these equations as functions of height, it is easy to locate the heights of reflection in the manner shown in Figure 2. Using a model of the ionosphere of the type employed in the next chapter, Figure 2 is drawn for daytime conditions in a middle lattitude. The two functions of height on the left-hand sides of Equations (31) are so nearly identical that duplicate curves cannot easily be shown for the O and X waves in Figure 2. The four curves refer to four frequencies. The first approximations to z_0 and z_X are given by the intersections of these

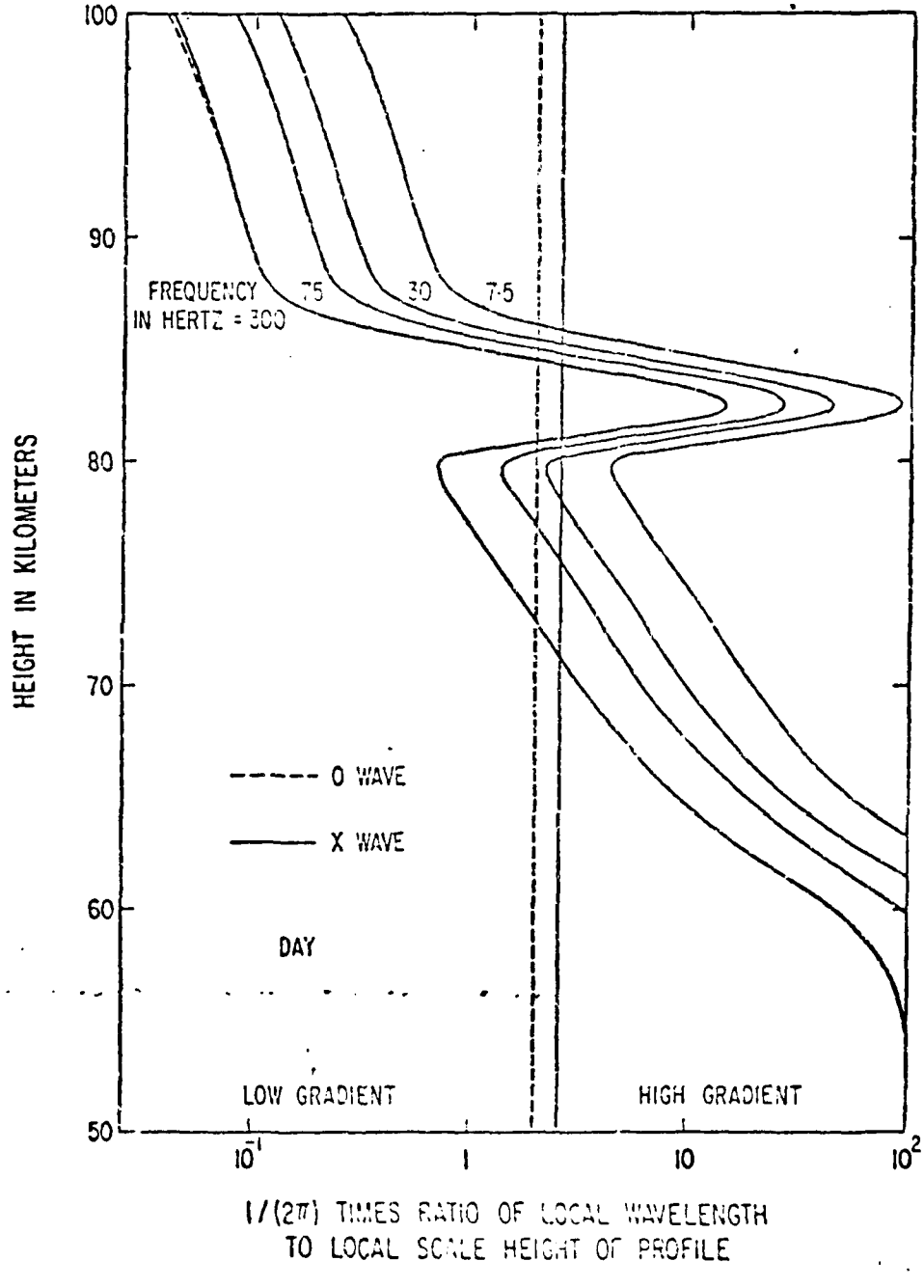

Chapter 3

Figure 2. Illustrating the determination of the day-time heights of reflection at four frequencies.

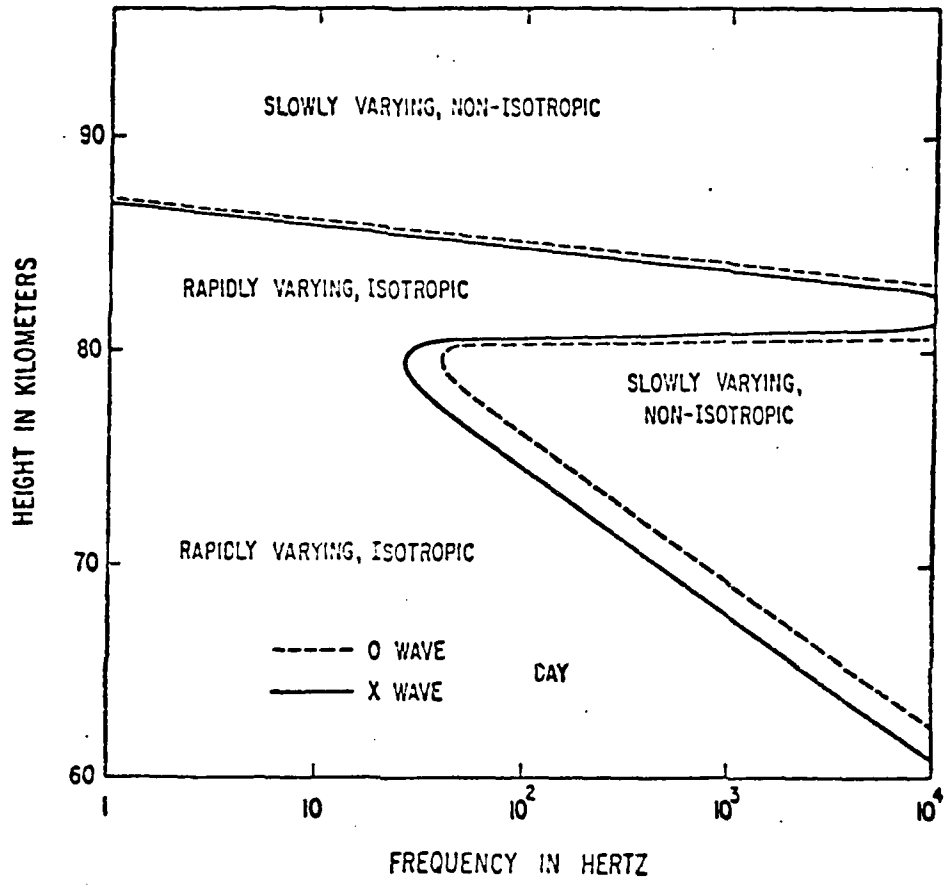

Chapter 3

Figure 3. Illustrating multiple solutions of Equations (2) under day-time conditions.

curves with the ordinates at 2.00 (O wave) and 2.57 (X wave). After correction by successive approximation as described in Section 2, the values of z_0 and z_X behave as shown in Figure 3.

For each wave, there is only a single solution of Equations (2) when the frequency is sufficiently low or sufficiently high. But there is an intermediate band of frequencies where three solutions exist. In this intermediate band the ionosphere is rendered isotropic both by the high gradient on the under side of the D region and by the high gradient on the underside of the E region. But the ionosphere functions as a slowly varying non-isotropic medium near the maximum of ionization density in the D region and also near the maximum of ionization density in the E region. We shall idealize this situation by applying the phase-integral treatment in the region of Figure 3 marked as slowly varying and non-isotropic, and a GG type solution in the region marked as rapidly varying and isotropic; the latter becomes the solution appropriate to a homogeneous isotropic medium below the refracting stratum at the bottom of the ionosphere.

6. Theory for three reflection heights

Consider a situation in which, for a particular magneto-ionic component (O wave or X wave), there are three heights of reflection z_1, z_2 and z_3 ($z_1 \leq z_2 \leq z_3$) as illustrated in Figure 3. Let n_1, n_2 and n_3 be the complex refractive indices for this wave at these heights. Let Q_1, Q_2 and Q_3 be the corresponding complex elliptical polarizations. While n_1, n_2 and n_3 are always markedly different, we have found in our calculations that the elliptical polarizations at the three levels are nearly always closely the same. We shall therefore assume that

$$Q_1 = Q_2 = Q_3 = Q \tag{32}$$

but that

$$n_1 \neq n_2 \neq n_3 \tag{33}$$

We use the axes of coordinates (x, y, z) shown in Figure 3 of Chapter 2, taking the positive y axis to be the horizontal direction of transmission in the Earth-ionosphere transmission line and the positive z axis to be vertically upwards. For a vertically propagating magnetic-ionic component, the complex phase-change between height z_1 and height z_2 is, according to the phase-integral theory,

$$\Phi_{12} = (2\pi/\lambda_o)\int_{z_1}^{z_2} n\, dz \tag{34}$$

and that between height z_2 and height z_3 is, according to the GG theory,

$$\Phi_{23} = (2\pi/\lambda_o)(z_3 - z_2) \tag{35}$$

For the horizontal components E_x and H_y of the complex electromagnetic fields, the matrix relating the values at height z_1 to those at height z_2 is

$$\begin{pmatrix} (n_1/n_2)^{-\frac{1}{2}} \cos\Phi_{12} & j\zeta_o (n_1 n_2)^{-\frac{1}{2}} \sin\Phi_{12} \\ j\zeta_o^{-1} (n_1 n_2)^{\frac{1}{2}} \sin\Phi_{12} & (n_1/n_2)^{\frac{1}{2}} \cos\Phi_{12} \end{pmatrix} \tag{36}$$

while that relating the values at height z_2 to those at height z_3 is

$$\begin{pmatrix} \cos\Phi_{23} & j\zeta_o \sin\Phi_{23} \\ j\zeta_o^{-1} \sin\Phi_{23} & \cos\Phi_{23} \end{pmatrix} \tag{37}$$

Multiplying the two matrices together we see that the matrix relating the values of E_x and H_y at height z_1 to those at height z_3 is

$$\begin{pmatrix} a & j\zeta_o b \\ j\zeta_o^{-1} c & d \end{pmatrix} \tag{38}$$

where

$$\left.\begin{aligned} a &= (n_1/n_2)^{-\frac{1}{2}} \cos\Phi_{12} \cos\Phi_{23} - (n_1 n_2)^{-\frac{1}{2}} \sin\Phi_{12} \sin\Phi_{23} \\ b &= (n_1/n_2)^{-\frac{1}{2}} \cos\Phi_{12} \sin\Phi_{23} + (n_1 n_2)^{-\frac{1}{2}} \sin\Phi_{12} \cos\Phi_{23} \\ c &= (n_1 n_2)^{\frac{1}{2}} \sin\Phi_{12} \cos\Phi_{23} + (n_1/n_2)^{\frac{1}{2}} \cos\Phi_{12} \sin\Phi_{23} \\ d &= -(n_1 n_2)^{\frac{1}{2}} \sin\Phi_{12} \sin\Phi_{23} + (n_1/n_2)^{\frac{1}{2}} \cos\Phi_{12} \cos\Phi_{23} \end{aligned}\right\} \tag{39}$$

Using a GG type theory between the Earth's surface and the height z_1, the matrix relating the values of E_x and H_y at the surface

to those at height z_1 is (cf Equation 9)

$$\begin{pmatrix} 1 & j\zeta_o(2\pi/\lambda_o)z_1 \\ j\zeta_o(2\pi/\lambda_o)(z_1 - S^2\tilde{z}_B) & 1 \end{pmatrix} \tag{40}$$

where

$$\tilde{z}_B = \int_0^{z_1} \frac{dz}{n^2(z)} \tag{41}$$

By multiplying the matrix (38) by the matrix (40) we see that the matrix relating the values of E_x and H_y at the Earth's surface to those at height z_3 is

$$\begin{pmatrix} a - c(2\pi/\lambda_o)z_1 & j\zeta_o\{b + d(2\pi/\lambda_o)z_1\} \\ j\zeta_o^{-1}\{a(2\pi/\lambda_o)(z_1 - S^2\tilde{z}_B) + c\} & d - b(2\pi/\lambda_o)(z_1 - S^2\tilde{z}_B) \end{pmatrix} \tag{42}$$

We also require corresponding matrices for E_y and H_x. If these are written as matrices for E_y and $-H_x$, the matrix (38) is unchanged and the matrix (40) is reflected in the leading diagonal. It follows that the matrix relating the values of E_y and H_x at the Earth's surface to those at height z_3 is

$$\begin{pmatrix} a - c(2\pi/\lambda_o)(z_1 - S^2\tilde{z}_B) & -j\zeta_o\{b + d(2\pi/\lambda_o)(z_1 - S^2\tilde{z}_B) \\ -j\zeta_o^{-1}\{a(2\pi/\lambda_o)z_1 + c\} & d - b(2\pi/\lambda_o)z_1 \end{pmatrix} \tag{43}$$

With the aid of the matrices (42) and (43), we are in a position to express the horizontal components E_x, H_y, E_y, H_x of the

complex electromagnetic field at the Earth's surface in terms of the horizontal components E_{x3}, H_{y3}, E_{y3}, H_{x3} at the height z_3. Moreover, at the height z_3, we have (cf Equations 26-29 of Chapter 2)

$$-\frac{E_{y3}}{H_{x3}} = \frac{E_{x3}}{H_{y3}} = \frac{1}{n_3}\,\zeta_o \tag{44}$$

and

$$-\frac{E_{x3}}{E_{y3}} = \frac{H_{y3}}{H_{x3}} = Q \tag{45}$$

These equations permit us to express E_{x3}, H_{y3} and E_{y3} in terms of H_{x3}. If we write

$$f = (a/n_3) + j\,b, \qquad g = d + j(c/n_3) \tag{46}$$

we obtain

$$\left.\begin{aligned} \zeta_o^{-1} E_x &= \{f + j\,g(2\pi/\lambda_o)z_1\}\,Q\,H_{x3} \\ H_y &= \{j\,f(2\pi/\lambda_o)(z_1 - S^2\tilde{z}_B) + g\}Q\,H_{x3} \\ \zeta_o^{-1} E_y &= -\{f + j\,g(2\pi/\lambda_o)(z_1 - S^2\tilde{z}_B)\}\,H_{x3} \\ H_x &= \{j\,f(2\pi/\lambda_o)z_1 + g\}H_{x3} \end{aligned}\right\} \tag{47}$$

In the second and fourth of Equations (47) the g terms dominate, and these equations may be simplified to

$$\left.\begin{aligned} H_x &= g\,H_{x3} \\ H_y &= g\,Q\,H_{x3} \end{aligned}\right\} \tag{48}$$

But in the first and third of Equations (47) it is necessary to avoid approximations. However, an equivalent complex height of reflection $\tilde{z}_R$ may be introduced such that

$$f + j\, g(2\pi/\lambda_o) z_1 = j\, g(2\pi/\lambda_o)\tilde{z}_R \tag{49}$$

The first and third of Equations (47) then become

$$\left.\begin{aligned} \zeta_o^{-1} E_x &= j\, g(2\pi/\lambda_o)\tilde{z}_R\, Q\, H_{x3} \\ \zeta_o^{-1} E_y &= -j\, g(2\pi/\lambda_o)(\tilde{z}_R - S^2\tilde{z}_B) H_{x3} \end{aligned}\right\} \tag{50}$$

With appropriate affixes 0 and X, Equations (48) and (50) apply to both the 0 wave and the X wave. Taking both waves into account, the complete expressions for the horizontal components (H_x, H_y, E_x, E_y) of the complex electromagnetic field at the Earth's surface are given by

$$\left.\begin{aligned} H_x &= g_0\, H^0_{x3} + g_X\, H^X_{x3} \\ H_y &= g_0\, Q_0\, H^X_{x3} + g_X Q_X H^X_{x3} \end{aligned}\right\} \tag{51}$$

and

$$\left.\begin{aligned} -j\,\frac{\lambda_o}{2\pi}\frac{1}{\zeta_o} E_x &= g_0 \tilde{z}_{R0}\, Q_0\, H^0_{x3} + g_X \tilde{z}_{RX}\, Q_X\, H^X_{x3} \\ j\,\frac{\lambda_o}{2\pi}\frac{1}{\zeta_o} E_y &= g_0(\tilde{z}_{R0} - S^2\tilde{z}_{B0}) H^0_{x3} + g_X(\tilde{z}_{RX} - S^2\tilde{z}_{BX}) H^X_{x3} \end{aligned}\right\} \tag{52}$$

We are now in a position to satisfy the boundary conditions at the surface of the Earth. Leakage of energy into the Earth is easily allowed for separately so that, in studying the effect of the ionosphere, we may take the boundary conditions at the surface of the Earth to be

$$E_x = E_y = 0 \tag{53}$$

Substitution from Equations (53) into Equations (52) gives

$$\left.\begin{aligned} Q_0 \tilde{z}_{R0} g_0 H_{x3}^0 + Q_X \tilde{z}_{RX} g_X H_{x3}^X &= 0 \\ (\tilde{z}_{R0} - s^2 \tilde{z}_{B0}) g_0 H_{x3}^X + (\tilde{z}_{RX} - s^2 \tilde{z}_{BX}) g_X H_{x3}^X &= 0 \end{aligned}\right\} \tag{54}$$

and elimination of $g_0 H_{x3}^0$ and $g_X H_{x3}^X$ then recovers Equation (16). The relative degree of excitation of the O and X waves above the height z_3 is given by the first of Equations (54) while the horizontal magnetic field at the Earth's surface is given by Equations (51).

We see that, when Equations (2) for the heights of reflection of the O and X waves each have a triplet of solutions instead of a single solution, the procedure for calculating the phase velocity and rate of attenuation in the Earth-ionsosphere transmission line is affected in only one respect. The equivalent complex heights of reflection for the O and X waves must be calculated, not from Equations (4), but from Equation (49). This equation gives

$$\tilde{z}_R = z_1 - j \frac{\lambda_o}{2\pi} \frac{f}{g} \tag{55}$$

or, using Equations (46) and (39),

$$\tilde{z}_R = z_1 + \frac{\lambda_o}{2\pi} \frac{n_2}{n_1 n_3} \frac{B - jA}{D + jC} \tag{56}$$

where

$$\left.\begin{aligned} A &= \cos\Phi_{12}\cos\Phi_{23} - (1/n_2)\sin\Phi_{12}\sin\Phi_{23} \\ B &= n_3\cos\Phi_{12}\sin\Phi_{23} + (n_3/n_2)\sin\Phi_{12}\cos\Phi_{23} \\ C &= (n_2/n_3)\sin\Phi_{12}\cos\Phi_{23} + (1/n_3)\cos\Phi_{12}\sin\Phi_{23} \\ D &= -n_2\sin\Phi_{12}\sin\Phi_{23} + \cos\Phi_{12}\cos\Phi_{23} \end{aligned}\right\} \tag{57}$$

The complex phase-change Φ_{23} in these equations is always small, and so are the terms involving $1/n_2$ and $1/n_3$. Hence Equations (57) may usually be simplified, if desired, to

$$\left.\begin{aligned} A &= \cos\Phi_{12} \\ B &= n_3\Phi_{23}\cos\Phi_{12} + (n_3/n_2)\sin\Phi_{12} \\ C &= (n_2/n_3)\sin\Phi_{12} \\ D &= -n_2\Phi_{23}\sin\Phi_{12} + \cos\Phi_{12} \end{aligned}\right\} \tag{58}$$

At the low-frequency end of the ELF band where reflection from the D region is comparatively unimportant, the complex phase-change Φ_{12} is also small and Equations (58) become approximately

$$\left.\begin{aligned} A &= 1 \\ B &= n_3\Phi_{23} + (n_3/n_2)\Phi_{12} \\ C &= (n_2/n_3)\Phi_{12} \\ D &= 1 \end{aligned}\right\} \tag{59}$$

Substitution from Equations (59) into Equation (56) then gives

$$\tilde{z}_R = z_1 - j\,\frac{\lambda_o}{2\pi}\,\frac{n_2}{n_1 n_3}\left\{1 + j\left(\frac{n_3}{n_2} - \frac{n_2}{n_3}\right)\phi_{12} + j\,n_3\,\phi_{23}\right\} \tag{60}$$

or, using Equations (34) and (35),

$$\tilde{z}_R = z_1 + \left(1 - \frac{n_2^2}{n_3^2}\right)\frac{1}{n_1}\int_{z_1}^{z_2} n\,dz + \frac{n_2}{n_1}(z_3 - z_2) - j\,\frac{\lambda_o}{2\pi}\,\frac{n_2}{n_1 n_3} \tag{61}$$

However, for numerical calculations it is usually better to use the unapproximated version in Equation (56).

To obtain $\tilde{z}_{RO}$ and $\tilde{z}_{XO}$ we use respectively the expressions for the O and X waves in Equations (57) to obtain A_O, B_O, C_O, D_O; A_X, B_X, C_X, D_X. We then have, in accordance with Equation (56),

$$\left.\begin{aligned}\tilde{z}_{RO} &= z_{1O} + \frac{\lambda_o}{2\pi}\,\frac{n_{2O}}{n_{1O} n_{3O}}\,\frac{B_O - jA_O}{D_O + jC_O}\\ \tilde{z}_{RX} &= z_{1X} + \frac{\lambda_o}{2\pi}\,\frac{n_{2X}}{n_{1X} n_{3X}}\,\frac{B_X - jA_X}{D_X + jC_X}\end{aligned}\right\} \tag{62}$$

Likewise, using Equation (41), we have

$$\tilde{z}_{BO} = \int_0^{z_{1O}} \frac{dz}{n_O^2(z)}, \qquad \tilde{z}_{BX} = \int_0^{z_{1X}} \frac{dz}{n_X^2(z)} \tag{63}$$

If these expressions for the equivalent complex heights of reflection and the equivalent complex heights of the bottom of the ionosphere are substituted into Equation (16), we can then obtain the phase velocity and the rate of attenuation in the Earth-ionosphere transmission line

from Equations (17) and (18).

There is little phase-change associated with intervals of height where the gradient of ionization density is high, so that the phase-change Φ_{23} in Equations (39) is always numerically small. If it is taken to be zero, a simple physical interpretation may be given for the calculations performed in this section. Figure 4 illustrates this interpretation for an individual magneto-ionic component (O wave or X wave) under day-time conditions. The smallest solution of the relevant Equation (2) is $z = z_1$, and this occurs in the high gradient on the under side of the D region. Calculation of reflection from this gradient is as though from a discontinuity of refractive index n_1-1, where n_1 is the complex refractive index at $z = z_1$. Calculation of reflection from the high gradient on the under side of the E region is as though from a discontinuity of refractive index n_3-n_2, where n_2 and n_3 are the complex refractive indices at heights z_2 and z_3, the second and third solutions of the relevant Equation (2). The complex phase-change between these two discontinuity levels is Φ_{12}, calculated in accordance with Equation (34). The process of combining the reflections from both discontinuity levels is then a standard calculation in optics or in transmission-line theory. However, it is necessary to switch from nearly vertical transmission to nearly horizontal transmission at the bottom of the ionosphere; this occurs in the refracting stratum in accordance with the theory of GG. It is also necessary to combine the calculations using the O and X waves before the boundary conditions at the surface of the Earth are satisfied.

AD-A083 097 CALIFORNIA UNIV SAN DEIGO LA JOLLA DEPT OF ELECTRICA--ETC F/G 20/14
A SIMPLIFIED THEORY OF ELF PROPAGATION IN THE EARTH-IONOSPHERE --ETC(U)
MAR 80 H G BOOKER N00014-78-C-0682
UNCLASSIFIED NL

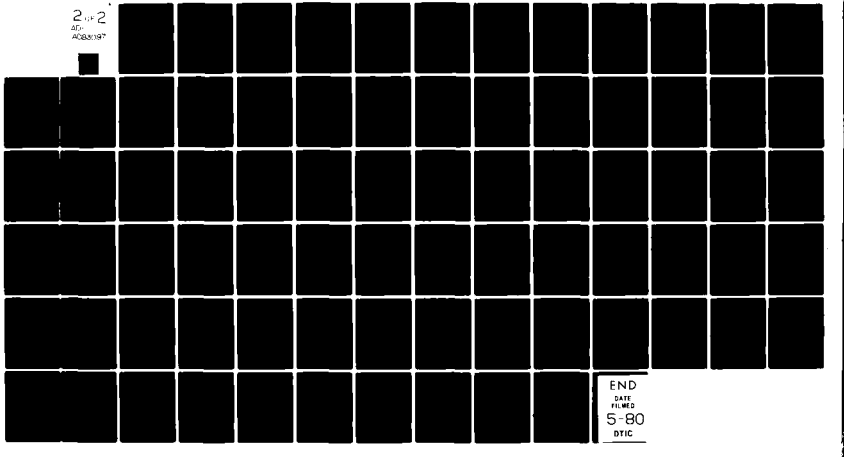

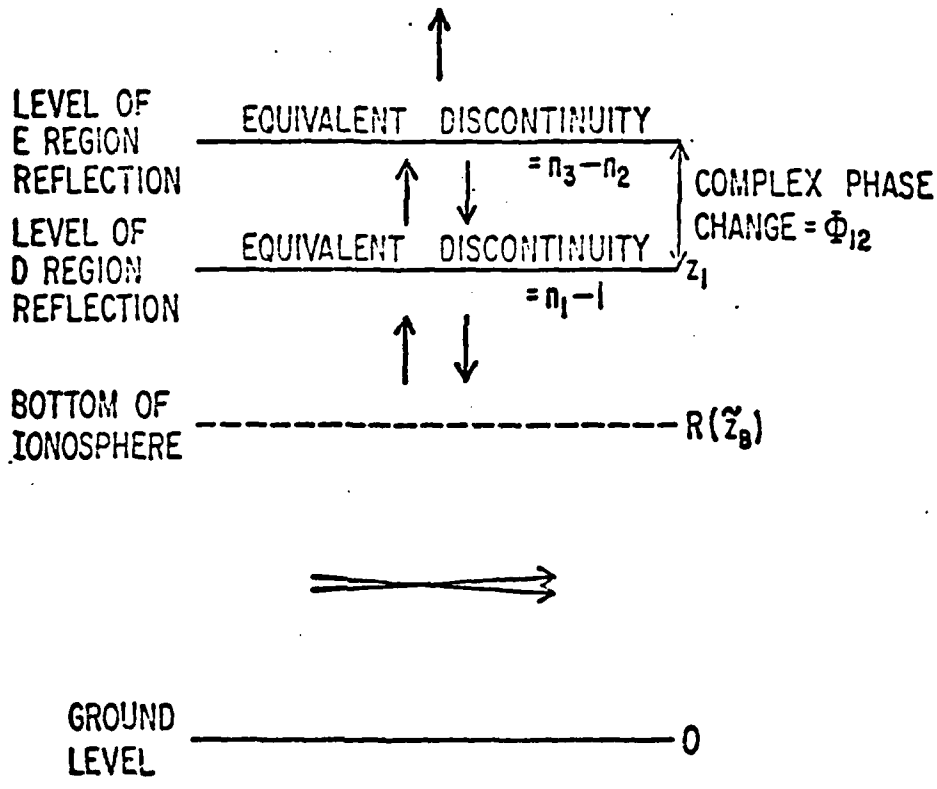

Figure 4. Illustrating simultaneous reflection of the O or X wave from the D and E regions at ELF when the relevant Equation (2) has a triplet of solutions z_1, z_2, z_3 $(z_1 < z_2 < z_3)$ at which the refractive indices are n_1, n_2, n_3 respectively.

7. Theory for five reflection heights

Under day-time conditions the theory presented in the previous section is required whenever there is significant reflection both from the high gradient on the under side of the D region and from the high gradient on the under side of the E region. However, the theory of the previous section is also required under night-time conditions unless the gradient on the top side of the E region is sufficiently low.

At night, reflection can occur both from the gradient on the under side of the E region and from the gradient on the top side of the E region. Moreover, on the under side of the E region there is sometimes a ledge of ionization, somewhat like a D region but at a greater height. Reflection can then occur from the gradient on the under side of the ledge, from the gradient on the under side of the E region, and from the gradient on the top side of the E region.

This behavior manifests itself by the occurrence of five solutions to one or both of Equations (2). Such a situation is illustrated in Figure 5, which is drawn for night-time conditions in a middle lattitude using a model of the ionosphere of the type employed in the next chapter. It is clear that we need to be able to deal with five reflection heights.

With five reflection heights z_1, z_2, z_3, z_4 and z_5 ($z_1 < z_2 < z_3 < z_4 < z_5$), we employ the following complex phase-changes (cf Equations 34 and 35):

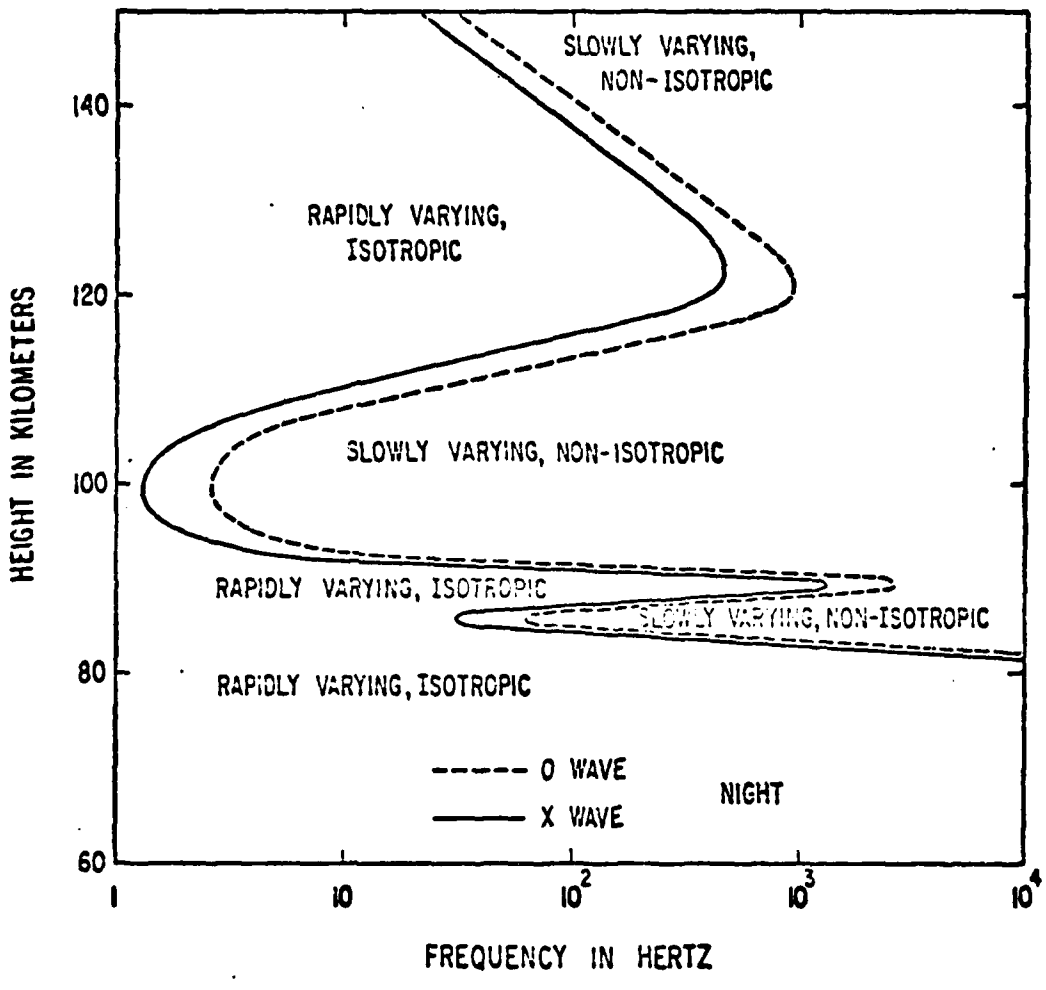

Chapter 3

Figure 5. Illustrating multiple solutions of Equations (2) under night-time conditions.

$$\left.\begin{aligned} \phi_{12} &= (2\pi/\lambda_o)\int_{z_1}^{z_2} n\,dz, \qquad & \phi_{34} &= (2\pi/\lambda_o)\int_{z_3}^{z_4} n\,dz \\ \phi_{23} &= (2\pi/\lambda_o)(z_3 - z_2) & \phi_{45} &= (2\pi/\lambda_o)(z_5 - z_4) \end{aligned}\right\} \tag{64}$$

The matrix (38) not only relates the values of E_x and H_y at height z_1 to those at height z_3, but also those at height z_3 to those at height z_5 if subscripts 1, 2 and 3 in Equations (39) are replaced by subscripts 3, 4 and 5. Moreover, if the two resulting matrices are multiplied together, we have the matrix that relates the values of E_x and H_y at the height z_1 to those at the height z_5. Performance of this multiplication is straightforward but lengthy. The product has the form of the matrix (38) but with more complicated expressions for a, b, c and d involving all the phase-changes appearing in Equations (64).

The rest of the calculation in the previous section subsequent to Equations (39) is, however, unchanged up to Equation (56), which becomes

$$\tilde{z}_R = z_1 + \frac{\lambda_o}{2\pi}\,\frac{n_2 n_4}{n_1 n_3 n_5}\,\frac{B - jA}{D + jC} \tag{65}$$

where A, B, C and D now have the values given in the Appendix to this chapter. If these expressions are evaluated for the O and X waves so as to obtain A_0, B_0, C_0, D_0 and A_x, B_x, C_x, D_x, then the equivalent complex heights of reflection for the O and X waves are

$$\left.\begin{aligned} \tilde{z}_{RO} &= z_{1O} + \frac{\lambda_o}{2\pi} \frac{n_{2O}n_{4O}}{n_{1O}n_{3O}n_{5O}} \frac{B_O - jA_O}{D_X + jC_X} \\ \tilde{z}_{RX} &= z_{1X} + \frac{\lambda_o}{2\pi} \frac{n_{2X}n_{4X}}{n_{1X}n_{3X}n_{5X}} \frac{B_X - jA_X}{D_X + jC_X} \end{aligned}\right\} \qquad (66)$$

We calculate $\tilde{z}_{RO}$ and $\tilde{z}_{RX}$ from these equations, $\tilde{z}_{BO}$ and $\tilde{z}_{BX}$ from Equations (63), the eigenvalue S from Equation (16), the phase velocity in the Earth-ionosphere transmission line from Equation (17), and the rate of attenuation from Equation (18).

The phase-changes Φ_{23} and Φ_{45} associated with the intervals of height where the gradient of ionization density is high are always numerically small. If they are taken to be zero, then the theory in this section reduces to one involving discontinuities of complex refractive index at three levels. The values of the discontinuities are $n_1 - 1$, $n_3 - n_2$ and $n_5 - n_4$. The height of the first discontinuity is z_1. The complex phase-change between the first discontinuity and the second is Φ_{12}. The complex phase-change between the second discontinuity and the third is Φ_{34}. The effect of reflection from all three discontinuities is calculated as in optics or in transmission-line theory.

For numerical work, however, there is no need to take Φ_{23} and Φ_{45} as zero. Moreover, it is convenient always to program for five solutions of each of Equations (2). If, for one or both of the magneto-ionic components, there are only three solutions z_1, z_2 and z_3, then we put z_4 and z_5 in the program equal to z_3. If there is only one solution z_R, then we put all five heights in the program equal to z_R.

8. Conclusion

It is concluded that a reasonable simplified procedure for evaluating the effect of the ionosphere on propagation in the Earth-ionosphere transmission line in the ELF band is as follows:

(i) Evaluate the heights of reflection for the O and X waves from Equations (2).

(ii) At these heights evaluate the complex refractive indices n_O and n_X for vertical propagation of the O and X waves.

(iii) At the same heights evaluate also the complex elliptical polarizations Q_O and Q_X as defined in Equation (72) of Chapter 2. Verify that Q_O and Q_X are approximately the same at all heights of reflection.

(iv) Calculate the equivalent complex heights of reflection $\tilde{z}_{RO}$ and $\tilde{z}_{RX}$ from Equations (66) using the expressions for A, B, C and D given in the Appendix to this chapter.

(v) Calculate the equivalent complex heights $\tilde{z}_{BO}$ and $\tilde{z}_{BX}$ of the bottom of the ionosphere from Equations (63).

(vi) Substitute into Equation (16), and deduce the phase velocity and the attenuation rate from Equations (17) and (18).

In the next chapter this method is applied to a simplified worldwide model of the ionosphere to estimate ELF propagation in the Earth-ionosphere transmission line for a range of frequencies and a range of ionospheric conditions.

Appendix to Chapter 3

When one of Equations (2) yields five heights of reflection z_1, z_2, z_3, z_4 and z_5 ($z_1 < z_2 < z_3 < z_4 < z_5$), let n_1, n_2, n_3, n_4 and n_5 be the complex refractive indices at these heights for vertical propagation of phase for the wave concerned. For this wave, let complex phase-changes Φ_{12}, Φ_{23}, Φ_{34} and Φ_{45} be defined by Equations (64).

The matrix (38) relates the values of E_x and H_y' at height z_1 to those at height z_3, where a, b, c and d are given by Equations (39). The same matrix relates the values of E_x and H_y at height z_3 to those at height z_5 if subscripts 1, 2 and 3 in Equations (39) are replaced by subscripts 3, 4 and 5. The two resulting matrices must be multiplied together.

If this is done, the values of A, B, C and D in Equation (65) evaluate to:

$$
\begin{aligned}
A = {} & \cos\Phi_{12}\cos\Phi_{23}\cos\Phi_{34}\cos\Phi_{45} \\
& - \frac{1}{n_4}\cos\Phi_{12}\cos\Phi_{23}\sin\Phi_{34}\sin\Phi_{45} \\
& - \frac{1}{n_2}\sin\Phi_{12}\sin\Phi_{23}\cos\Phi_{34}\cos\Phi_{45} \\
& + \frac{1}{n_2 n_4}\sin\Phi_{12}\sin\Phi_{23}\sin\Phi_{34}\sin\Phi_{45} \\
& - n_3\cos\Phi_{12}\sin\Phi_{23}\sin\Phi_{34}\cos\Phi_{45} \\
& - \frac{n_3}{n_4}\cos\Phi_{12}\sin\Phi_{23}\cos\Phi_{34}\sin\Phi_{45} \\
& - \frac{n_3}{n_2}\sin\Phi_{12}\cos\Phi_{23}\sin\Phi_{34}\cos\Phi_{45} \\
& - \frac{n_3}{n_2 n_4}\sin\Phi_{12}\cos\Phi_{23}\cos\Phi_{34}\sin\Phi_{45} \qquad (67)
\end{aligned}
$$

$$
\begin{aligned}
B = {} & n_5 \cos\Phi_{12} \cos\Phi_{23} \cos\Phi_{34} \sin\Phi_{45} \\
& + \frac{n_5}{n_4} \cos\Phi_{12} \cos\Phi_{23} \sin\Phi_{34} \cos\Phi_{45} \\
& - \frac{n_5}{n_2} \sin\Phi_{12} \sin\Phi_{23} \cos\Phi_{34} \sin\Phi_{45} \\
& - \frac{n_5}{n_2 n_4} \sin\Phi_{12} \sin\Phi_{23} \sin\Phi_{34} \cos\Phi_{45} \\
& - n_3 n_5 \cos\Phi_{12} \sin\Phi_{23} \sin\Phi_{34} \sin\Phi_{45} \\
& + \frac{n_3 n_5}{n_4} \cos\Phi_{12} \sin\Phi_{23} \cos\Phi_{34} \cos\Phi_{45} \\
& - \frac{n_3 n_5}{n_2} \sin\Phi_{12} \cos\Phi_{23} \sin\Phi_{34} \sin\Phi_{45} \\
& + \frac{n_3 n_5}{n_2 n_4} \sin\Phi_{12} \cos\Phi_{23} \cos\Phi_{34} \cos\Phi_{45}
\end{aligned} \tag{68}
$$

$$
\begin{aligned}
C = {} & \frac{n_2 n_4}{n_3 n_5} \sin\Phi_{12} \cos\Phi_{23} \cos\Phi_{34} \cos\Phi_{45} \\
& - \frac{n_2}{n_3 n_5} \sin\Phi_{12} \cos\Phi_{23} \sin\Phi_{34} \sin\Phi_{45} \\
& + \frac{n_4}{n_3 n_5} \cos\Phi_{12} \sin\Phi_{23} \cos\Phi_{34} \cos\Phi_{45} \\
& - \frac{1}{n_3 n_5} \cos\Phi_{12} \sin\Phi_{23} \sin\Phi_{34} \sin\Phi_{45} \\
& - \frac{n_2 n_5}{n_5} \sin\Phi_{12} \sin\Phi_{23} \sin\Phi_{34} \cos\Phi_{45}
\end{aligned}
$$

$$- \frac{n_2}{n_5} \sin\Phi_{12} \sin\Phi_{23} \cos\Phi_{34} \sin\Phi_{45}$$

$$+ \frac{n_4}{n_5} \cos\Phi_{12} \cos\Phi_{23} \sin\Phi_{34} \cos\Phi_{45}$$

$$+ \frac{1}{n_5} \cos\Phi_{12} \cos\Phi_{23} \cos\Phi_{34} \sin\Phi_{45} \qquad (69)$$

$$D = - \frac{n_2 n_4}{n_3} \sin\Phi_{12} \cos\Phi_{23} \cos\Phi_{34} \sin\Phi_{45}$$

$$- \frac{n_2}{n_3} \sin\Phi_{12} \cos\Phi_{23} \sin\Phi_{34} \cos\Phi_{45}$$

$$- \frac{n_4}{n_3} \cos\Phi_{12} \sin\Phi_{23} \cos\Phi_{34} \sin\Phi_{45}$$

$$- \frac{1}{n_3} \cos\Phi_{12} \sin\Phi_{23} \sin\Phi_{34} \cos\Phi_{45}$$

$$+ n_2 n_4 \sin\Phi_{12} \sin\Phi_{23} \sin\Phi_{34} \sin\Phi_{45}$$

$$- n_2 \sin\Phi_{12} \sin\Phi_{23} \cos\Phi_{34} \cos\Phi_{45}$$

$$- n_4 \cos\Phi_{12} \cos\Phi_{23} \sin\Phi_{34} \sin\Phi_{45}$$

$$+ \cos\Phi_{12} \cos\Phi_{23} \cos\Phi_{34} \cos\Phi_{45} \qquad (70)$$

If these expressions are evaluated for the 0 and X waves respectively so as to obtain A_0, B_0, C_0, D_0 and A_X, B_X, C_X, D_X, then the equivalent complex heights of reflection for the 0 and X waves are given by Equations (66).

If in Equations (67) - (70) we put $z_4 = z_5$, they reduce to Equations (57). If in Equations (67) - (70) we put $z_1 = z_2 = z_3 = z_4 = z_5 = z_R$, then Equations (66) reduce to Equations (4).

Bibliography

Booker, H. G. 1936 Oblique propagation of electromagnetic waves in a slowly-varying non-isotropic medium, Proc. Roy. Soc. A155, 235-257.

Booker, H.G. and Lefeuvre, F. 1977 The relation between ionospheric profiles and ELF propagation in the Earth-ionosphere transmission line, J. Atmos. Terr. Phys. 39, 1277-1299.

Budden, K. G. 1952 The theory of the limiting polarization of radio waves reflected from the ionosphere, Proc. Roy. Soc. A215, 215-233.

Budden, K. G. 1961a Radio waves in the ionosphere, Cambridge University Press, Cambridge.

Budden, K. G. 1961b The wave-guide mode theory of wave propagation, Logos Press, London.

Galejs, J. 1972 Terrestrial propagation of long electromagnetic waves, Pergamon Press.

Greifinger, C. and Greifinger, P. 1978 Approximate method for determining ELF eigenvalues in the earth-ionosphere waveguide, Radio Science 13, 831-837.

Greifinger, C. and Greifinger, P. 1979 On the ionospheric parameters which govern high latitude ELF propagation in the earth-ionosphere waveguide, Radio Science 14, 889-895.

Hayes, M.G.W. 1971 Theory of the limiting polarization of radio waves emerging obliquely from the ionosphere, Proc. Roy. Soc. A324, 369-390.

Wait, J. R. 1962 Electromagnetic waves in stratified media, Macmillan, New York.

Wait, J. R. 1974 Special issue on extremely low frequency (ELF) communications, IEEE Trans. Commun. 22, 353-587.

Chapter 4. Calculations of ELF Propagation in Earth-ionosphere Transmission Line

1. Introduction

In Chapter 3 a simplified theory was derived for evaluating the effect of the ionosphere on ELF propagation in the Earth-ionosphere transmission line. It is the objective of this chapter to apply the theory to a simplified worldwide model of the ionosphere.

In the theory, phase (and group) propagation below the bottom of the ionosphere is practically horizontal, and phase propagation above the bottom of the ionosphere (but not, in general, group propagation) is practically vertical. A precise definition of the bottom of the ionosphere has been given by Greifinger and Greifinger (1978, 1979). It is a complex height, the positive imaginary part of which is a measure of the absorption experienced in the lowest layer of the ionosphere. An indispensable feature of the theory presented in Chapter 3 is the use, in a high gradient of refractive index, of a solution of the equations of propagation of the type developed by Greifinger and Greifinger (1978, 1979). Use is also made in Chapter 3 of equivalent complex heights of reflection for the O and X waves. These are based on the ELF reflection theory of Booker and Lefeuvre (1977) described in Chapter 2.

The basic procedure is to compare the local vertical gradient of refractive index with the local wavelength, thereby classifying altitude into intervals where the gradient is high and ones where it is low. Where the gradient is low, the phase-integral treatment is adequate. An interval where the gradient is high may, to a first

approximation, be replaced by a discontinuity. The amount of the discontinuity is the difference between the refractive indices at the top and bottom of the interval of high gradient, judged in relation to local wavelength. It is then a matter of combining reflections from the several discontinuities. This requires calculation of the complex phase-changes between the discontinuities, that is, in the intervals of height where the phase-integral treatment is satisfactory.

An improvement on the discontinuity theory is obtained by making allowance for the small change of phase that occurs in an interval of high gradient. This may be done using the type of treatment developed by Greifinger and Greifinger (1977, 1979). If this improvement is incorporated, calculations are made as follows:

(i) Evaluate the heights of reflection z_0 and z_X for the 0 and X waves in accordance with Equations (2) of Chapter 3. These are algebraic relations that will be referred to as the reflection equations.

(ii) At these heights, evaluate the complex refractive indices n_0 and n_X for the 0 and X waves for vertical propagation of phase in the ionosphere in the presence of the Earth's magnetic field.

(iii) At the same heights, evaluate also the complex elliptical polarizations Q_0 and Q_X for the 0 and X waves. Verify that Q_0 and Q_X are approximately the same at all heights of reflection.

(iv) Evaluate the equivalent complex heights of reflection $\tilde{z}_{R0}$ and $\tilde{z}_{RX}$ for the 0 and X waves as described in Chapter 3.

(v) Evaluate the equivalent complex heights $\tilde{z}_{B0}$ and $\tilde{z}_{BX}$ of the bottom of the ionosphere using the method of Greifinger and

Greifinger (1978, 1979); see Equations (63) of Chapter 3.

(vi) Calculate the eigenvalue S (the sine of the complex angle of incidence upon the ionosphere) from the formula (Equation 16 of Chapter 3)

$$S = \left[\frac{Q_O^{-1} - Q_X^{-1}}{Q_O^{-1}(\tilde{z}_{BO}/\tilde{z}_{RO}) - Q_X^{-1}(\tilde{z}_{BX}/\tilde{z}_{RX})} \right]^{\frac{1}{2}} \tag{1}$$

(vii) Deduce the ratio of the velocity c of light in free space to the phase velocity v in the Earth-ionosphere transmission line from the formula (Equation 17 of Chapter 3)

$$c/v = R(S) \tag{2}$$

and the rate of attenuation in nepers per unit distance from the formula (Equation 18 of Chapter 3)

$$\alpha = -(2\pi/\lambda_o) I(S) \tag{3}$$

where λ_o is the wavelength in free space, and where R and I denote real and imaginary parts.

For the day-time ionosphere, the method of calculation takes into account reflection from the gradient on the under side of the D region and reflection from the gradient on the under side of the E region. The method would also take into account reflection from a gradient on the top side of the E region, but no significant such gradient exists in the ionospheric model used in this chapter for the day-time ionosphere.

For the night-time ionosphere, the method of calculation takes into account reflection from the gradient on the under side of the E

region and reflection from the gradient on the top side of the E region. However, the model of the night-time ionosphere used in this chapter incorporates a ledge of ionization below the E region, somewhat like a D region but at a greater height. Reflection can then be important from the gradient on the under side of the ledge as well as from those on the under side and the top side of the E region. All three sources of reflection are taken into account in this chapter.

However, it will transpire that, at the low-frequency end of the ELF band, a considerable amount of energy is transmitted through the E region at night and, in the form of both the whistler mode and the Alfvén mode, is reflected from the F region. Reflection of ELF waves from the F region, although important at night at frequencies below the ionic gyrofrequency, is not treated in this chapter.

When reflection from the F region is important, some variation with height in the elliptical polarizations of the O and X waves occurs above 100 km and may be important. However, in all of the circumstances actually treated in this chapter, we have found that the complex elliptical polarizations of the magneto-ionic components are practically independent of height at all relevant heights. Consequently, Equations (32) of Chapter 3 are well satisfied.

For a magneto-ionic component (O wave or X wave), reflecting strata occur where $1/(4\pi)$ times the local wavelength λ is approximately equal to the local scale-height h, defined in terms of the profile of $n^2 - 1$, where n is the ionospheric refractive index for vertical propagation of phase. The theory in Chapter 3 contemplates a situation in which five such levels may exist at the heights z_1, z_2, z_3, z_4 and

z_5 ($z_1 < z_2 < z_3 < z_4 < z_5$). These are the solutions of the reflection equations (Equations 2 of Chapter 3) for the magneto-ionic component concerned. In practice, the level z_1 is in the gradient on the under side of the D region (or, at night, of a ledge below the E region if such a ledge exists). The level z_2 is close to the maximum of ionization density in the D region, and the level z_3 is in the gradient on the under side of the E region. By day, the levels z_4 and z_5 do not exist because of the absence of a substantial gradient on the top side of the E region. By night, however, the levels z_4 and z_5 frequently do exist and occur in the gradient above the level of maximum ionization density in the E region.

Below the level z_1, $\lambda/(4\pi h)$ is mostly large and the field takes the form described by Greifinger and Greifinger (1978, 1979). Between the levels z_1 and z_2, $\lambda/(4\pi h)$ is mostly small and the field conforms reasonably well to the theory for a slowly varying medium. The complex phase-change between these two levels is

$$\Phi_{12} = (2\pi/\lambda_o) \int_{z_1}^{z_2} n \, dz \qquad (4)$$

Between the levels z_2 and z_3, $\lambda/(4\pi h)$ is again large and the field takes the form described by Greifinger and Greifinger, except that only vertical propagation of phase is now involved. Between these two levels there is a phase-change Φ_{23} which is always numerically small. Between the levels z_3 and z_4 we are again back in a slowly varying medium, and the complex phase-change between these levels is

$$\Phi_{34} = (2\pi/\lambda_o) \int_{z_3}^{z_4} n \, dz \qquad (5)$$

Between the levels z_4 and z_5 we return to a rapidly varying medium and the corresponding phase-change Φ_{45} is small. Above the level z_5 we are in a slowly varying medium and we simply have a wave for which phase travels vertically upwards indefinitely.

If the small phase-changes Φ_{23} and Φ_{45} associated with the intervals of high gradient are taken to be zero, a simple physical interpretation of the theory in Chapter 3 is possible. It is illustrated in Figure 1 for an individual magneto-ionic component (O wave or X wave). Reflection from the high gradient on the under side of the E region is now reflection from a discontinuity of refractive index $n_3 - n_2$, where n_2 and n_3 are the complex refractive indices at the heights z_2 and z_3. Reflection from the high gradient on the top side of the E region is reflection from a discontinuity of refractive index $n_5 - n_4$, where n_4 and n_5 are the complex refractive indices at the heights z_4 and z_5. Moreover, reflection from the high gradient on the under side of the D region is reflection from a discontinuity of refractive index $n_1 - 1$, where n_1 is the complex refractive index at the height z_1. Reflection from the three discontinuities must be combined, taking into account the complex phase-change Φ_{12} (Equation 4) between the D level and lower E level, and the complex phase-change Φ_{34} (Equation 5) between the lower E level and the upper E level. This is a standard calculation in optics or

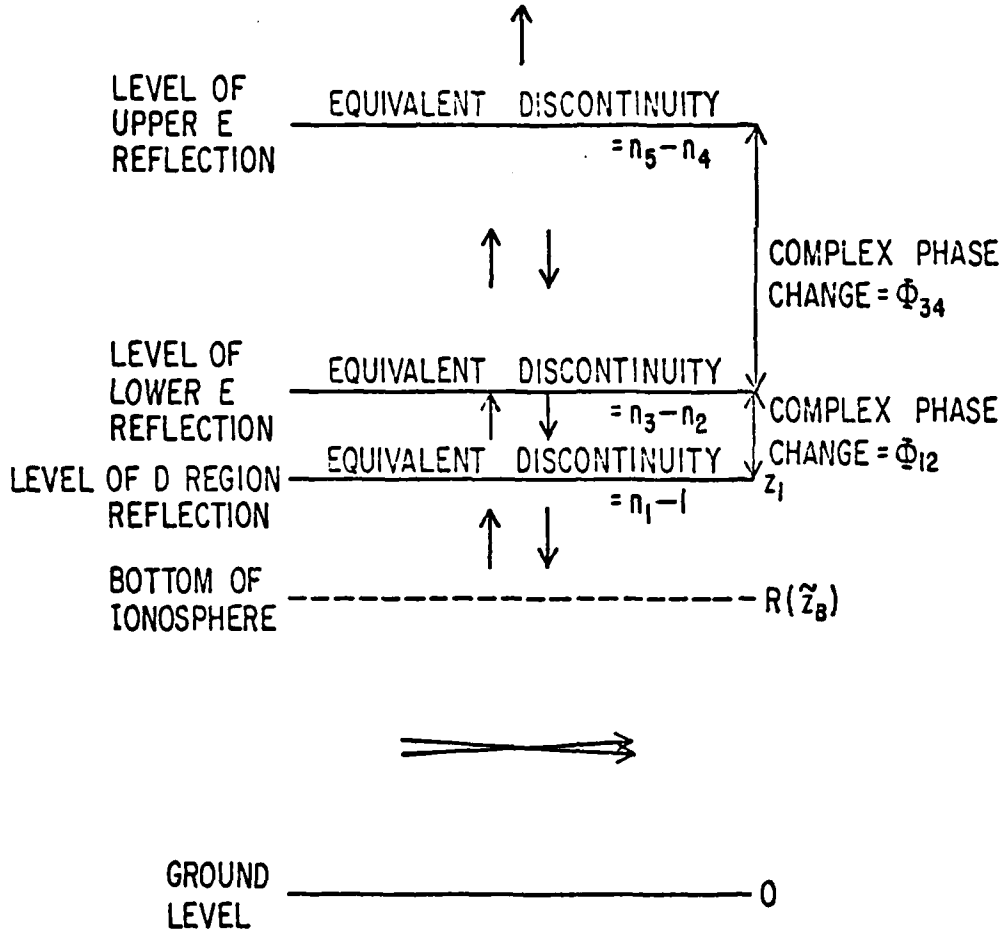

Chapter 4

Figure 1. Illustrating simultaneous reflection of the O or X wave from (i) a high gradient on the under side of the D region, (ii) a high gradient on the under side of the E region, and (iii) a high gradient on the top side of the E region.

in transmission-line theory.

Below the level z_1 in Figure 1 it is, of course, necessary to switch from nearly vertical propagation to nearly horizontal propagation at the bottom of the ionosphere; this occurs in a refracting stratum as described by Greifinger and Greifinger (1978, 1979). It is also necessary to remember that the calculation for an individual magneto-ionic component (O wave or X wave) does not satisfy the boundary conditions at the surface of the Earth because the field is elliptically polarized. It is the combination of the O and X wave calculations that is significant at low heights and that satisfies the boundary conditions at the Earth's surface.

Figure 1 illustrates in a simple way the basis of the calculations made in this chapter. In the actual computations, however, the phase-changes Φ_{23} and Φ_{45} associated with the intervals of high gradient were not taken to be zero. Neither was any use made of approximations based on the assumption that Φ_{23} and Φ_{45} are numerically small. We simply used without approximation the formulae given in the Appendix of Chapter 3.

2. A simplified model of the ionosphere

To apply Equations (1), (2) and (3) to the study of ELF propagation in the Earth-ionosphere transmission line, we need a worldwide model of the ionosphere. In principle, it is desirable to use the International Reference Ionosphere (Rawer, Bilitza and Ramakrishnan 1978 ; Rawer, Ramakrishnan, and Bilitza 1978). However, we have used a simpler model, but nevertheless one that is likely to illustrate many of the features that arise in worldwide ELF propagation.

We have made no attempt to model the ionosphere above a height of 150 km. At E region levels and below, the profile of electron density that we have used under quiet ionospheric conditions is illustrated in Figure 2. All profiles were represented as analytic functions of height using the method of Booker (1977); Table 1 shows the parameters used to reproduce Figure 2. The electron density is assumed to depend on the sunspot number R in the manner shown at the head of Table 1. Electron density was taken to be proportional to the square root of the cosine of the sun's zenith angle χ, an assumption that is satisfactory for the E region but less so for the D region. Figure 2 shows that we have given the under side of the E region quite a high gradient at a height of a little over 80 km. This was done in accordance with the preliminary version of the International Reference Ionosphere (Rawer, Ramakrishnan and Bilitza, 1975).

The profile of electron density that we have used at night under quiet ionospheric conditions is based on Table 2 and is illustrated in Figure 3. There is no dependence on time during the night, but there is a dependence on latitude Λ. Higher values of electron density were

Table 1

Quiet day profile of electron density (Figure 1)

$m=5$, $N_0=2.12 \times 10^{11} (1 + 0.01R)^{1/2} \cos^{1/2}\chi$, $z_0=200$

n	1	2	3	4	5	
z_n	62.5	82.5	84	100	120	
$A_{n-1,n}$	0.2	0.001	$1.\dot{3}$	0.03125	0.0	0.0025
B_n	0.5	2.0	1.5	0.2	0.2	

Table 2

Quiet night profile of electron density (Figure 2)

$m=5$, $N_0=1.83 \times 10^{9} (1 + 0.02R)^{1/2} (1 - 0.6 \cos 2\Lambda)$, $z_0=220$

n	1	2	3	4	5	
z_n	80	89	90	112	127	
$A_{n-1,n}$	0.75	0.0	0.75	0.0022727	$-0.10\dot{3}$	$0.01\dot{6}$
B_n	0.65	2.0	2.0	$0.\dot{3}$	0.2	

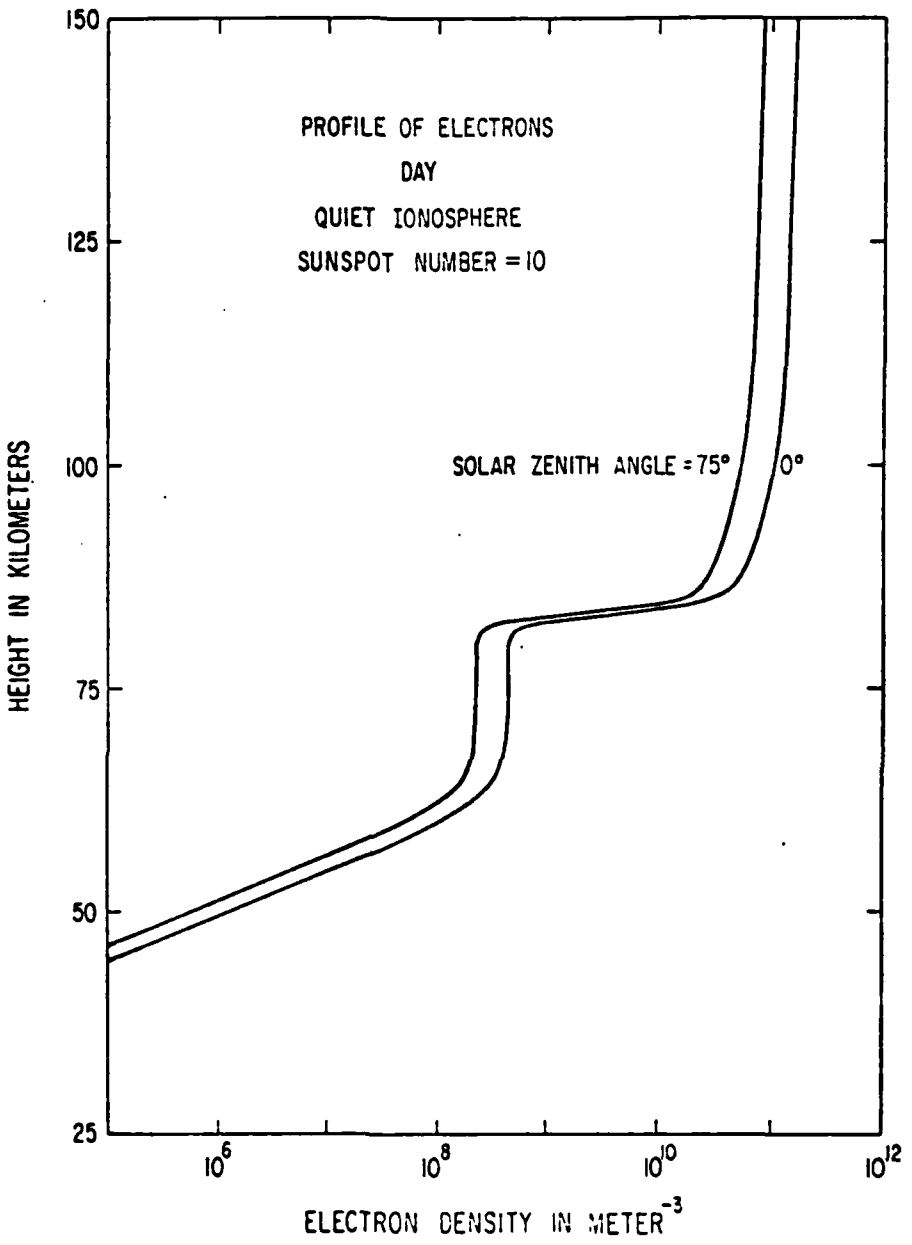

Chapter 4

Figure 2. Day-time profiles of electron density under quiet ionospheric conditions

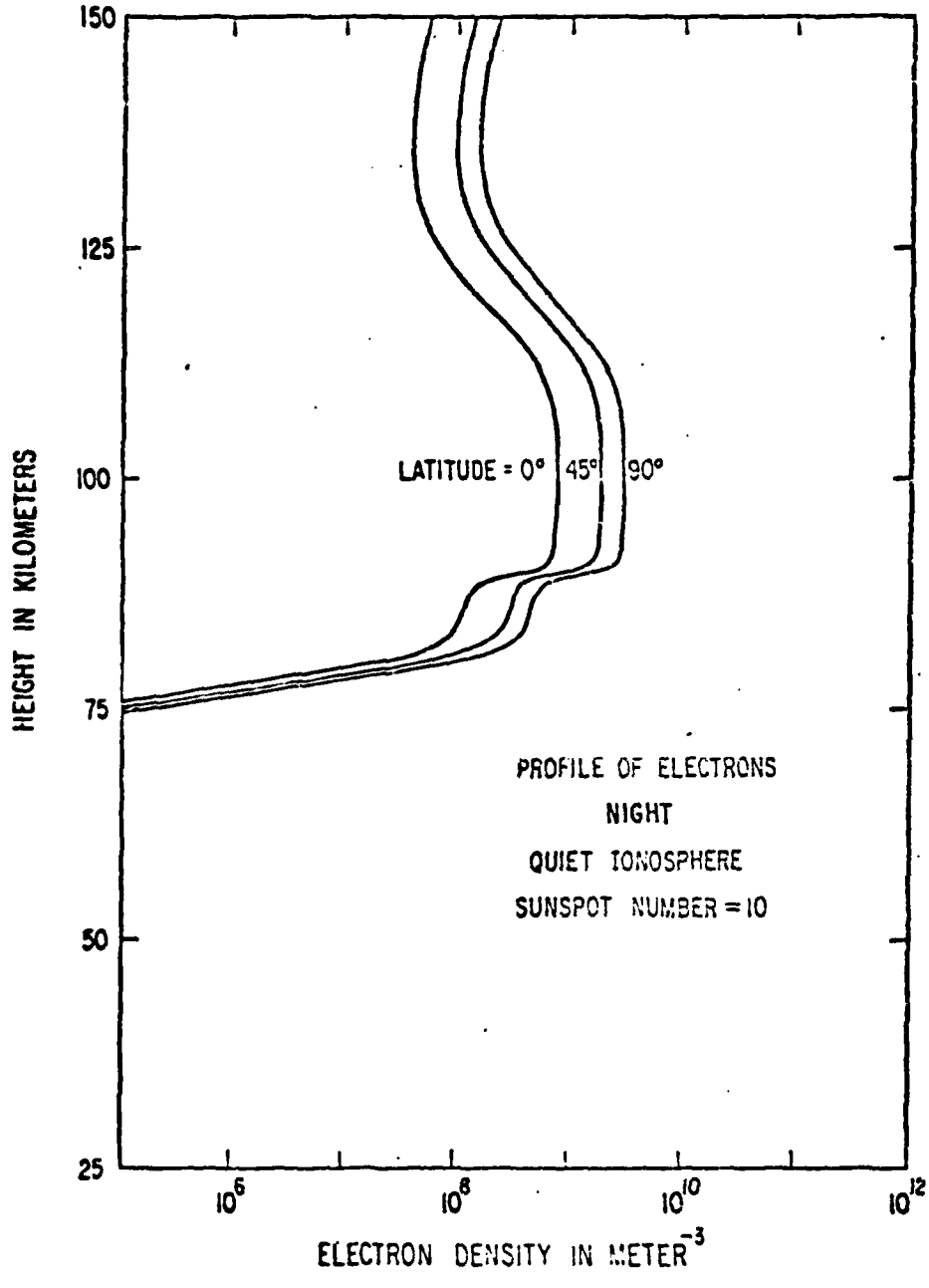

Chapter 4

Figure 3. Night-time profiles of electron density under quiet ionospheric conditions.

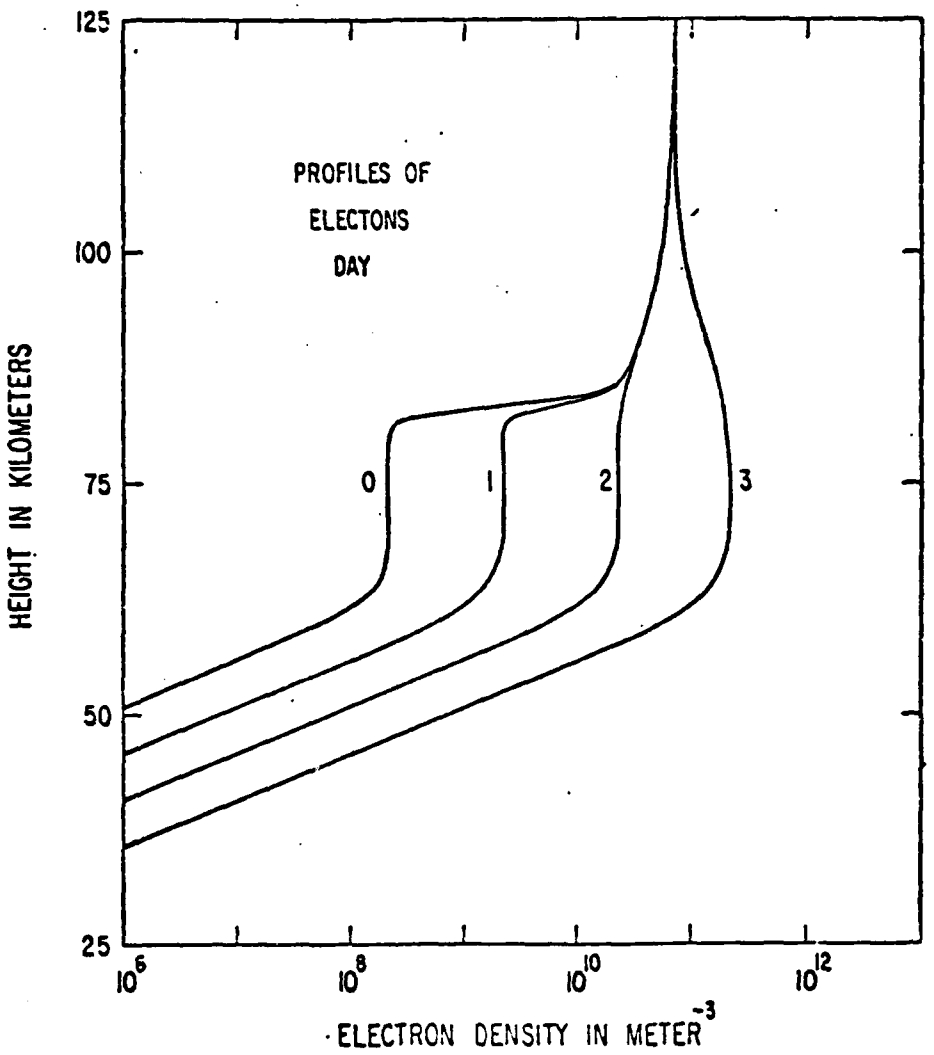

Chapter 4

Figure 4. Illustrating three degrees of disturbance in the midday profile of electron density at latitude 75^{o}.

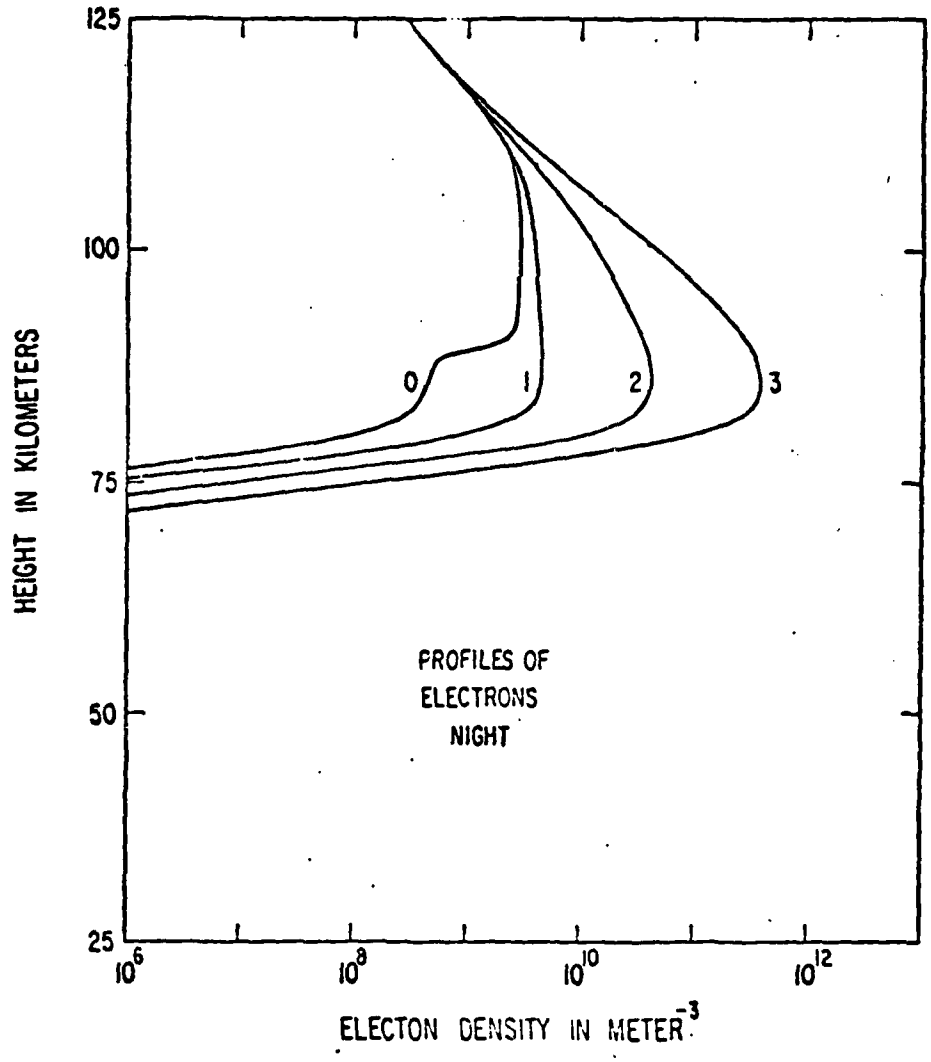

Figure 5. Illustrating three degrees of disturbance in the nighttime profile of electron density at latitude 75°.

used at high latitudes because of auroral effects. Figure 3 shows that the adopted night-time profile of electron density has a high gradient on the under side of the E region at a height of about 90 km, with a ledge of ionization below. The ledge was added in the light of such night-time rocket profiles as were available to us.

No attempt was made to include a sporadic E layer. Nevertheless such a layer is important because it can reflect the whistler mode transmitted into the ionosphere (Barr 1977, Pappert and Moler 1978).

In order to study the effects of enhanced ionization below the E region on ELF propagation in the Earth-ionosphere transmission line, calculations were performed for the series of profiles of electron density shown in Figure 4. The profile marked 0 is the profile already adopted for latitude 75° at midday under quiet conditions. For the profiles marked 1, 2 and 3 in Figure 4, the D region electron density has been increased by 1, 2 and 3 powers of ten respectively. A similar series of profiles for night conditions is shown in Figure 5. Profile 3 might be appropriate to a polar cap absorption event, and profiles 1 and 2 to events of this type having lesser intensity. A sudden ionospheric disturbance associated with a solar flare might correspond roughly to profile 1 in Figure 4 extrapolated to the rest of the day-time ionosphere on the assumption that the electron density is proportional to $\cos^{\frac{1}{2}}\chi$.

At ELF, ions play a role, especially at the lower end of the band. Nevertheless, the ion profiles are not well established. The

profiles assumed for negative ions are shown in Figure 6 (day) and Figure 7 (night). The profiles marked 0 are used under quiet ionospheric conditions. The profiles marked 1, 2 and 3 are used in conjunction with the corresponding electron profiles 1, 2 and 3 in Figures 4 and 5. The positive ion content is adjusted to maintain neutrality. It is assumed that all ions are molecular and have an atomic mass 29. Consequently, the effect of dissociation on transmission into the ionosphere above 100 km is not included.

In addition to the profiles of electron density and ion density, knowledge is required of the profiles of collisional frequency. The collisional frequencies of greatest importance at ELF are ν_e and ν_i, of which the first is that for electrons with neutral molecules and the second is that for ions with neutral molecules. Their values in sec^{-1} as functions of height z in km are assumed to be given by:

$$\left.\begin{aligned} \log_{10}\nu_e &= 5.4 - 0.077\ (z-90) \\ \log_{10}\nu_i &= 4.6 - 0.077\ (z-90) \end{aligned}\right\} \qquad (6)$$

At the levels of greatest importance for ELF propagation in the Earth-ionosphere transmission line, Equations (6) are in reasonable agreement with values given by Banks and Kockarts (1973).

The Earth's magnetic field is taken to be that of a central dipole, and no allowance is made for the difference between geographic and geomagnetic latitude. The variation with height in the magnitude of the Earth's magnetic field is taken into account in calculating the the scale-heights h_0 and h_X defined in Equations (1) of Chapter 3.

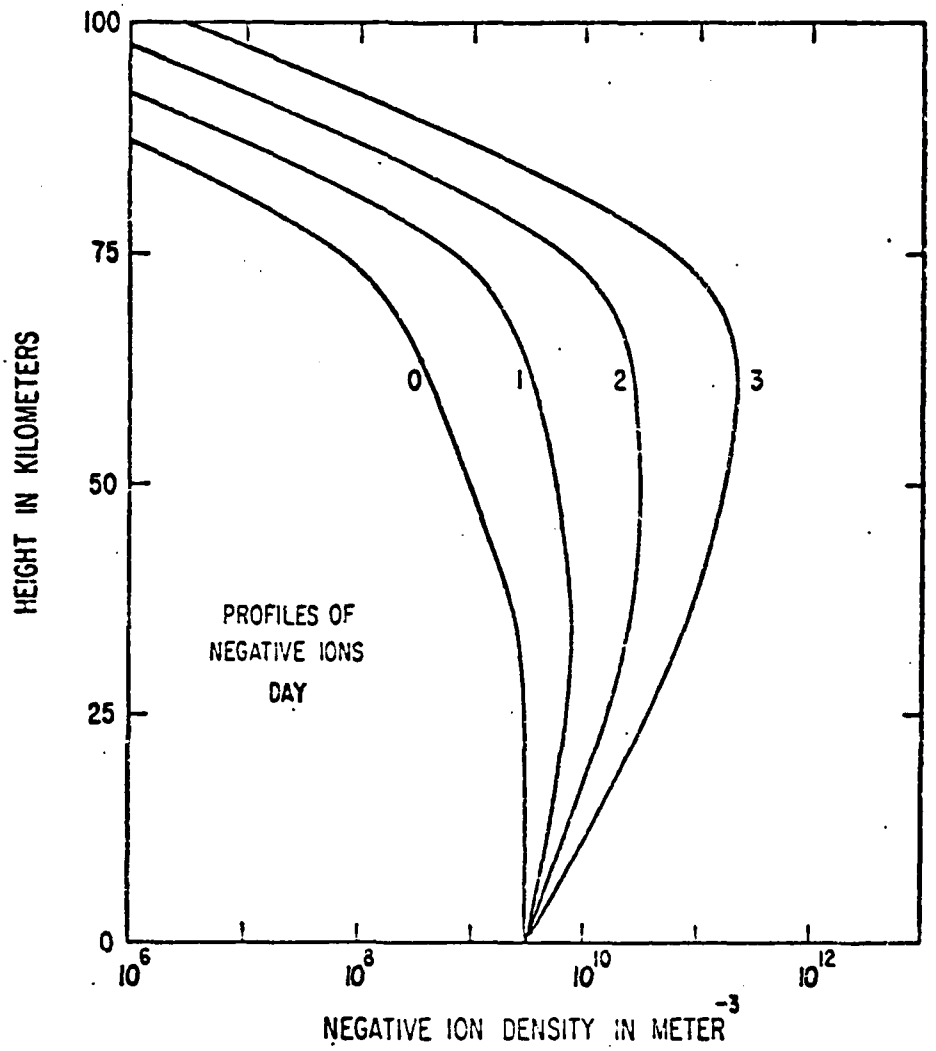

Chapter 4

Figure 6. Illustrating four day-time profiles of negative ion density.

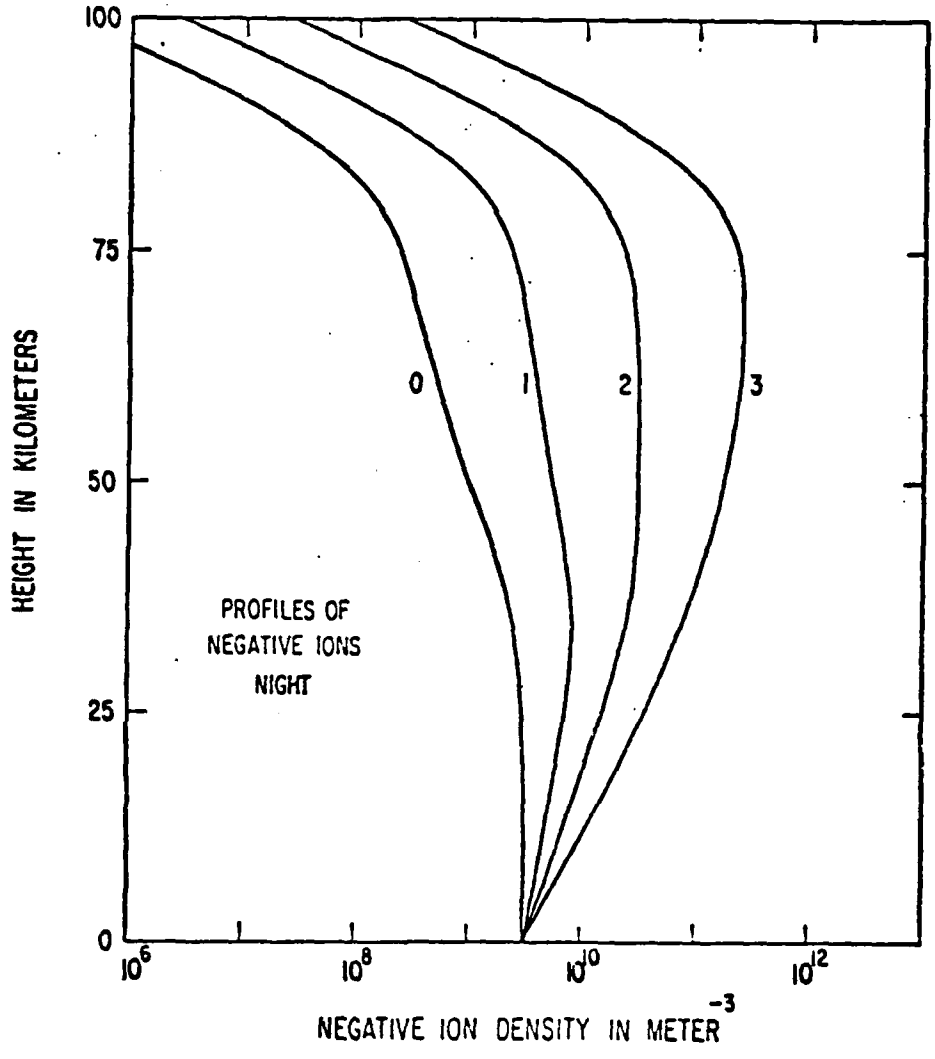

Chapter 4

Figure 7. Illustrating four night-time profiles of negative ion density.

In calculating the scale-heights, it is necessary to evaluate height-derivatives not only for the magnitude of the Earth's magnetic field but, more importantly, for the electron density, the ion densities and the collisional frequencies. These derivatives need to be calculated analytically from analytic functions of height. Confusion results if unsmoothed numerically estimated profiles are used and the derivatives are calculated by taking differences. Confusion also results if profiles are employed that are discontinuous or that have discontinuous derivatives. These difficulties are avoided by specifying the profiles using the method of Booker (1977).

In calculating the complex refractive indices n_0 and n_X at each height, the square root of a complex number has to be evaluated. One sign before the square root gives the value for the 0 wave and the other sign that for the X wave. The computer cannot be allowed to make this choice according to any rules that happen to be programmed into it. If this is done, integrals such as those in Equations (4) and (5) are liable to use the 0 wave value of n over part of the range of integration and the X wave value over the remainder. The refractive index for a particular magneto-ionic component (0 wave or X wave) must be calculated in such a way that continuity is maintained over the entire range of heights in use.

Leakage of energy into the Earth causes small additions to the values of c/v and α calculated in Equations (2) and (3). These additions are easily made; they are not included in the numerical results summarized in the remainder of this chapter.

3. Day-time mid-latitude frequency dependence

Let us begin by considering the frequency dependence of ELF propagation at a middle latitude under day-time conditions. Let the sunspot number be low (R = 10) and the latitude be 45°. Let the time of day be noon, and let us assume equinoctial conditions. The model of a quiet ionosphere described in the previous section then specifies all the profiles, and we can proceed to solve Equations (2) of Chapter 3 to obtain the heights of reflection. The results are presented in Figure 8. The actual points calculated are connected by rectilinear segments.

At frequencies below about 30 Hz there is a single solution of the reflection equation for the O wave (marked z_{30} in Figure 8) and a single solution of the reflection equation for the X wave (marked z_{3X}); they occur in the high gradient on the under side of the E region. As the frequency increases, two additional solutions appear for each wave. The solutions marked z_{10} and z_{1X} occur in the high gradient on the under side of the D region, while the solutions marked z_{20} and z_{2X} are located near the level of maximum ionization density for the D region.

For each magneto-ionic component the curves for the three heights connect up to form a single continuous curve. These curves separate (i) situations in which the gradient of ionization density is sufficiently small for the phase-integral treatment to be satisfactory from (ii) situations in which the gradient of ionization density is sufficiently large for the Greifinger and Greifinger (1978, 1979) type of treatment to be satisfactory; below the refracting stratum

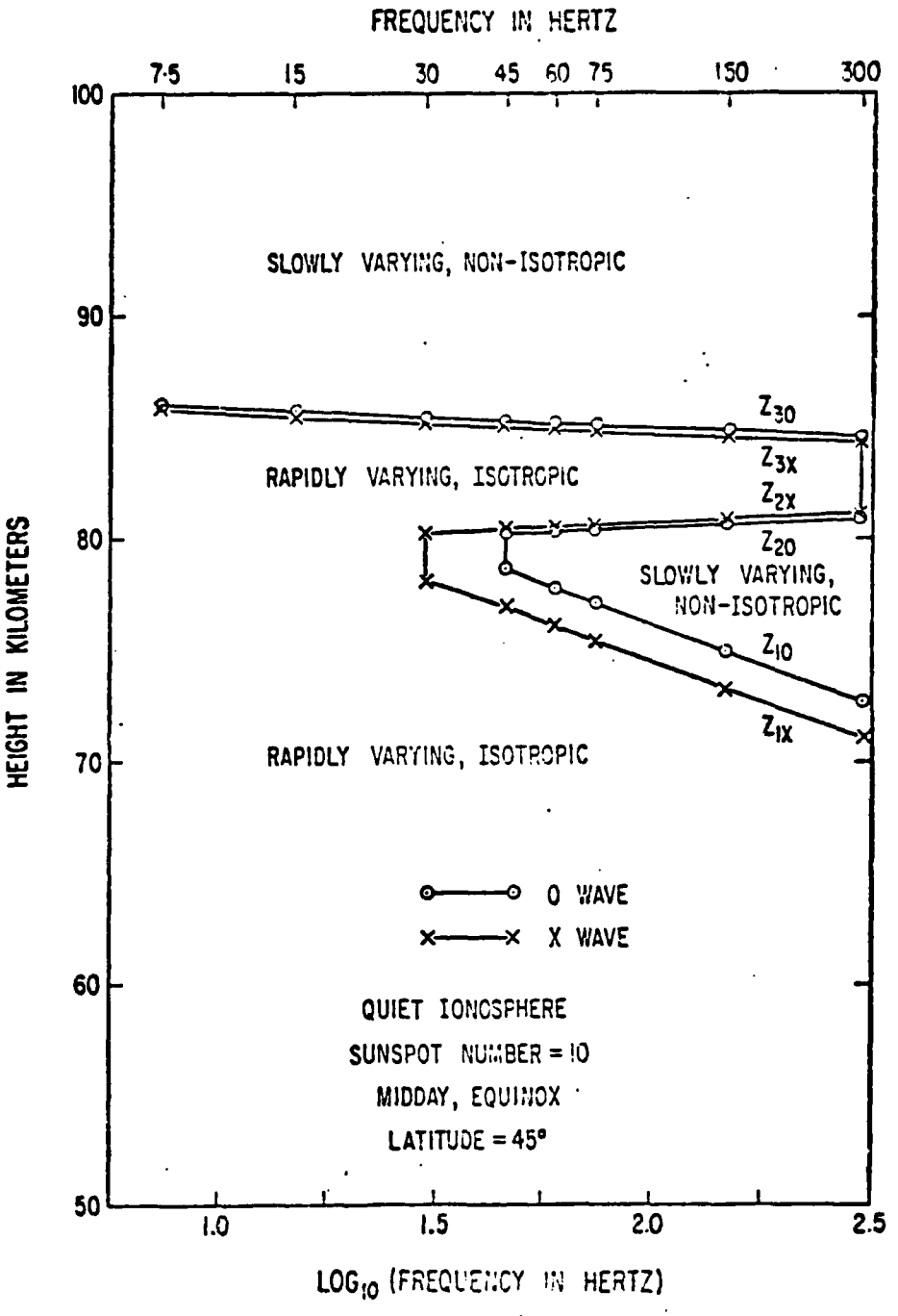

Chapter 4

Figure 8. Illustrating, as functions of frequency at a middle latitude, the solutions of the reflection equations (Equations 2 of Chapter 3) under day-time conditions.

at the bottom of the ionosphere, this becomes a situation corresponding to a homogeneous isotropic medium. The connections between the z_2 and z_3 curves in Figure 8 in reality occur, not at 300 Hz (the highest frequency for which we have performed calculations), but in the VLF band. The z_1 curves in Figure 8 drop to the bottom of the ionosphere as the frequency is increased to VLF values. In so doing, they lose their reflecting ability ($\propto n_1 - 1$ in Figure 1). At sufficiently high frequencies the z_1 level becomes the level at which the limiting polarizations of downcoming O and X waves are determined.

From Figure 8 we see that, at frequencies below about 30 Hz, reflection is controlled primarily by the high gradient on the under side of the E region. At the frequency increases, however, reflection from the D region starts to play a role. At frequencies above about 1000 Hz reflection from the D region is dominant. But there is a substantial range of frequency in which reflection from the high gradients on the under sides of both the D and E regions must be taken into account.

Because the refractive index is bigger in the E region than in the D region, the discontinuity $n_3 - n_2$ in Figure 1 turns out, in the ELF band, to be about a power of ten bigger than the discontinuity $n_1 - 1$. This means that the high gradient on the under side of the E region is potentially much more effective for blocking transmission of energy into the upper ionosphere than is the high gradient on the under side of the D region. The relative importance of the two in a particular situation depends on the value of the complex phase-change Φ_{12} shown in Figure 1 and defined in Equation (4).

The real and imaginary parts of Φ_{12} are shown in Figure 9 as functions of frequency for the circumstances of Figure 8. For the X wave, Φ_{12} is roughly real because this wave is the propagating whistler wave. For the O wave, Φ_{12} is roughly imaginary and negative because this wave behaves quite evanescently. From Figure 9 we see that the attenuation of the whistler wave in going through the D region has only reached about 1 db even at a frequency as high as 300 Hz. The whistler wave penetrates in strength to the E region in the VLF band, and this is even truer in the ELF band. Moreover, Figure 9 shows that the phase-change through the D region for the whistler wave has only reached about 30° at 300 Hz. For frequencies less than 100 Hz, the phase-change through the D region for the X wave is small, and the attenuation is negligible. Even for the largely evanescent O wave the attenuation through the D region has only reached about 4 db at 300 Hz and it is less than 1.5 db at frequencies less than 100 Hz. Below about 100 Hz the D region is an optically thin, largely transparent attachment to the under side of the day-time E region. It is only when the frequency exceeds about 100 Hz that the D region starts to play a significant role in the reflection process. It is only when the frequency exceeds about 1000 Hz that the D region takes over as the dominant reflector in middle latitudes.

We need to calculate the effect of interference between reflection from the high gradient on the under side of the D region and reflection from the high gradient on the under side of the E region. As described in Chapter 3, this involves calculating equivalent complex heights of reflection $\tilde{z}_{RO}$ and $\tilde{z}_{RX}$ for the O and X waves. The values

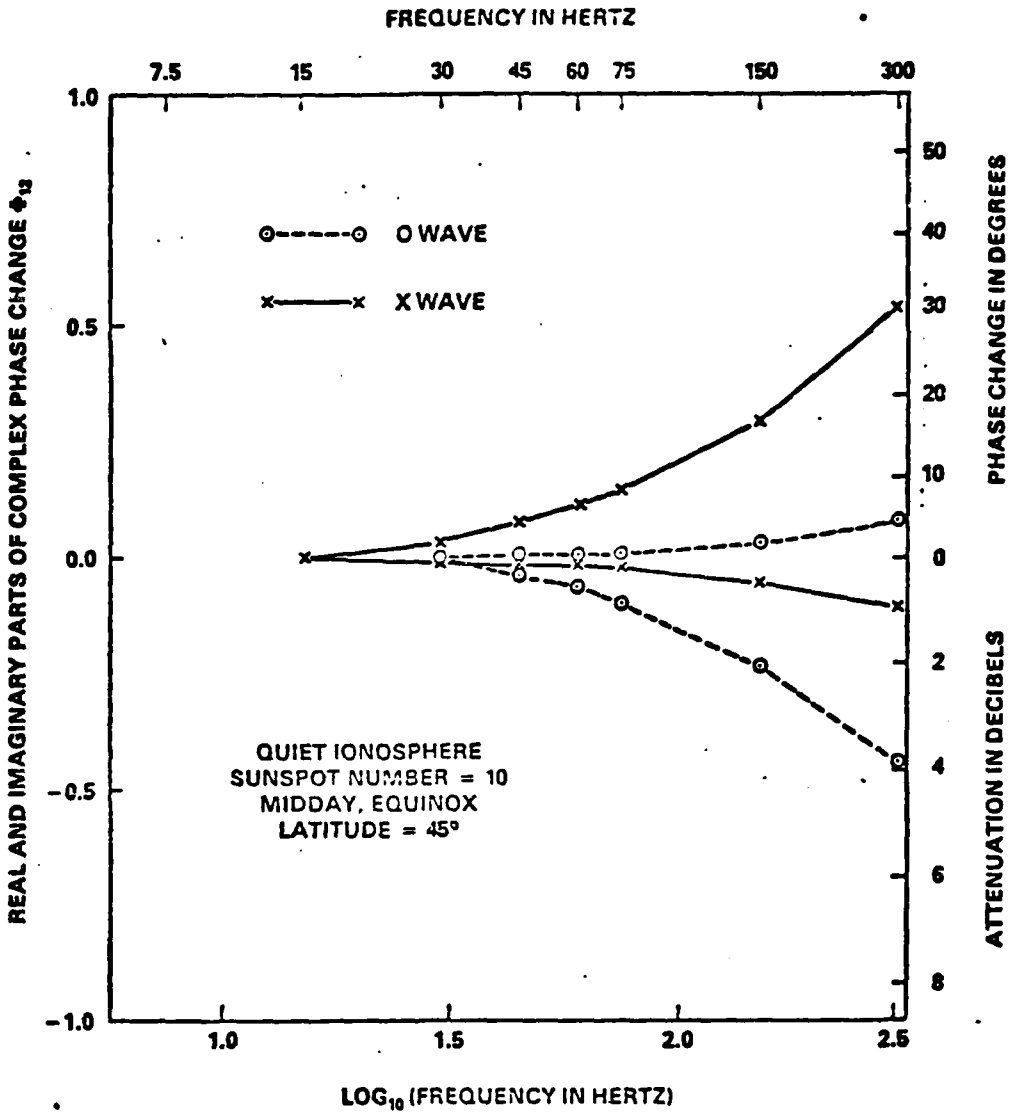

Chapter 4

Figure 9. Illustrating the variation with frequency of the complex phase-change Φ_{12} through the D region at a middle latitude under day-time conditions.

derived from Figures 8 and 9 are shown in Figure 10. The values for the equivalent complex height of the bottom of the ionosphere are also shown. The quantities $\tilde{z}_{BO}$ and $\tilde{z}_{BX}$ were calculated from Equations (63) of Chapter 3; they are indistinguishable from each other in Figure 10, and are shown as the real and imaginary parts of a single complex height $\tilde{z}_B$. The quantities $\tilde{z}_{RO}$ and $\tilde{z}_{RX}$ were calcualted from Equations (66) of Chapter 3 using formulae given in the Appendix of Chapter 3. However, for frequencies less than about 100 Hz, adequate results can be obtained using the approximate expression in Equation (61) of Chapter 3.

The equivalent complex height of reflection includes the effect of phase-change at reflection and, in the imaginary part, the effect of energy-loss in association with reflection, particularly leakage into the upper ionosphere. At 7.5 Hz Figure 10 shows that the real part of $\tilde{z}_{RX}$ is almost identical to the actual height of reflection shown in Figure 8. Reflection of the whistler wave is taking place from the high gradient on the under side of the E region with no significant change of phase. But the imaginary part of $\tilde{z}_{RX}$ in Figure 10 shows that there is significant leakage of energy into the upper ionosphere via the whistler mode. On the other hand, the negligible imaginary part of $\tilde{z}_{RO}$ in Figure 10 shows that, for the O wave at 7.5 Hz, there is no significant leakage of energy into the upper ionosphere by day. This is because the O wave is largely evanescent. The storage field above the level of reflection in the E region does, however, cause significant change of phase at reflection, and this results in the real part of $\tilde{z}_{RO}$ in Figure 10 being substantially in excess of the actual height of reflection shown in Figure 8. Except

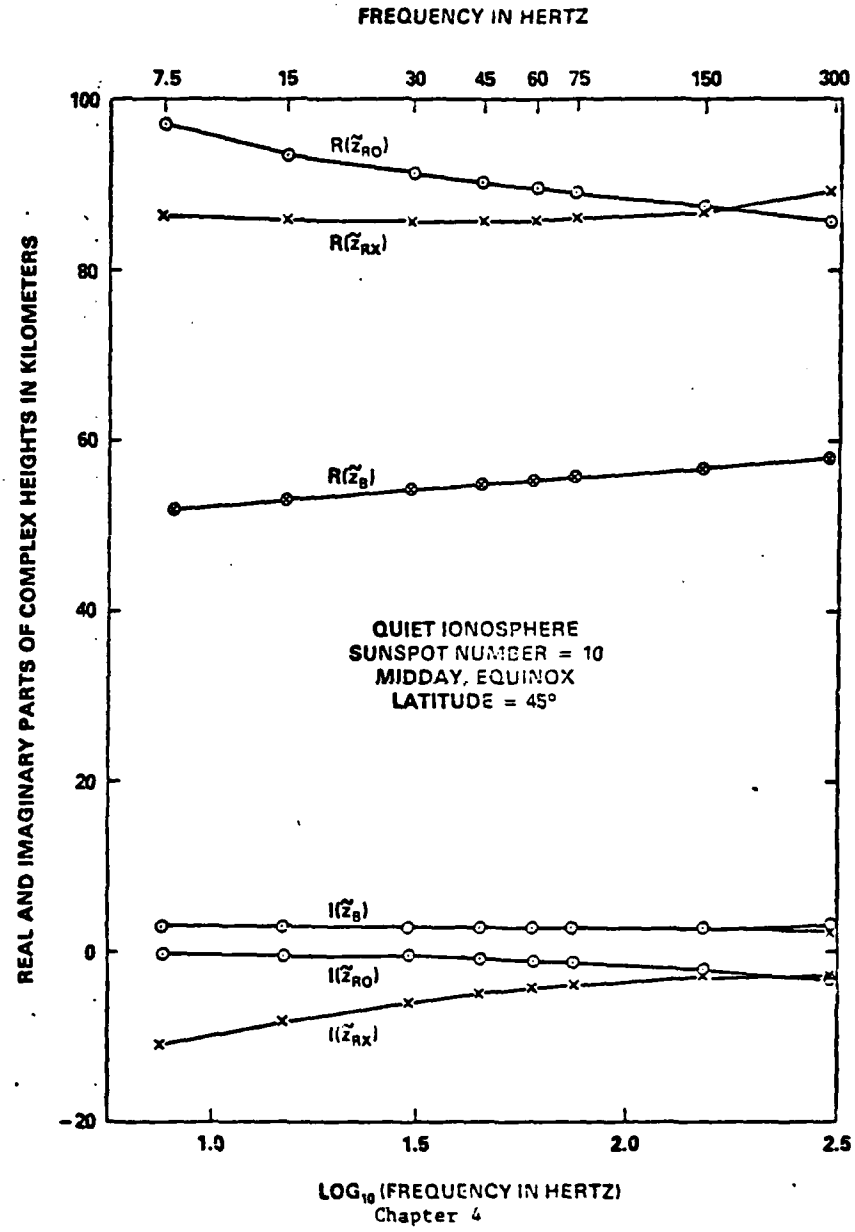

Chapter 4

Figure 10. Illustrating, as functions of frequency at a middle latitude, the complex heights of reflection and the complex height of the bottom of the ionosphere under day-time conditions.

at low latitudes, it is storage of O wave energy above the level of reflection that affects the phase velocity in Earth-ionosphere transmission line, while it is leakage of X wave energy into the upper ionosphere that is a prime cause of attenuation. However, some attenuation in the Earth-ionosphere transmission line is also caused by absorption in the D region and, using the method of Greifinger and Greifinger (1977, 1979), this appears in Figure 10 via the imaginary part of the equivalent height of the bottom of the ionosphere.

We notice that, although Figure 8 shows the D region as coming into action as the frequency increases through about 30 Hz for the X wave and about 45 Hz for the O wave, no corresponding discontinuities appear in the equivalent complex heights of reflection shown in Figure 10. This is because, as shown in Figure 9, the complex phase-change Φ_{12} between the D and E region levels of reflection is small, and increases quite gradually with frequency. The real part of $\tilde{z}_{RX}$ increases with frequency up to 300 Hz in Figure 10 because of the effect of phase-change at reflection.

To calculate the phase velocity v and the attenuation rate α in the Earth-ionosphere transmission line, the complex heights derived in Figure 10 have to be used in Equation (1), and hence in Equations (2) and (3). Because we are not at a low latitude, the elliptical polarizations of both waves are close to circular at all relevant heights, so that Q_O and Q_X in Equations (1) are almost exactly -j and +j respectively. The results for c/v and α are shown in Figure 11.

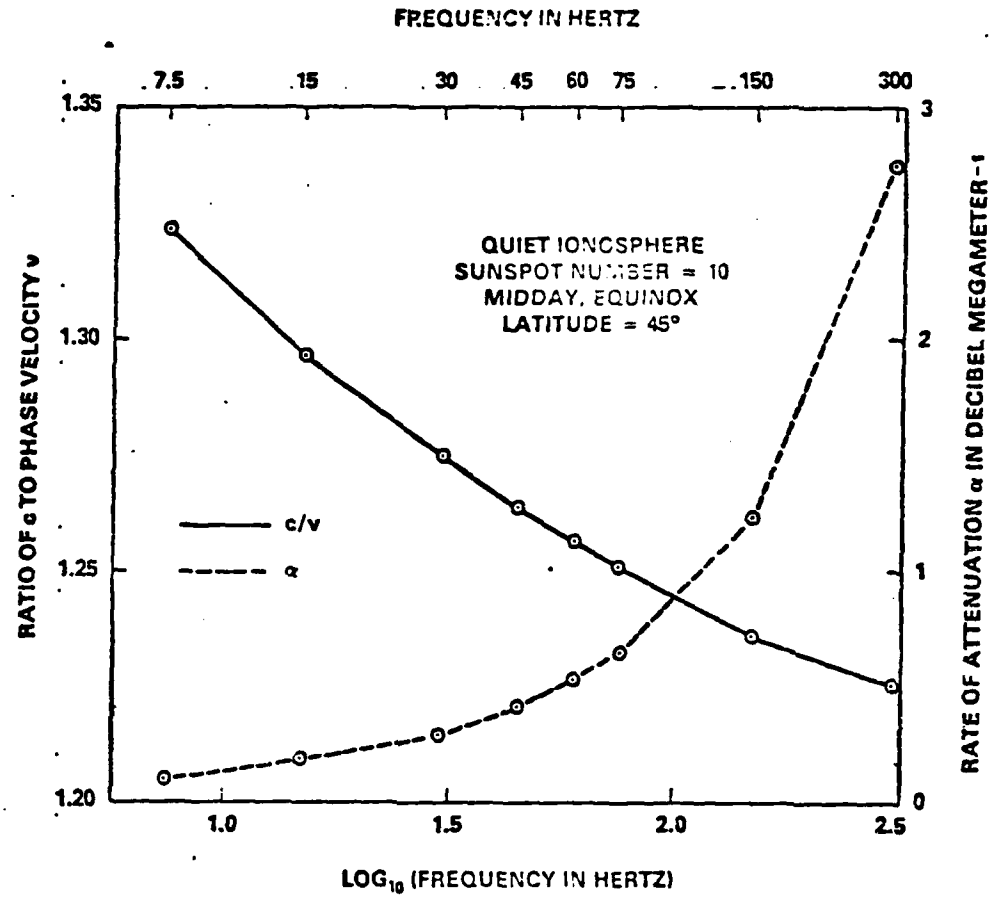

Figure 11. Illustrating the variation with frequency of the velocity of phase propagation and the rate of attenuation at a middle latitude under day-time conditions.

4. Day-time latitude dependence at the equinox

Let us now examine the latitude dependence of ELF propagation in the day-time, starting with a frequency of 45 Hz. We again consider equinoctial conditions. Likewise, we again let the time of day be noon and the sunspot number be low (R = 10). Solution of Equations (2) of Chapter 3 for the heights of reflection yields the curves shown in Figure 12. Derivation of the equivalent complex heights of reflection and the equivalent complex height of the bottom of the ionosphere leads to the results shown in Figure 13.

Figure 12 verifies that, for 45 Hz, the D region is involved in the reflection process in the day-time at middle latitudes. But the diagram shows that the influence of the D region disappears both at low latitudes and at high latitudes. The low latitude effect is caused by the Earth's magnetic field. The high latitude effect is caused by the decrease in ionization density at high solar zenith angles. Even at a latitude of 45° the effect of the D region on the reflection process is minor at a frequency of 45 Hz as described in the previous section. It follows that, at all latitudes, reflection at 45 Hz in the day-time is controlled primarily by the high gradient on the under side of the E region.

Figure 13 shows that, at 45 Hz under day-time equinoctial conditions, the real part of $\tilde{z}_{RX}$ is nearly independent of latitude and has an E region value. The imaginary part of $\tilde{z}_{RX}$, however, increases steadily with latitude. This is because reflection at the equator is metallic in character but, as the latitude increases, the effect of the Earth's magnetic field brings into play leakage of energy into

the upper ionosphere via the whistler mode. For the same reason the character of the transmitted O wave changes from metallic to evanescent as one moves away from the equator. The associated change of phase at reflection causes a steady increase with latitude in the real part of $\tilde{z}_{RO}$.

As the frequency decreases from 45 Hz, the D region behavior shown in Figure 12 shrinks out of existence. But as the frequency increases from 45 Hz, the D region behavior spreads in latitude, and at 150 Hz it extends from the equator to polar regions. At 300 Hz the effect of the D region on the reflection process is still moderate at high latitudes, but it is quite substantial at low latitudes. This is illustrated in Figure 14 which shows, as functions of latitude at 300 Hz, the real and imaginary parts of the complex phase change Φ_{12} associated with passage through the D region.

At the equator, vertical propagation at ELF between the high gradients in the D and E regions is metallic in character. In these circumstances the real and imaginary parts of Φ_{12} are almost exactly equal in magnitude, and the values are almost exactly the same for the O and X waves. This behavior is seen in Figure 14 for a frequency of 300 Hz. At this frequency the attenuation associated with passage through the D region at the equator amounts to about 6 db. Consequently the skin depth for the D region at the equator at 300 Hz is less than the separation between the levels of reflection associated with the high gradients on the under sides of the D and E regions. Reflection from the D region is therefore dominant at the equator at 300 Hz.

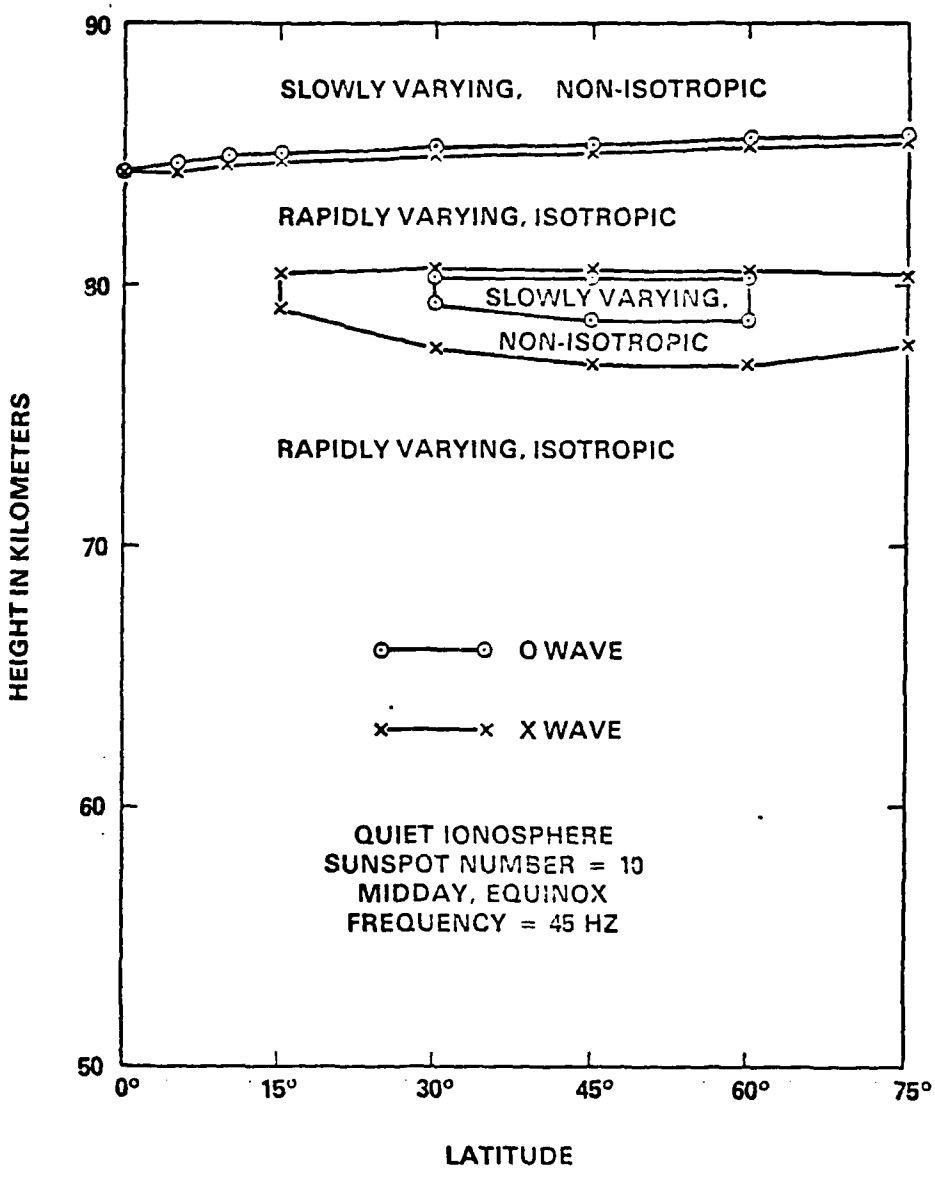

Chapter 4

Figure 12. Illustrating, as functions of latitude at 45 Hz, the solutions of the reflection equations (Equations 2 of Chapter 3) under day-time conditions.

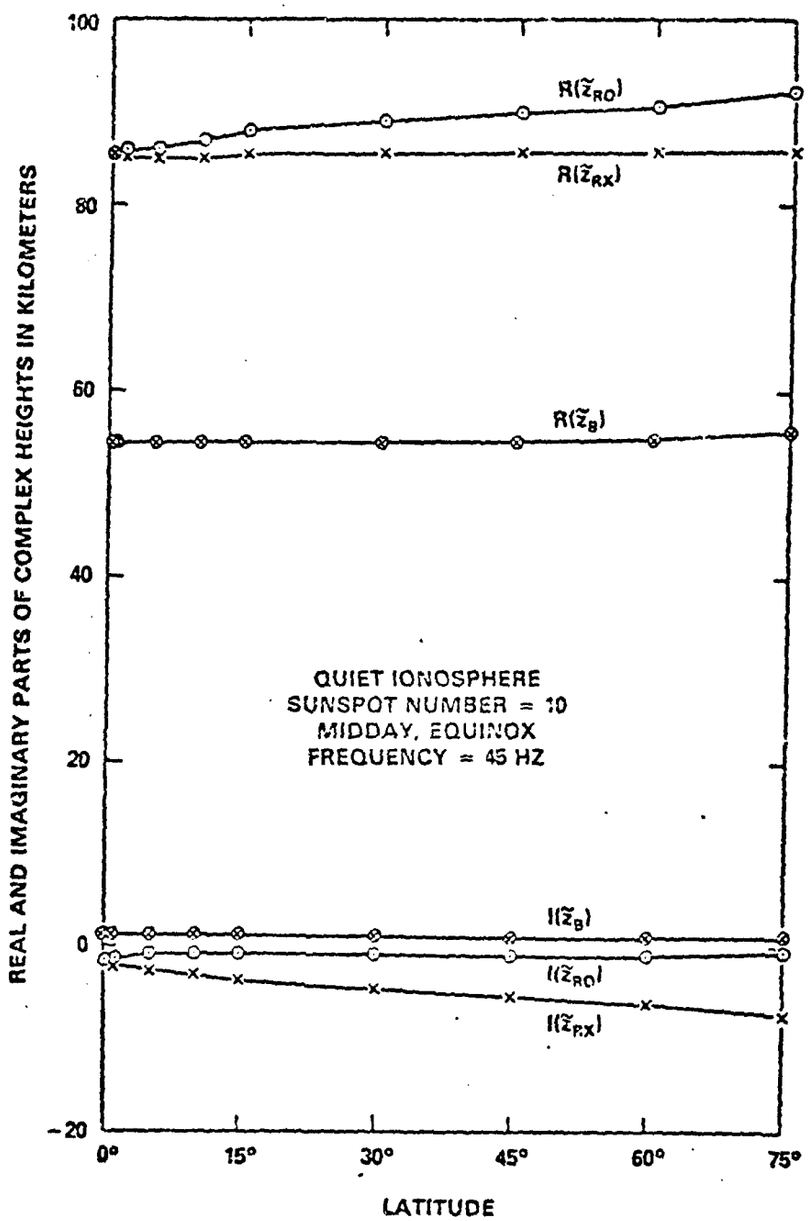

Chapter 4

Figure 13. Illustrating, as functions of latitude at 45 Hz, the complex heights of reflection and the complex height of the bottom of the ionosphere under day-time conditions.

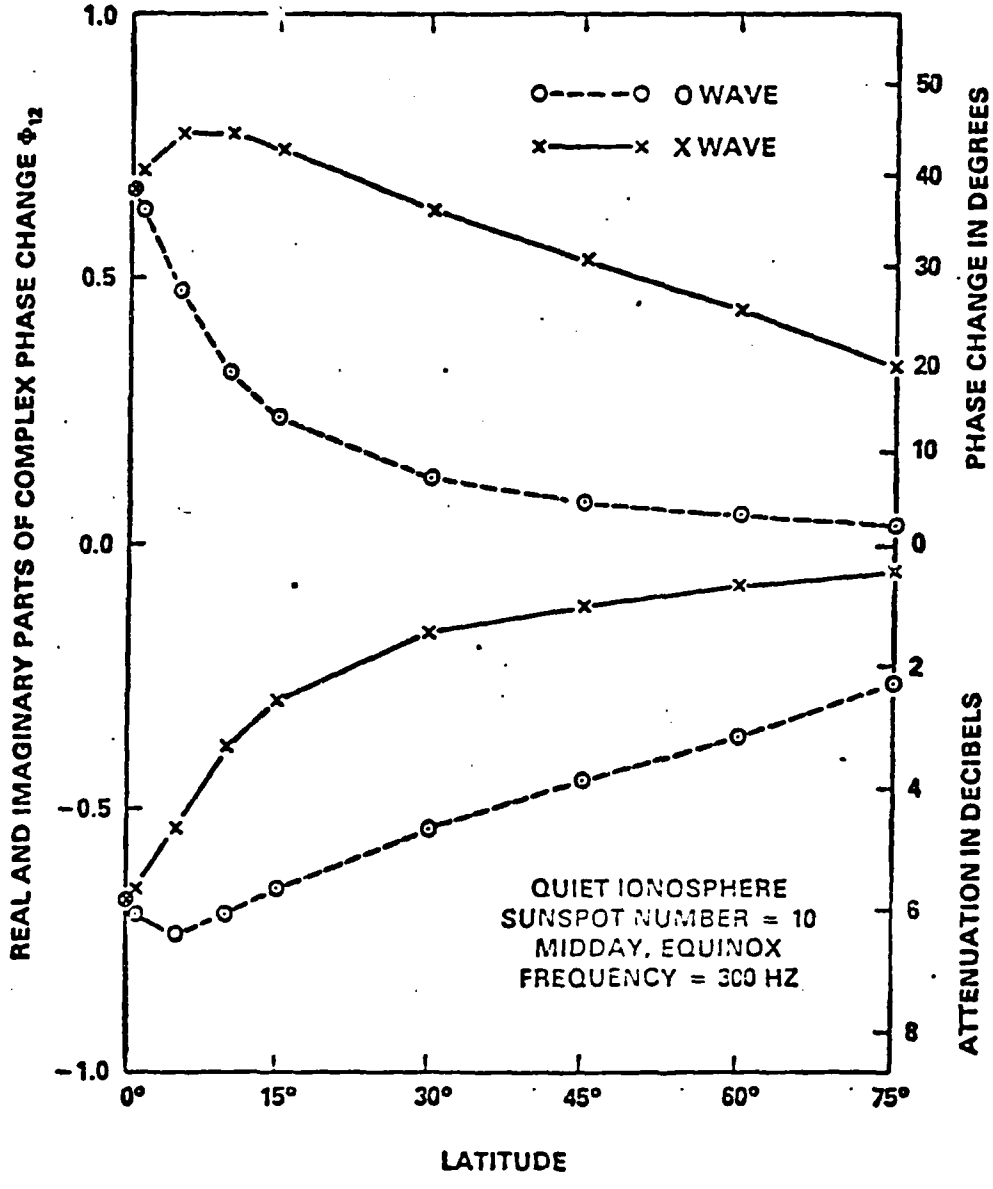

Chapter 4

Figure 14. Illustrating the variation with latitude of the complex phase-change Φ_{12} through the D region at 300 Hz under day-time conditions.

However, this quickly changes as one moves to higher latitudes. The effect of the Earth's magnetic field causes a change in the X wave from metallic behavior to whistler behavior, and in the O wave from metallic behavior to evanescent behavior. Figure 14 shows that, at latitude 45°, the attenuation of the evanescent wave in passing through the D region at 300 Hz is down to 4 db and that for the whistler wave is down to 1 db. By latitude 75° these figures are still lower, and even the phase-change for the whistler wave in going through the D region is then down to 20°. At 300 Hz by day, reflection is controlled by the high gradient on the under side of the D regions at low latitudes but by the high gradient on the under side of the E region at high latitudes. As the frequency is increased, the D region dominance spreads from low latitudes towards the poles; it extends to all latitudes at frequencies above 1000 Hz.

We are now in a position to calculate the phase velocity v and the attenuation rate α in the Earth-ionosphere transmission line as functions of latitude for a range of frequencies in the ELF band. Results are shown in Figure 15a for c/v and Figure 15b for α. The diagrams show the change in behavior at a frequency of about 100 Hz as the D region begins to take over reflection at low latitudes. At 300 Hz in Figure 15a there is a drop in c/v as the latitude decreases from 15° to 0°. This is because the height of reflection is falling to a D region value while the bottom of the ionosphere is remaining at about the same height; it is roughly the square-root of the ratio of these two heights that controls the value of c/v (Greifinger and Greifinger 1978, 1979). At 300 Hz in Figure 15b there is a continuous

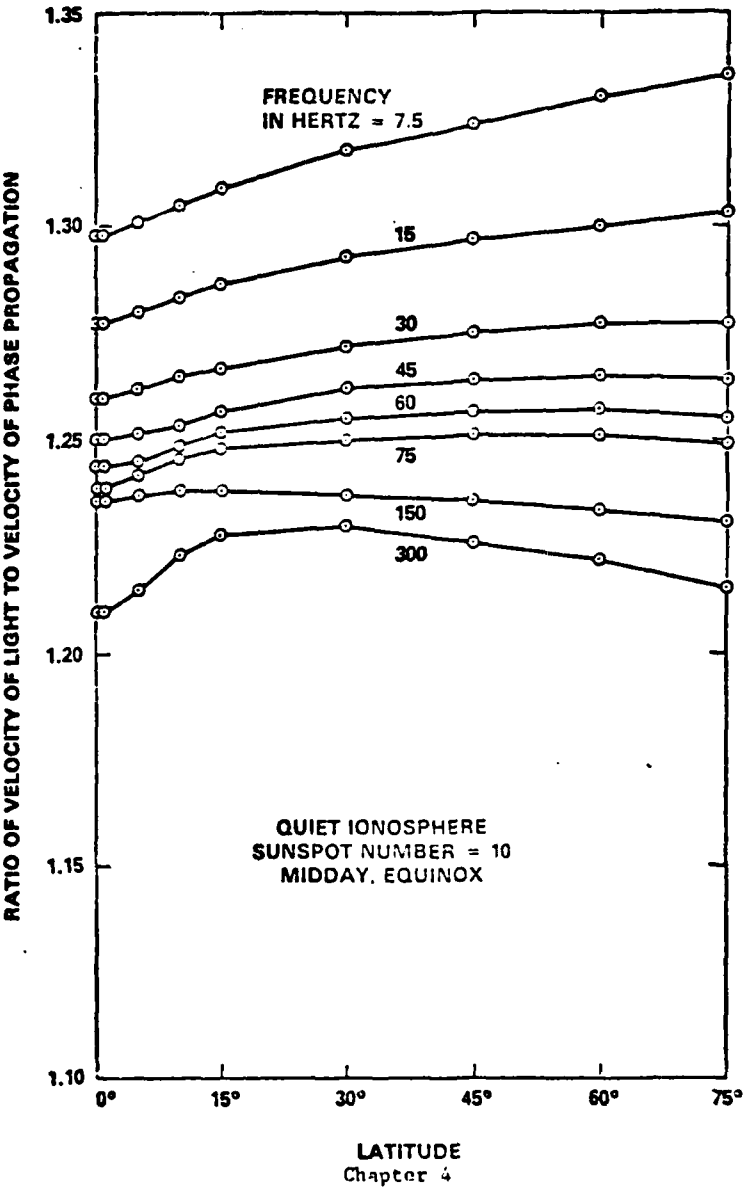

Chapter 4

Figure 15a. Illustrating the variation of the velocity of phase propagation with latitude and frequency under day-time conditions.

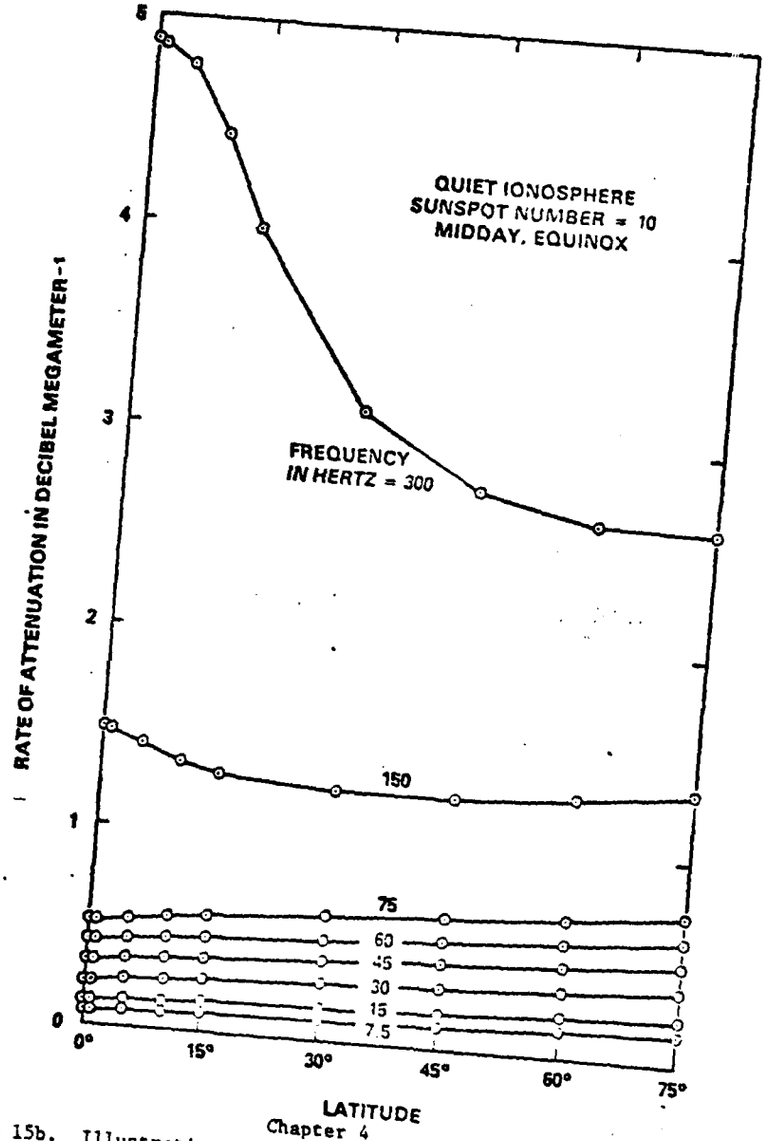

Figure 15b. Illustrating the variation of the rate of attenuation with latitude and frequency under day-time conditions.

rise in α as one moves from polar regions to the equator. This is caused by the transition from E region reflection to D region reflection. At ELF the discontinuity $n_1 - 1$ in Figure 1 is about a power of ten smaller than the discontinuity $n_3 - n_2$. The D region gradient lets more energy through than the E region gradient, and if this energy is absorbed before encountering the E region, propagation in the Earth-ionosphere transmission line is adversely affected.

5. Sunspot, seasonal and diurnal variations

For three frequencies, the effect of increasing the sunspot number from 10 to 100 is shown in Figures 16a and 16b for midday equinoctial conditions. At 7.5 and 45 Hz attenuation in the Earth-ionosphere transmission line is slightly reduced. At 75 Hz the attenuation is slightly reduced at high latitudes, and slightly increased at low latitudes. The last effect is due to increased influence of the D region.

For two frequencies, the effect of seasonal variation is shown in Figures 17a and 17b for noon conditions with a low sunspot number. At latitudes of 75° and 90° under winter conditions the sun is below the horizon and the night-time profiles described in Section 2 are used. A nocturnal profile is also used for latitude 90° under equinoctial conditions. Provided that the sun is well above the horizon, the seasonal variation is not large. In comparison with equinoctial values, attenuation rates are somewhat increased in the winter and somewhat reduced in the summer.

For a frequency of 75 Hz, the diurnal variation is shown in Table 3 for equinoctial conditions with a low sunspot number. The upper entry gives c/v and the lower entry α in db Mm^{-1}. When the sun is low in the sky, the attenuation rate in the Earth-ionosphere transmission line is increased. However, the main feature of diurnal variation is the difference between the day and night values.

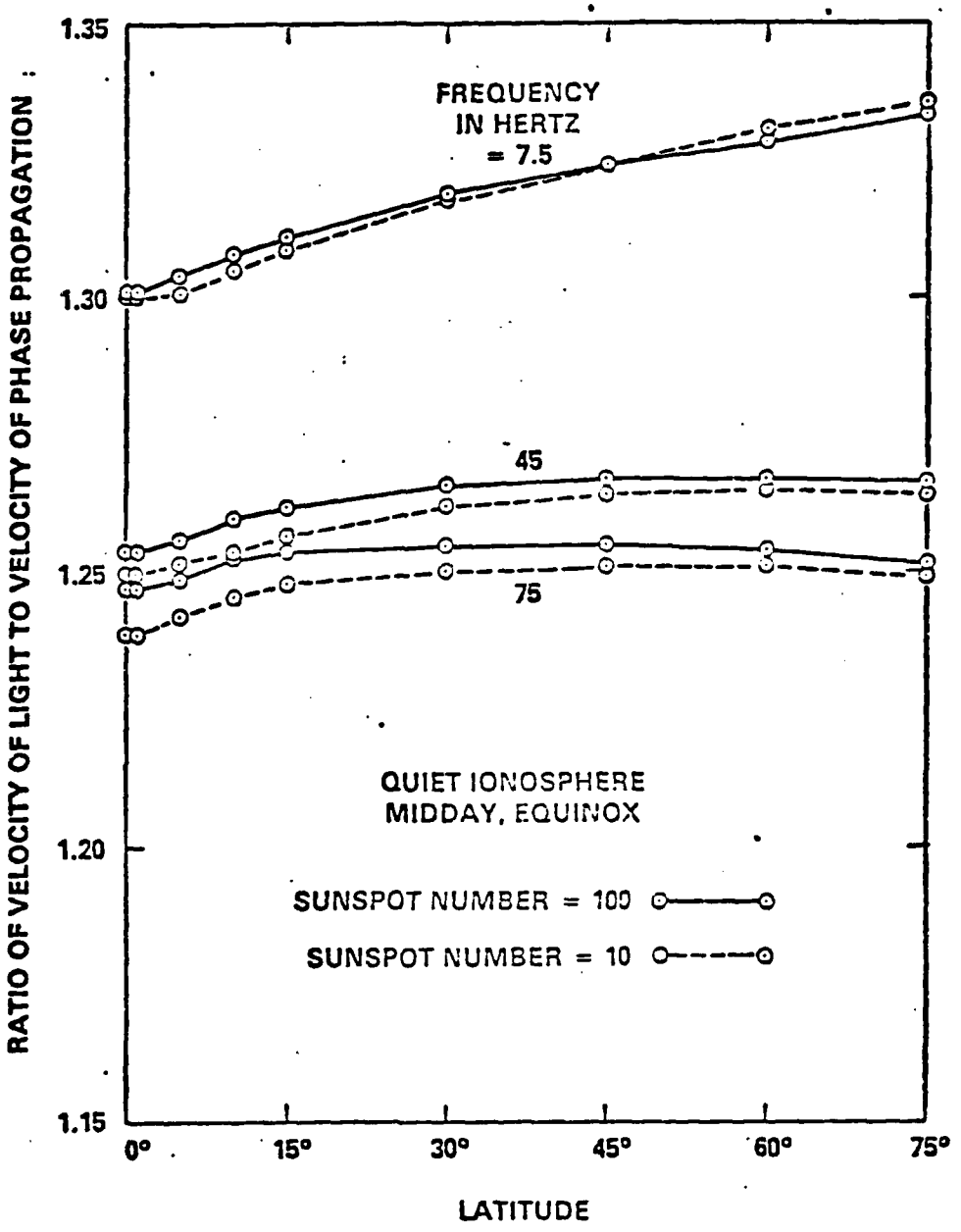

Chapter 4

Figure 16a. Illustrating the change in the velocity of phase propagation with sunspot number.

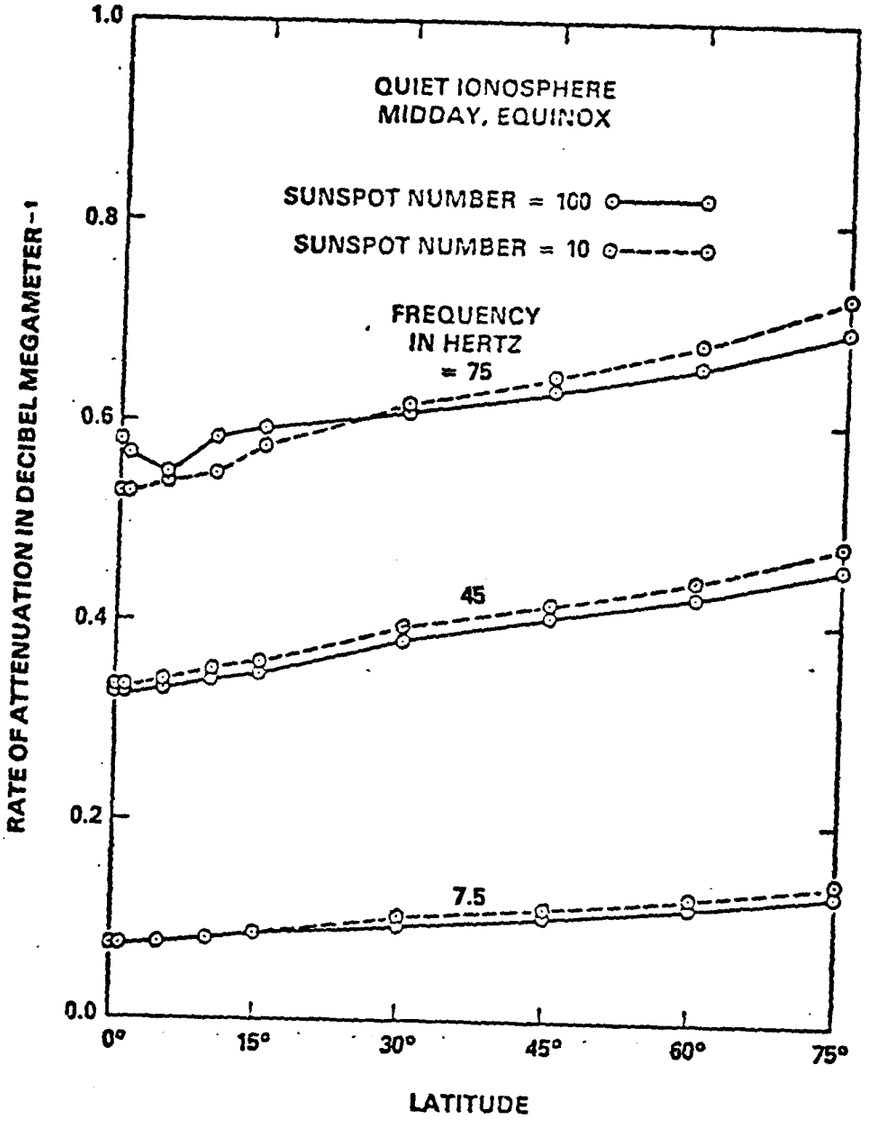

Chapter 4

Figure 16b. Illustrating the change in the rate of attenuation with sunspot number.

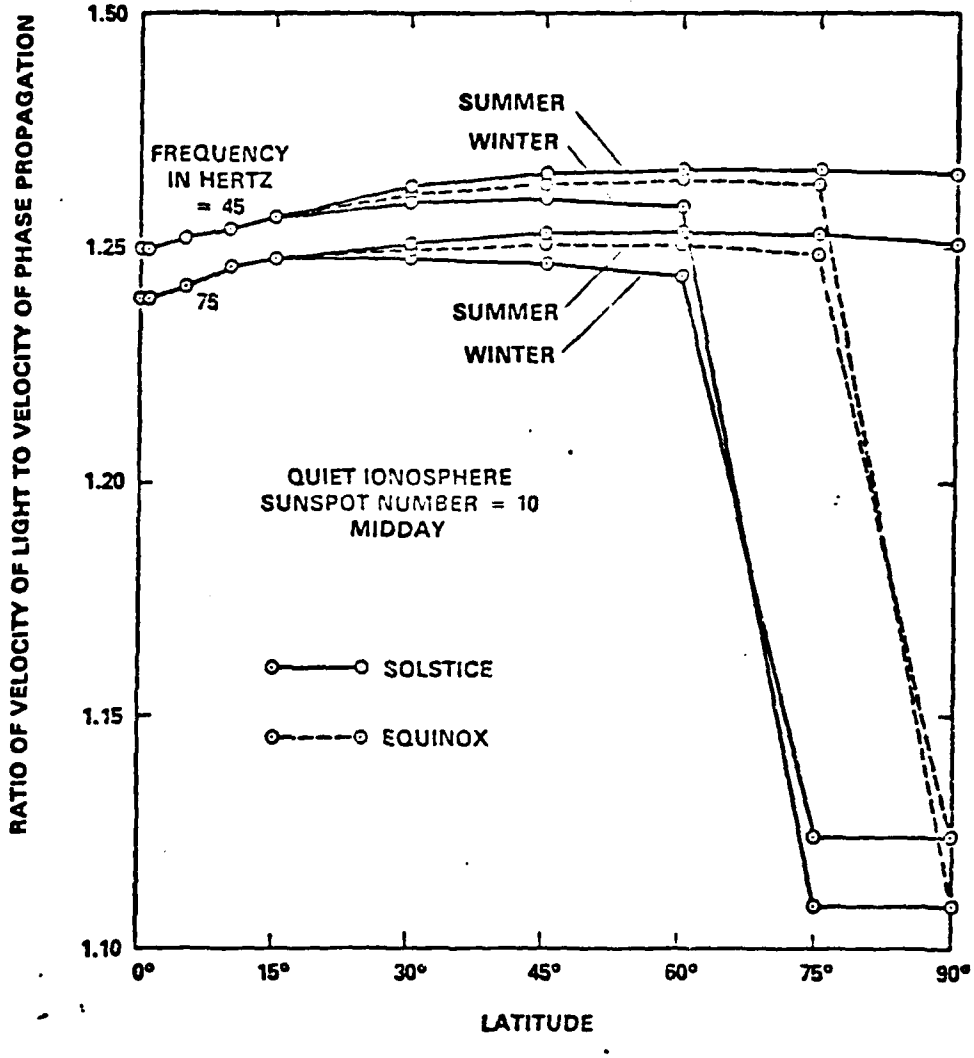

Chapter 4

Figure 17a. Illustrating the change in the velocity of phase propagation with season.

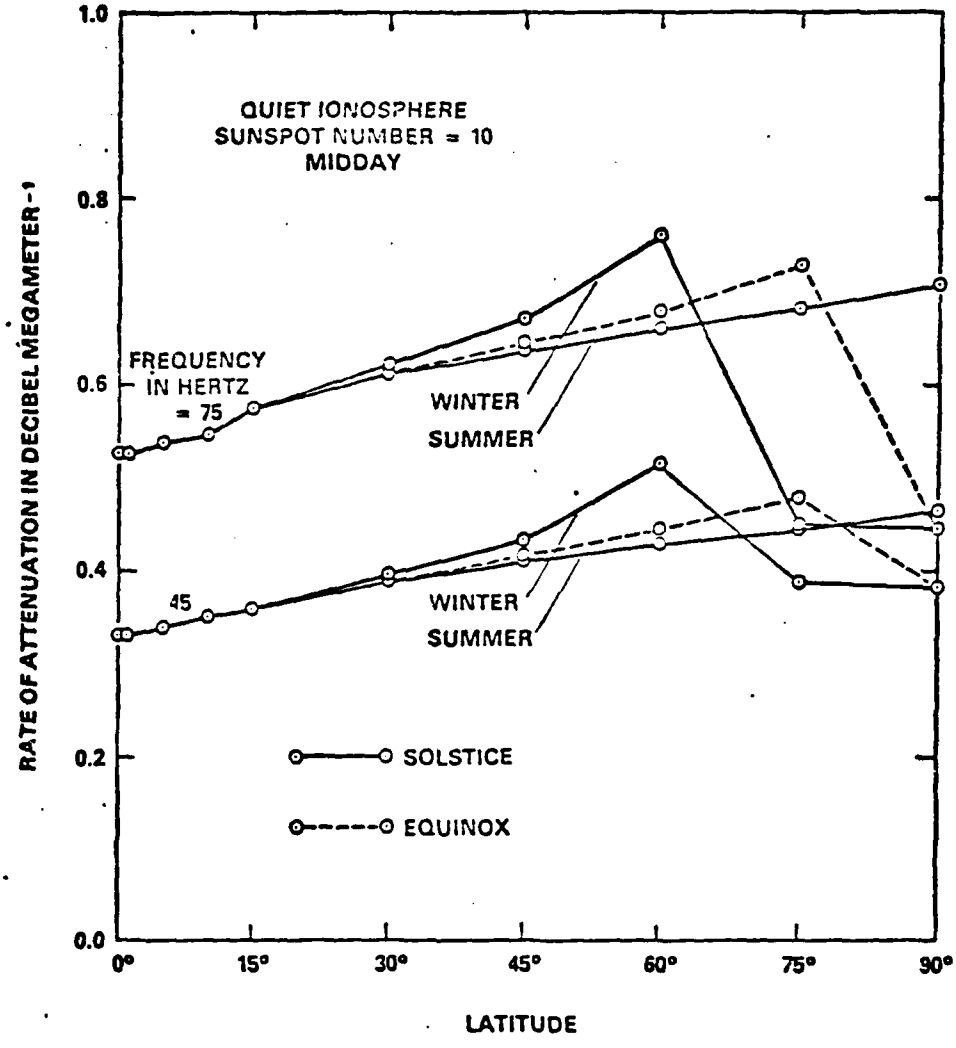

Chapter 4

Figure 17b. Illustrating the change in the rate of attenuation with season.

Table 3

Diurnal variation of c/v and α (db Mm^{-1}) at 75 Hz

(equinox, sunspot number = 10)

Latitude	Local time			
	Night	0800 1600	1000 1400	1200 noon
0°	1.11	1.23	1.24	1.24
	0.48	0.54	0.53	0.53
15°	1.13	1.24	1.25	1.25
	0.46	0.57	0.57	0.57
30°	1.12	1.25	1.25	1.25
	0.49	0.63	0.62	0.61
45°	1.12	1.25	1.25	1.25
	0.48	0.67	0.65	0.65
60°	1.12	1.25	1.25	1.25
	0.46	0.71	0.69	0.68
75°	1.12	1.25	1.25	1.25
	0.45	0.77	0.74	0.73

6. Night-time propagation ignoring reflection above 100 km

Night-time propagation in the ELF band presents the difficulty that reflection from above the level of maximum ionization density in the E region needs to be considered. Nevertheless, let us begin by excluding this phenomenon. We are then discussing, not the profiles of electron density actually shown in Figure 3, but ones that are modified so as to keep the electron density more-or-less uniform at heights above about 100 km.

Calculations are then qualitatively similar to those for the day-time ionosphere, the ledge of ionization below the E region in Figure 3 playing the role of the day-time D region in Figure 2. Figures 15a and 15b for day-time conditions are replaced by Figures 18a and 18b for night-time conditions in circumstances when reflection from above the level of maximum ionization density in the E region is ignored.

Comparison of Figure 18a with Figure 15a shows that the values of c/v are less by night than they are by day. The height of reflection is greater by night, but the height of the bottom of the ionosphere is substantially greater. The ratio of the two is changed so as to reduce the values of c/v.

Comparison of Figure 18b with Figure 15b shows that, at frequencies below about 100 Hz, the attenuation rate is greater by night than it is by day. In both cases reflection is primarily from the high gradient on the under side of the E region. But the lower values of the ionization density at night lead to lower values of the refractive indices, and consequently to lower values of the disconti-

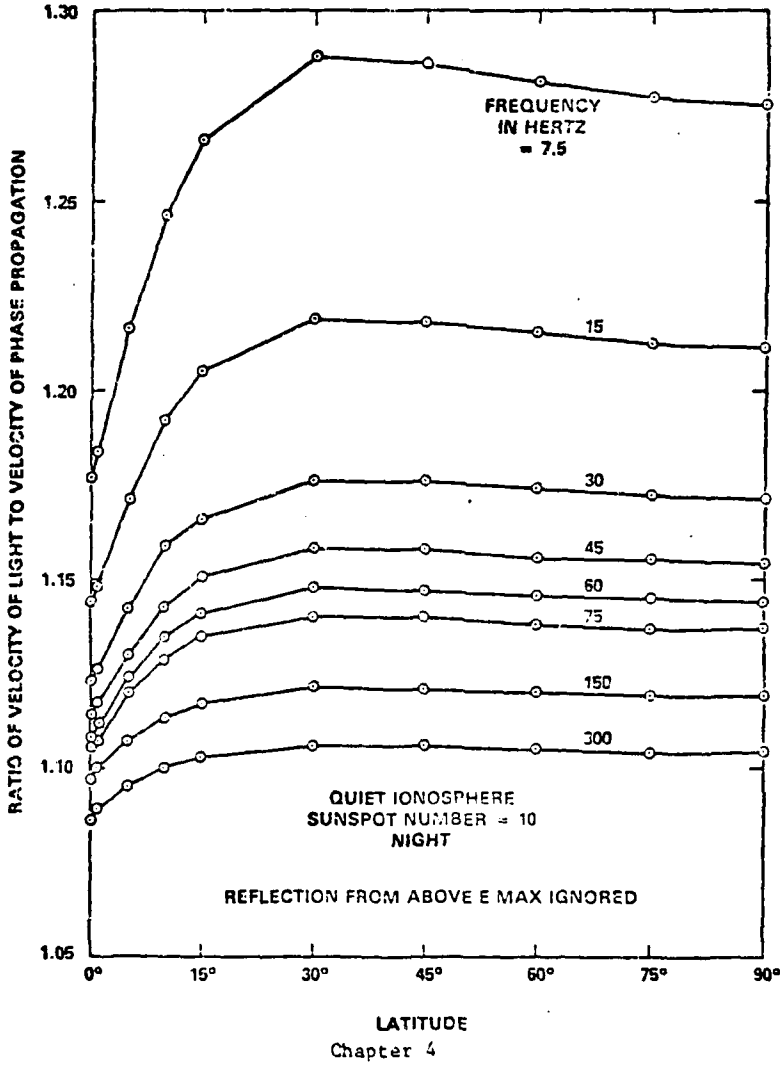

Chapter 4

Figure 18a. Illustrating the variation of the velocity of phase propagation with latitude and frequency under nighttime conditions, ignoring reflection from above the level of maximum ionization density in the E region.

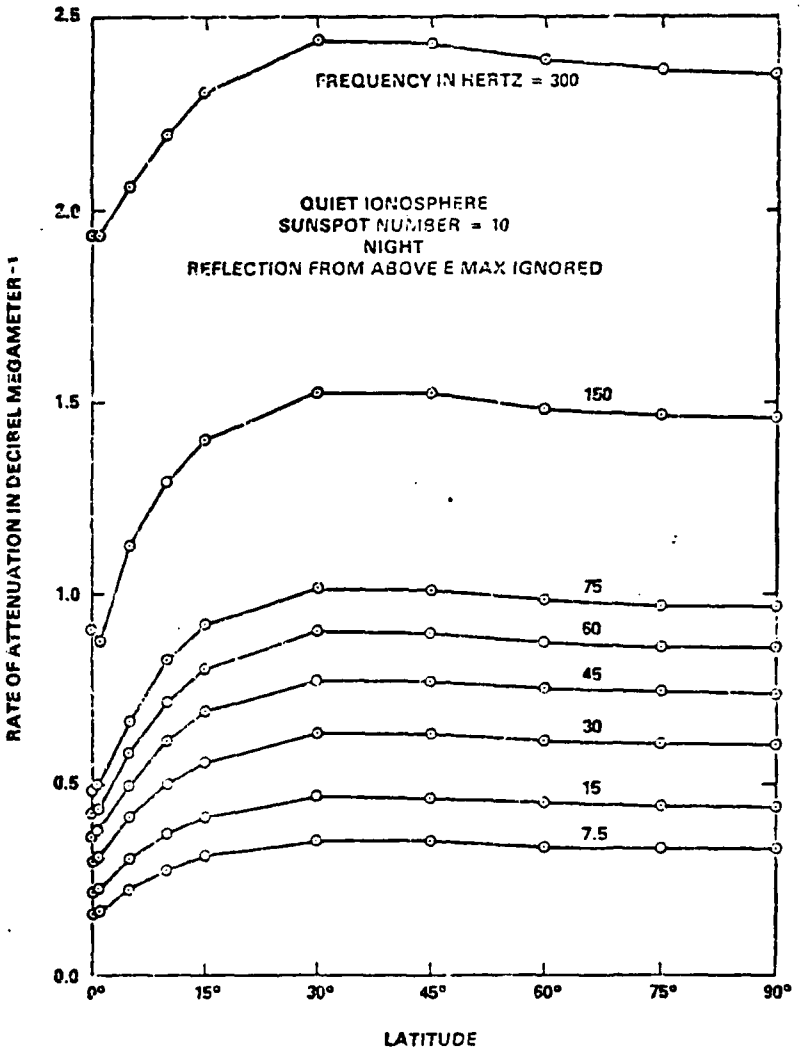

Chapter 4

Figure 18b. Illustrating the variation of the rate of attenuation with latitude and frequency under night-time conditions, ignoring reflection from above the level of maximum ionization density in the E region.

nuities n_1-1 and n_3-n_2 in Figure 1. This means that the gradient on the under side of the night-time E region is substantially less effective in blocking transmission of energy into the upper ionosphere than is that for the day-time E region. In consequence, rates of attenuation in the Earth-ionosphere transmission line at frequencies below about 100 Hz are greater by night than they are by day if reflection from the top side of the E region is ignored.

The same is true at frequencies above about 1000 Hz; reflection is then from the ledge below the E region. However, with the model of the ledge that we have used, the transition from E reflection to ledge reflection at night takes place at a higher frequency than does the transition from E reflection to D reflection by day. At 300 Hz this results in the night-time attenuation in Figure 18b being less than the day-time attenuation in Figure 15b.

Diagrams such as those in Figure 18a and 18b would constitute a reasonable representation of ELF propagation at night if this were entirely controlled by reflection below the level of maximum ionization density in the E region. In fact, however, this is not so.

7. Night-time propagation incorporating reflection above 100 km

Let us now use the night-time profiles of electron density shown in Figure 3 without modification above 100 km. The decrease of electron density that we now have on the top side of the E region causes the reflection equations to have an extra pair of solutions both for the O wave and for the X wave, except at low latitudes. This produces the type of behavior illustrated in Figure 1, except that the D region is replaced by the ledge on the under side of the E region. The degree of importance of reflection of a magneto-ionic component from the gradient on the top side of the E region is strongly influenced by the complex phase-change Φ_{34} experienced in traversing the E region. This complex phase-change is illustrated as a function of frequency in Figure 19 for a middle latitude and a low sunspot number.

At 300 Hz we see that the attenuation of the O wave in passing through the E region exceeds 20 db. This is because of the largely evanescent behavior of the O wave in the E region. In consequence, reflection of the O wave at 300 Hz is confined to the under side of the E region. However, the situation is very different for the X wave. Figure 19 shows that attenuation of the whistler wave in passing through the E region at 300 Hz is less than 0.5 db. Hence the whistler mode penetrates in great strength to the gradient on the top side of the nocturnal E region.

Furthermore, Figure 19 shows that the phase-change for the whistler mode between the gradient on the bottom side of the E region and the gradient on the top side is close to 180° at 300 Hz. The E region is then a slab with an optical thickness for the whistler

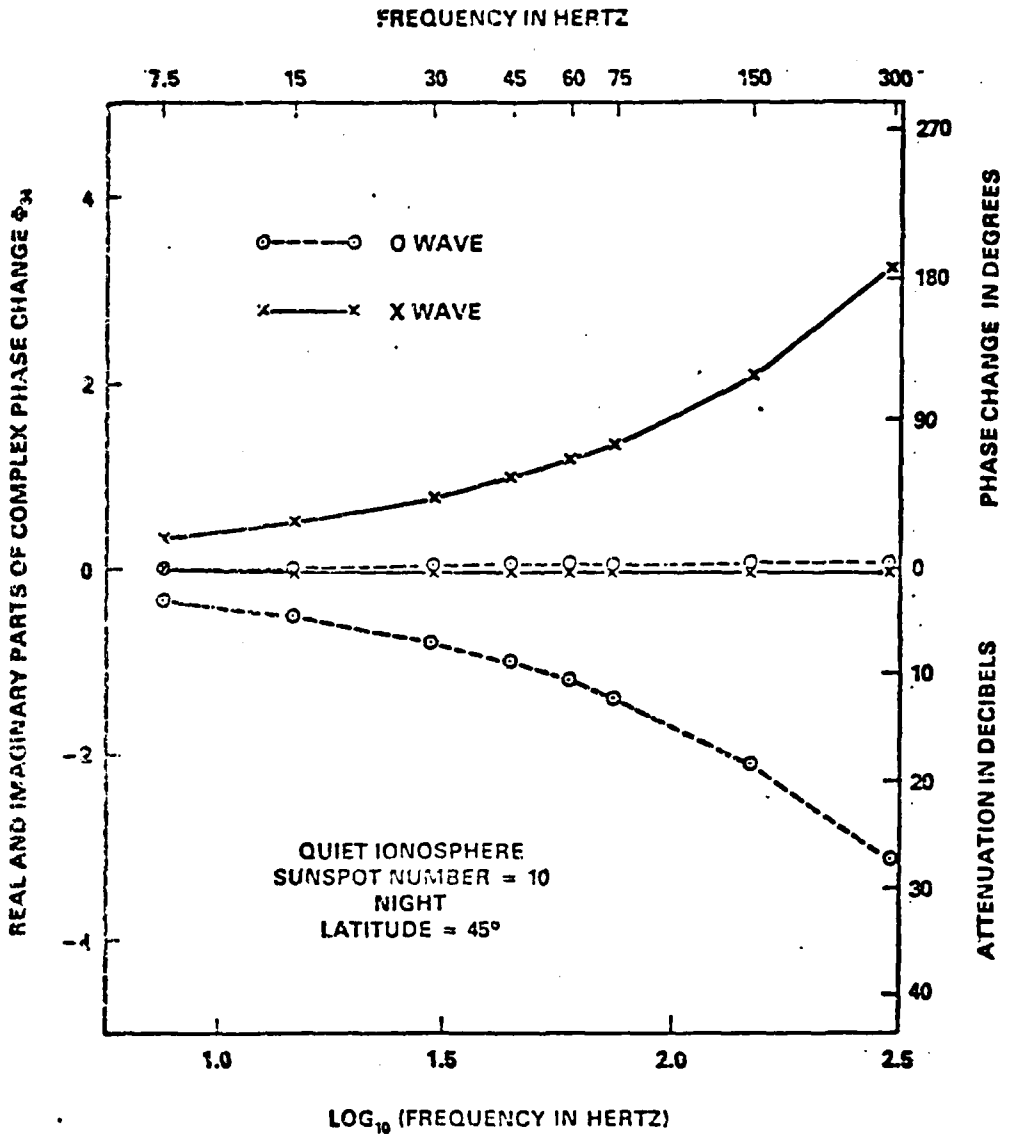

Chapter 4

Figure 19. Illustrating the variation with frequency of the complex phase-change Φ_{34} through the E region at a middle latitude under night-time conditions.

wave close to half a wavelength. This produces a resonance phenomenon. The E region would be perfectly transparent to the whistler mode at the resonant frequency in the absence of absorption. Near the resonant frequency high field strength occurs in the E region and, in the presence of collisional damping, substantial loss ensues.

There is no harmonic of this resonant frequency because reflection from the top side of the E region becomes ineffective before this frequency is reached. Even for the fundamental frequency, reflection from the top side of the E region becomes ineffective at low latitudes because of the modified influence of the Earth's magnetic field. This is illustrated in Figures 20a and 20b, which present c/v and α as functions of latitude over the frequency range 30-300 Hz for the night-time profiles shown in Figure 3. The non-standard behavior at 300 Hz caused by the resonance phenomenon is immediately apparent. However, the high attenuation rate for 300 Hz in Figure 20b disappears between latitude 30° and latitude 15°. Closer to the equator there is no significant reflection from the gradient on the top side of the E region. In the latitude range 0°-15° results for 300 Hz in Figures 20a and 20b are the same as those in Figures 18a and 18b.

Comparison of these pairs of diagrams shows that reflection from the gradient on the top side of the E region extends to progressively lower latitudes as the frequency is decreased below 300 Hz. Whereas it disappears between 30° and 15° at 300 Hz, it disappears between 10° and 5° at 150 Hz. Moreover, at higher latitudes, interference between the reflections from the gradients on the top and bottom sides of the E region is non-resonant at 150 Hz. This reduces

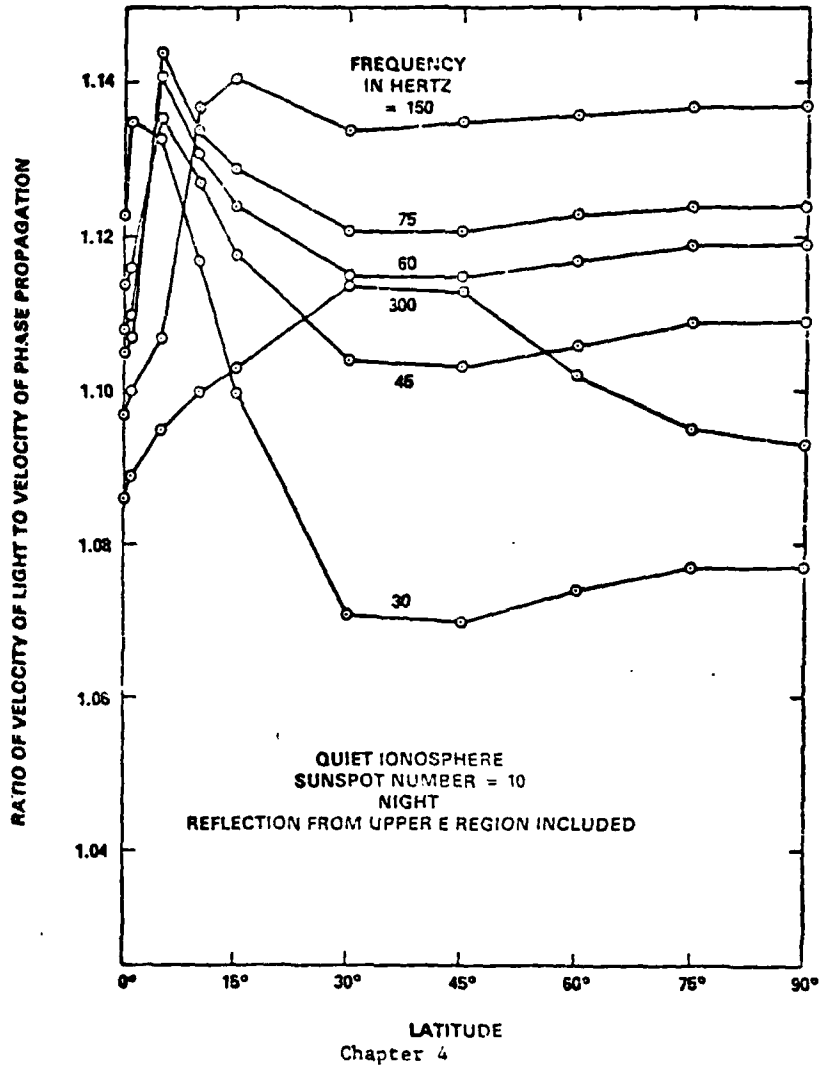

Chapter 4

Figure 20a. Illustrating the variation of the velocity of phase propagation with latitude and frequency under night-time conditions, incorporating reflection from the gradient on the top side of the E region.

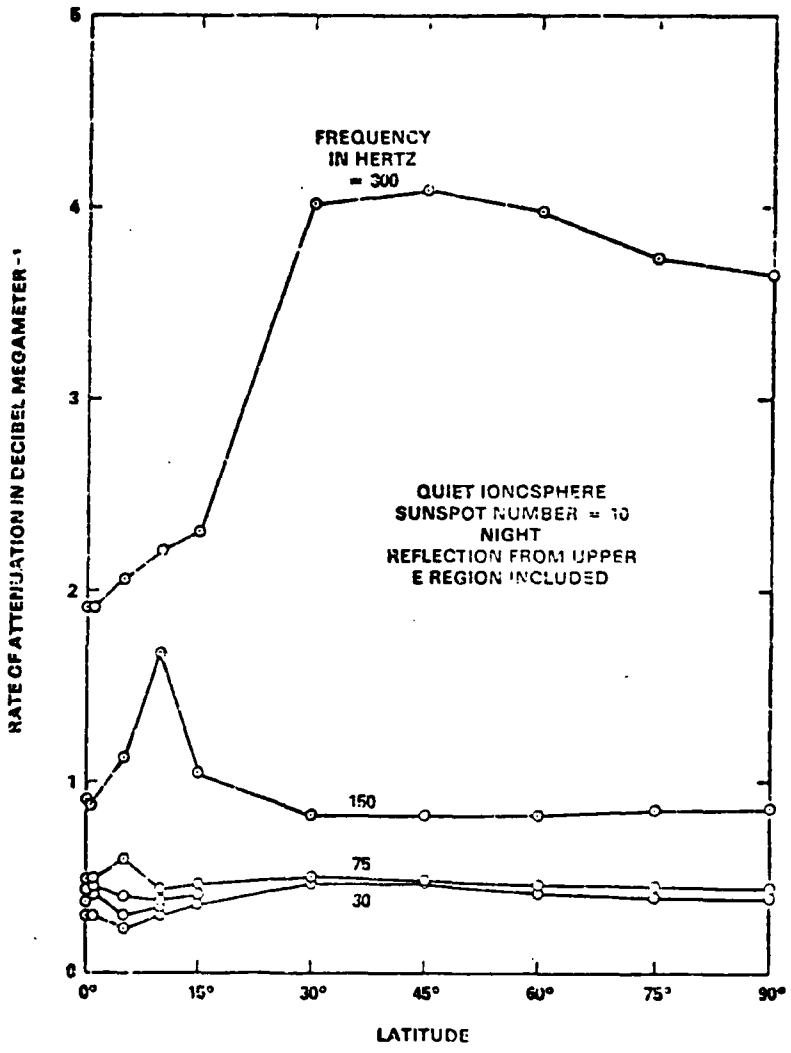

Chapter 4

Figure 20b. Illustrating the variation of the rate of attenuation with latitude and frequency under night-time conditions, incorporating reflection from the gradient on the top side of the E region.

the rate of attenuation at 150 Hz below the value that would apply in the absence of reflection from the top side, whereas the resonant interference at 300 Hz has the opposite effect. The upshot at 150 Hz is a maximum in the attenuation rate at a latitude in the vicinity of 10° as shown in Figure 20b. At 75 Hz, this maximum occurs at a latitude in the vicinity of 5°.

Except at low latitudes, vertical cross-sections of Figures 20a and 20b give the resonance curves associated with the E region resonance for the whistler mode. However, because calculations have not been made at frequencies above 300 Hz, only the behavior below the resonant frequency is depicted.

Let us now turn to a frequency of 7.5 Hz, using the night-time profiles shown in Figure 3. From Figure 19 we see that attenuation of the X wave in traversing the E region at night is completely negligible at 7.5 Hz (0.06 db). Even the phase-change is only about 20°. For the whistler wave at 7.5 Hz at night, therefore, the E region is an optically thin, nearly transparent windowpane. Reflection comes from the F region. This is confirmed by the fact that the fifth solution of the reflection equations for the X wave at 7.5 Hz at night occurs well above the greatest height included in Figure 3.

Even for the O wave at 7.5 Hz at night, we see from Figure 19 that the attenuation through the E region is only about 3 db. Although the O wave is largely evanescent in the E region, nevertheless it tunnels through to a significant extent at 7.5 Hz at night. Moreover, because 7.5 Hz is below the ionic gyrofrequency, the O wave above the

E region becomes a propagating Alfvén mode. This too is reflected from the F region, although significant attenuation is involved. The loss of energy caused by partial transmission of the O wave through the E region is quite significant, and is a prime cause of attenuation in the Earth-ionosphere transmission line at 7.5 Hz by night.

Nocturnal propagation at 7.5 Hz in the Earth-ionosphere transmission line depends on reflection from the F region. Because we have not incorporated an F region in our model of the ionosphere, we are unable to include curves for 7.5 Hz in Figure 20a and 20b. Curves for 15 Hz are omitted for the same reason.

There are major differences between (i) the curves in Figures 18a and 18b and (ii) the curves in Figures 20a and 20b. These differences arise from the assumption in the latter case that a substantial drop in ionization density occurs between the E and F regions as shown in Figure 3. It is clear that the magnitude and other features of this drop have an important influence on ELF propagation in the Earth-ionosphere transmission line at night. They change the effect of the interference phenomenon that takes place between reflections from the gradients on the top and bottom sides of the E region. The extent and character of the drop are not well established. The drop that we have assumed was suggested by the preliminary version of the International Reference Ionosphere (Rawer, Ramakrishnan and Bilitza, 1975). The actual drop may be different and may be a function of latitude and other parameters. Results are likely to be affected by various phenomena including the presence of sporadic E ionization (Barr 1977, Pappert and Moler 1978).

8. Ionospheric disturbances

Let us examine the likely effect on day-time ELF propagation of a sudden ionospheric disturbance (SID) caused by a solar flare. Let us suppose that the SID occurs at midday under equinoctial conditions. We regard the SID as creating a Disturbance 1 condition as described in Section 2. This increases the ionization density by about a power of ten in the D region while leaving it relatively unaffected elsewhere. The effect on c/v and α is shown in Figures 21a and 21b for three frequencies.

At 7.5 Hz and 45 Hz the SID lowers the height of the bottom of the ionosphere and consequently increases the values of c/v as shown in Figure 21a. The same is true at 75 Hz at high latitudes. At low latitudes, however, reflection at 75 Hz is transferred from the E region to the D region by the SID. Consequently the ratio of the height of reflection to the height of the bottom of the ionosphere is reduced, and with it the value of c/v. Transfer of reflection from the E region to the D region begins at low latitudes and spreads to all latitudes as the frequency is increased. For a quiet ionosphere this transfer takes place at a frequency of about 300 Hz (Figures 15a and 15b), but during an SID the transfer of reflection to the D region is already well under way at a frequency of 75 Hz.

Figure 21b shows that an SID increases the attenuation rate in the Earth-ionosphere transmission line at 7.5 Hz only slightly. At 45 Hz the increased loss is more substantial. In Figure 1, the enhanced D region increases the value of the discontinuity $n_1 - 1$ but reduces the value of the discontinuity $n_3 - n_2$, and it is the latter

that is the more serious effect at 45 Hz. At 75 Hz the decrease in $n_3 - n_2$ is also important, but the increase in $n_1 - 1$ makes itself felt at low latitudes (Figure 21b).

Let us now consider the likely effect on ELF propagation of a polar cap absorption (PCA) event caused by particle emission from the sun. At a latitude of 75° we regard PCA events of progressively increasing strength as represented by the Disturbance 1, 2 and 3 conditions described in Section 2. The effect of the various degrees of disturbance on ELF propagation in polar regions is shown in Table 4 for three frequencies. At these frequencies disturbance increases attenuation in the Earth-ionosphere transmission line. The principal reason is that, under quiet ionospheric conditions, the D region plays little role in the reflection process below 100 Hz, and leakage of energy into the upper ionosphere is controlled primarily by the high gradient on the under side of the E region. This advantage is weakened under Disturbance 1 conditions and destroyed under Disturbance 2 conditions. When the reflection process has been firmly taken over by ionization below the E region, further increase in disturbance reduces attenuation in the Earth-ionosphere transmission lire. Nevertheless, under Disturbance 3 conditions, the attenuation rates at 45 and 75 Hz are greater than they are for a quiet ionosphere--a result that could, however, be changed by making the gradient on the under side of the ionosphere greater for greater degrees of disturbance. On the other hand, at a frequency of 1000 Hz, reflection is from the D region (or at night from the ledge on the under side of the E region) even under quiet ionospheric conditions. The effect

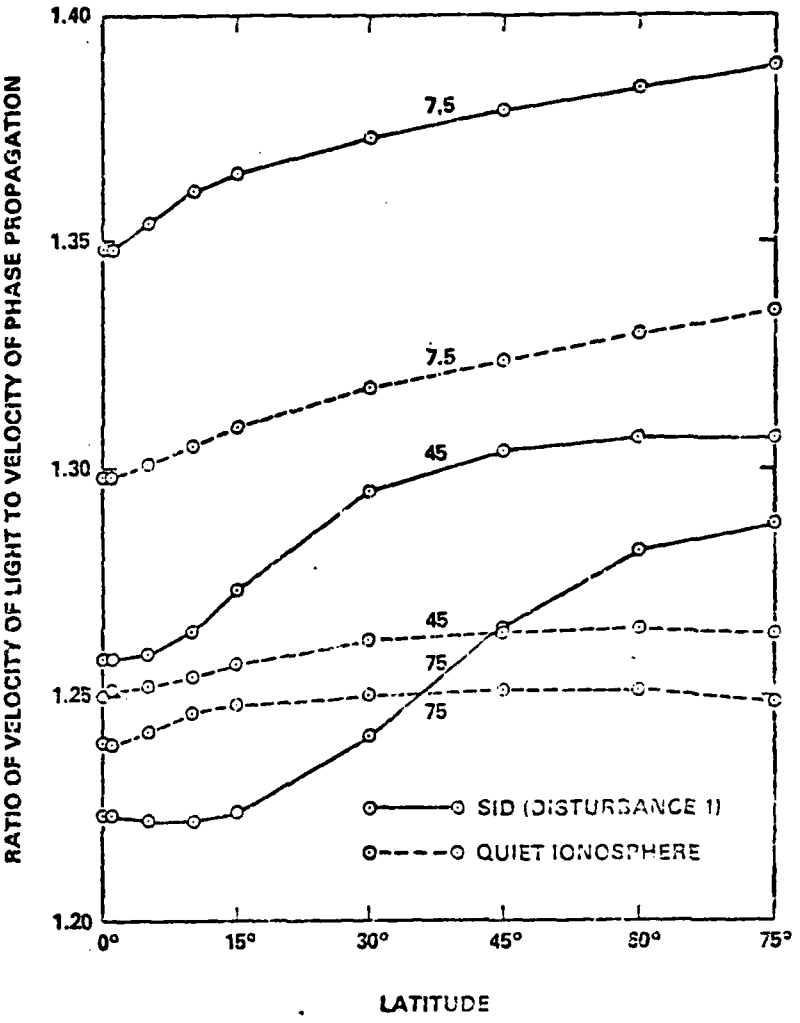

Chapter 4

Figure 21a. Illustrating the change in the velocity of phase propagation caused by a sudden ionospheric disturbance.

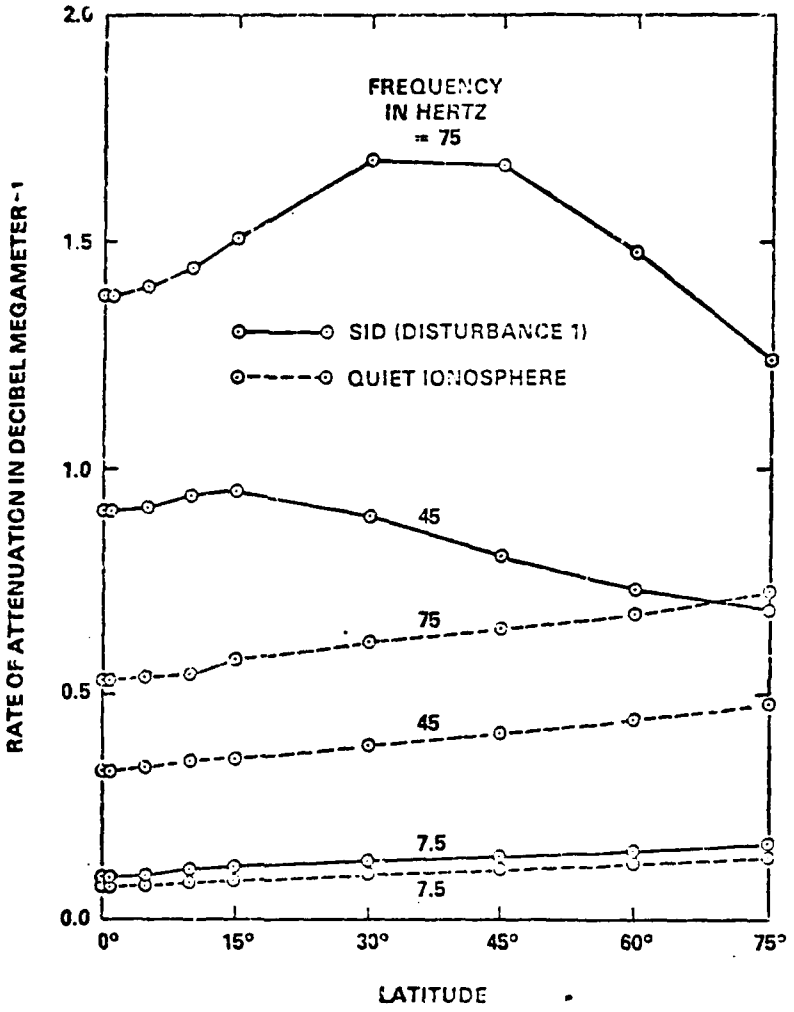

Chapter 4

Figure 21b. Illustrating the change in the rate of attenuation caused by a sudden ionospheric disturbance.

of disturbance is then to reduce the attenuation rate in the Earth-ionosphere transmission line.

Table 4

Effect on c/v and α (db Mm^{-1}) of

enhanced ionization below the E region in the polar caps

(latitude = 75°)

Frequency (hertz)	Day profiles (Figs. 4 and 6)				Night profiles (Figs. 5 and 7)			
	0	1	2	3	0	1	2	3
7.5	1.34 0.14	1.39 0.17	1.36 0.24	1.34 0.20	F region is involved		1.34 0.18	1.41 0.16
45	1.26 0.48	1.31 0.68	1.23 0.84	1.22 0.73	1.11 0.39	1.14 0.65	1.18 0.86	1.28 0.78
75	1.25 0.73	1.29 1.24	1.20 1.24	1.20 1.08	1.12 0.45	1.14 0.94	1.13 1.26	1.25 1.22

Table 5

Calculations of Pappert and Moler

for comparison with Table 4

Frequency (hertz)	Day profiles (Figs. 4 and 6)				Night profiles (Figs. 5 and 7)			
	0	1	2	3	0	1	2	3
7.5	1.32 0.12	1.35 0.16	1.32 0.21	1.32 0.17	F region is involved		1.37 0.18	1.43 0.16
45	1.26 0.46	1.26 0.82	1.21 0.73	1.21 0.67	1.14 0.28	1.17 0.70	1.22 0.88	1.29 0.81
75	1.25 0.77	1.23 1.47	1.18 1.07	1.19 1.00	1.15 0.40	1.14 1.98	1.16 1.56	1.27 1.26

9. Comparison with the method of Papper and Moler (1974)

The method of calculation described in Chapter 3 and applied in this chapter was designed primarily to reveal the physics of ELF propagation. As a method for calculating the numerical values of c/v and α it is only approximate. Let us compare these values with those obtained by Pappert and Moler (1974) using a method in which the only errors should be those arising from digitization of the profiles. Using their method, Papper and Moler (private communication) have kindly performed calculations corresponding to those presented in Table 4. Their results are shown in Table 5.

Comparison of Tables 4 and 5 shows that, while the numbers are not identical, trends are the same. The comments about the effect of disturbance on the polar ionosphere made in the previous section on the basis of Table 4 are unchanged if use is made of Table 5 instead.

However, there is a place in Tables 4 and 5 where an appreciable discrepancy occurs in the rate of attenuation. This happens for 75 Hz at night under Disturbance 1 conditions. In these circumstances, the height of reflection is between 83 and 84 km, and this is on the sharp bend of Profile 1 in Figure 5. A small increase in the estimate of height would then appreciably increase the estimate of local scale-height. This would increase the rate of attenuation, thereby creating better agreement between the values shown in Tables 4 and 5 for 75 Hz at night under Disturbance 1 conditions. It should be remembered that the method of calculation described in Chapter 3 assumes that the profile of electron density is approximately exponential in behavior

across the relevent reflecting stratum. This condition is often reasonably well satisfied, but when it is not, some error occurs.

A respect in which we disagree with the calculations of Pappert and Moler (1974) occurs at low latitudes. They find a substantial dependence of ELF propagation on Δ, the angle made with the north by the horizontal direction of transmission in the Earth-ionosphere transmission line. They obtain different results when Δ is changed by 180°, implying non-reciprocal transmission. Other authors (Field 1969, Galejs 1972) have also obtained non-reciprocal effects in the ELF band. At VLF the phenomenon is well known (Budden 1961, Galejs 1972). Pappert and Moler (1974) encounter non-reciprocal behavior at ELF not only by night but also by day. In contrast, we have obtained no numerically important variation with Δ, reciprocal or non-reciprocal, under any circumstances in the ELF band that we have investigated.

If non-reciprocity exists, it must be caused by the Earth's magnetic field. Moreover, it cannot be caused at any level in the ionosphere where the propagation of phase is vertical. It must be caused where the transition is taking place from nearly horizontal propagation of phase to nearly vertical propagation. In the ELF band (but not in the VLF band) this transition is confined to a refracting stratum at the bottom of the ionosphere. But in this stratum there is never any substantial difference between the refractive indices for the O and X waves. This is especially true by day; the height of the bottom of the ionosphere is then illustrated in Figures 10 and 13 by the curves for the real part of $\tilde{z}_B$. By day

the refracting stratum occurs where the gyrofrequencies are small compared with the collisional frequencies, and consequently where the Earth's magnetic field cannot play an important role. We are therefore unable to identify a convincing physical basis for significant non-reciprocity in the ELF band by day. By night some non-reciprocity is reasonable. The calculations of Pappert and Moler (1974) do show less non-reciprocity by day than by night, and perhaps this is to be regarded as adequeately consistent with the physical argument. But we doubt it. So far as we are able to judge, the computer program of Pappert and Moler is giving correct results near the magnetic poles but not near the magnetic equator.

When this point has been cleared up, the method of Pappert and Moler will give greater accuracy in the calculation of c/v and α than can be obtained by the method described in Chapter 3. However, this greater accuracy will be achieved using far more arithmetical operations, and with considerably less insight into the physics of the propagation phenomena. For some purposes it is physical insight that is required rather than precise arithmetic.

10. The Schumann resonances

As an example of the need for physical insight rather than precise arithmetic, let us consider the Schumann resonances associated with the Earth-ionosphere cavity. For years it was taken for granted that loss of energy from the cavity arose primarily from absorption below the E region. By some workers this view still seems to be held (Tran and Polk, 1979a,b). Yet the results presented in this paper suggest that the physics of the Schumann resonance phenomenon may be otherwise.

An important cause for loss of energy from the Earth-ionosphere cavity at the Schumann resonant frequency (~ 7.5 Hz) is leakage through the nocturnal E region not merely via the whistler mode but also via the Alfvén mode. To recognize that this is so, it is only necessary to use Equation (5) to prepare a diagram of the type appearing in Figure 19. High numerical accuracy is not needed.

Attenuation at the Schumann resonant frequency in the day hemisphere is in all probability quite low. To understand how this can be, it is first necessary to recognize that reflection occurs in a stratum where $1/(4\pi)$ times the local wavelength is of the same order of magnitude as the local scale-height of the profile. Even with now obsolescent profiles, quite a simple calculation places the level of reflection in the E region at the Schumann resonant frequency. With profiles based on rocket observations that exhibit a high gradient on the under side of the E region, the reason for the low rate of attenuation at 7.5 Hz in Figure 15b can easily be understood. High numerical accuracy is not needed in order to ascertain that the

attenuation rate in the Earth ionosphere transmission line over the day hemisphere can be quite low at 7.5 Hz.

The important arithmetical weaknesses of the curves presented in this chapter for ELF propagation in the Earth-ionosphere transmission line are not connected with the approximations employed in the method described in Chapter 3. They arise from the weaknesses of the ionospheric model to which the method is applied in this chapter. While there is a need to improve the model of the day-time ionosphere, a far greater need exists to improve the model of the night-time ionosphere. In studying the damping of the Schumann resonances, a shift in emphasis is probably required away from absorption of energy in the day-time D region towards leakage of energy through the night-time E region. To do this, and to study other aspects of ELF propagation at night, necessitates a better model of the night-time ionosphere, especially above 100 km, than has been employed in this chapter.

11. Conclusion

It is concluded that the method of investigating ELF propagation in the Earth-ionosphere transmission line described in Chapter 3 and applied in this chapter (i) gives more physical insight than any other method currently available, (ii) requires less effort than any other profile-based method currently available, and (iii) provides reasonable accuracy in spite of approximations.

However, to handle reflection from the F region at the low frequency end of the ELF band at night, further development of the method is needed. In particular, between the E and F regions some coupling takes place between the O and X waves at frequencies less than the ionic gyrofrequency. The extent and consequences of this coupling need to be investigated.

Bibliography

Banks, P. M. and Kockarts, G.	1973	Aeronomy, Academic Press, New York.
Barr, R.	1977	The effect of sporadic-E on the nocturnal propagation of ELF waves, Journal of Atmospheric and Terrestrial Physics 39, 1387-1397.
Booker, H. G.	1977	Fitting of multi-region ionospheric profiles of electron density by a single analytic function of height, Journal of Atmospheric and Terrestrial Physics 39, 619-623.
Booker, H. G. and Lefeuvre, F.	1977	The relation between ionospheric profiles and ELF propagation in the Earth-ionosphere transmission line, Journal of Atmospheric and Terrestrial Physics 39, 1277-1292.
Budden, K. G.	1961	Radio waves in the ionosphere, Cambridge University Press, Cambridge
Field, E. C.	1969	Propagation of ELF waves under normal and naturally disturbed conditions, J. Geophys. Res. 74, 3639-3650.
Galejs, J.	1972	Terrestrial propagation of long electromagnetic waves, Logos Press, London.
Greifinger, C. and Greifinger, P.	1978	Approximate method for determining ELF eigenvalues in the Earth-ionosphere waveguide, Radio Science 13, 831-837.
Greifinger, C. and Greifinger, P.	1979	On the ionospheric parameters which govern high latitude ELF propagation in the Earth-ionosphere waveguide, Radio Science 14, 889-895.
Pappert, R. A. and Moler, W. F.	1974	Propagation theory and calculations at lower ELF, IEEE Transactions on Communications 22, 438-451.

Pappert, R. A. and Moler, W.F. 1978 A theoretical study of ELF normal mode reflection and absorption produced by nighttime ionospheres, J. Atmos. Terr. Phys. 40, 1031-1045.

Rawer, K., Ramakrishnan, S. and Bilitza, D. 1975 Preliminary reference profiles for electron and ion densities and temperatures proposed for the International Reference Ionosphere, Institüt für physikalishe Weltraumforschung, Scientific Report W. B. 2.

Rawer, K., Bilitza, D. and Ramakrishnan, S. 1978 Goals and status of the International Reference Ionosphere, Reviews of Geophysics and Space Physics 16, 177-181.

Rawer, K. Ramakrishnan, S. and Bilitza, D. 1978 International Reference Ionosphere 1978, International Union of Radio Science, Brussels.

Tran, A. and Polk, C. 1979a Schumann resonances and electrical conductivity of the atmosphere and lower ionosphere. Part I: Effects of conductivity at various altitudes on resonance frequencies and attenuation, J. Atmos. Terr. Phys. 41, 1241-1248.

Tran, A. and Polk, C. 1979b Schumann resonances and conductivity of the atmosphere and lower ionosphere. Part II: Evaluation of conductivity profiles from experimental Schumann resonance data, J. Atmos. Terr. Phys. 41, 1249-1261.